



Norwegian University of  
Science and Technology

# Hydrogen Storage: Thermophysical data and flow properties for some porous media

Ole Kristoffer Abrahamsen

Master of Science in Product Design and Manufacturing

Submission date: June 2010

Supervisor: Erling Næss, EPT



# Problem Description

## 1. Permeability:

a) A test rig for the measurement of permeability in porous materials shall be designed and documented. Required instrumentation and measurement accuracies shall be specified. The experimental uncertainty shall be evaluated.

b) An experimental program for the determination of permeability of selected porous materials shall be performed. The materials shall be described, and measurement results shall be analyzed, discussed and presented.

## 2. Thermal Conductivity:

a) Based on the results of the project work, a complete setup for the measurement of thermal conductivity on porous materials shall be designed. All required equipment specifications and instrument accuracies shall be determined, and suitable equipment shall be selected. A complete uncertainty analysis shall be performed. Additionally, numerical analyses shall be performed in order to assess the temperature and heat flow distributions on the test setup.

b) Experiments shall be performed on the test setup. Materials and material combinations for analysis shall be selected in cooperation with the Department. The experimental results shall be analyzed, presented and discussed. A comparison with available literature models shall be performed and the results discussed.

3. Suggestions for further work shall be presented and discussed.

Assignment given: 18. January 2010

Supervisor: Erling Næss, EPT



EPT-M-2010-5

## MASTER THESIS

for

Stud.techn. Ole Kristoffer Abrahamsen

Spring 2010

*Hydrogen storage: Thermophysical data and flow properties for some porous media*  
*Hydrogenlagring: Termofysikalske data og strømningssegenskaper for noen porøse medier*

### **Background and objective.**

Hydrogen on-board storage is a critical matter for development and commercialization of hydrogen based vehicles. However, the hydrogen storage systems presently available do not meet standards imposed by the U.S. Department of Energy and the automobile industry and needs improvements. Sorption type materials have been identified as a viable option. They are characterized by high porosity and surface area. However, the thermal effects that occur during the filling and discharging of a storage system play an important role in the utilization of the hydrogen adsorption storage systems.

The objective of the project is to design experimental test rigs and perform experiments for the characterization of thermal properties of some adsorption type storage materials.

The work is a continuation of the project work.

### **The following questions should be considered in the project work:**

1. Permeability:
  - a. A test rig for the measurement of permeability in porous materials shall be designed and documented. Required instrumentation and measurement accuracies shall be specified. The experimental uncertainty shall be evaluated.
  - b. An experimental program for the determination of permeability of selected porous materials shall be performed. The materials shall be described, and measurement results shall be analyzed, discussed and presented. A comparison to relevant literature data shall be made, if possible.
2. Thermal conductivity:
  - a. Based on the results of the project work, a complete setup for the measurement of thermal conductivity on porous materials shall be designed. All required equipment specifications and instrument accuracies shall be determined, and suitable equipment shall be selected. A complete experimental uncertainty analysis shall be performed. Additionally, numerical analyses shall be performed in order to assess the temperature and heat flow distributions in the test setup.

- b. Experiments shall be performed on the test setup. Materials and material combinations for analysis shall be selected in cooperation with the Department. The experimental results shall be analyzed, presented and discussed. A comparison with available literature models shall be performed and the results discussed.
3. Suggestions for further work shall be presented and discussed.

Within 14 days of receiving the written text on the diploma thesis, the candidate shall submit a research plan for his project to the department.

When the thesis is evaluated, emphasis is put on processing of the results, and that they are presented in tabular and/or graphic form in a clear manner, and that they are analyzed carefully.

The thesis should be formulated as a research report with summary both in English and Norwegian, conclusion, literature references, table of contents etc. During the preparation of the text, the candidate should make an effort to produce a well-structured and easily readable report. In order to ease the evaluation of the thesis, it is important that the cross-references are correct. In the making of the report, strong emphasis should be placed on both a thorough discussion of the results and an orderly presentation.

The candidate is requested to initiate and keep close contact with his/her academic supervisor(s) throughout the working period. The candidate must follow the rules and regulations of NTNU as well as passive directions given by the Department of Energy and Process Engineering.

Pursuant to "Regulations concerning the supplementary provisions to the technology study program/Master of Science" at NTNU §20, the Department reserves the permission to utilize all the results and data for teaching and research purposes as well as in future publications.

One – 1 complete original of the thesis shall be submitted to the authority that handed out the set subject. (A short summary including the author's name and the title of the thesis should also be submitted, for use as reference in journals (max. 1 page with double spacing)).

Two – 2 – copies of the thesis shall be submitted to the Department. Upon request, additional copies shall be submitted directly to research advisors/companies. A CD-ROM (Word format or corresponding) containing the thesis, and including the short summary, must also be submitted to the Department of Energy and Process Engineering

Department of Energy and Process Engineering, 12. January 2010



Olav Bolland  
Department Manager



Erling Næss  
Academic Supervisor

Research Advisor:  
Professor II Ulrich Bünger, NTNU

## ABSTRACT

Two rigs have been developed and built to measure thermal conductivity and permeability for porous materials. The intention of the rigs is to investigate the properties of some hydrogen adsorption materials. The materials are only available in small volumes which have been taken into consideration under the development.

Fourier's law of heat conduction has been used as a basis for the development of the thermal conductivity rig. A cylindrical geometry with centered heater was chosen to ensure that all heat must be transported through the specimen. The temperature and heat distribution have been evaluated numerically to find the required insulation on top and bottom. Based on the chosen insulation, the rig is able to measure the conductivity for specimens with minimum conductivity of  $0.1 \frac{W}{mK}$ . To make the rig capable of measurements at different temperatures, a side wall cooling system has been developed where fluid is transported on the outer side of the rig. Depending on the coolant fluid, the rig is capable of measurements within a wide temperature range. Liquid nitrogen and tap water have been used in the measurements where the lowest measurement was performed at  $\div 137^{\circ}C$ . The uncertainties have been determined where the positioning of the thermocouples have been shown to be most affecting due to the small dimensions of the rig. The results have an uncertainty of  $\pm 10\%$ .

The permeability rig have been developed using the principles of Darcy's law. To estimate the magnitude of the flow rate and pressure loss for a given material, a set of empirical equations has been used. Based on the estimations it turned out that great variations in pressure loss can be expected depending on the pore size diameter of the material. They also stated the validation of Darcy's law which is for slow viscous flow only. The uncertainties in the equipment have been estimated and indicated that results can be obtained with an uncertainty less than 10%. The measurements pointed out that the geometry of the rig should be modified as the pressure loss turned out to be too small.

Due to delays, the adsorption materials were not available when the rigs were ready for measurements; therefore, other materials were chosen to test the rigs. The permeability results has been compared to the estimation based on the pore size diameter of the materials. For the conductivity rig, the results were harder to verify since the properties such as porosity and conductivity of the solid phase not were known.





## PREFACE

This master thesis is a part of a research project between NTNU, Max Planck Institut für Metallforschung, and Technische Universität Dresden. It has been written in the period from January to June 2010 and is a continuation of the project work.

I would like to thank Erling Næss for our weekly meetings this spring, they have been valuable for the progression of the project and for my own learning. My work in the laboratory has been done with help from Halvor Flatberg and Reidar Tellebon, I am very grateful for all the time they have spent helping me. In addition, I would like to thank my fellow students at office B432 for a year filled with fun, laughter and several coffee runs.

The work has given me the opportunity to take part in the development from the first prestudies to actually performing measurements on the rigs that have been built.



Kristoffer Abrahamsen  
Trondheim, June 14 2010



# CONTENTS

<b>1. Introduction</b>	<b>1</b>
1.1. Background . . . . .	1
1.2. Project Description . . . . .	2
<b>I Design and Prestudy of Test Rigs</b>	<b>3</b>
<b>2. Thermal Conductivity Rig</b>	<b>5</b>
2.1. Introduction . . . . .	5
2.2. Rig Design and Dimensions . . . . .	6
2.3. Fourier's Law of Heat Conduction . . . . .	7
2.4. Temperature Distribution and Heat Flow . . . . .	8
2.5. Equipment and Instrumentation . . . . .	12
2.6. Uncertainty Analysis . . . . .	13
2.7. Thermal Conductivity Estimation . . . . .	18
2.8. Discussion . . . . .	18
<b>3. Permeability Rig</b>	<b>19</b>
3.1. Introduction . . . . .	19
3.2. Rig Design . . . . .	19
3.3. Darcy's Law . . . . .	20
3.4. Equipment and Instrumentation . . . . .	21
3.5. Estimation of Permeability . . . . .	23
3.6. Estimation of Pressure Loss . . . . .	27
3.7. Uncertainty Analysis . . . . .	29
3.8. Discussion . . . . .	32
<b>II Test Rigs</b>	<b>33</b>
<b>4. Thermal Conductivity Rig, Completion</b>	<b>35</b>
4.1. Introduction . . . . .	35
4.2. Equipment and Instrumentation . . . . .	36
4.3. Evaluation of Data . . . . .	36
4.4. Calibration and Determination of Uncertainties . . . . .	37
4.5. Side Wall Cooling . . . . .	40
4.6. Assembly . . . . .	43
4.7. Discussion . . . . .	43
<b>5. Permeability Rig, Completion</b>	<b>45</b>
5.1. Introduction . . . . .	45
5.2. Equipment and Instrumentation . . . . .	46

5.3. Evaluation of Data and Estimation of Uncertainties . . . . .	46
5.4. Assembly . . . . .	50
5.5. Preparation and Accomplishment of a Measurement . . . . .	51
5.6. Discussion . . . . .	51
<b>III Experimental Results</b>	<b>53</b>
<b>6. Thermal Conductivity Measurement Results</b>	<b>55</b>
6.1. Introduction . . . . .	55
6.2. Sugar . . . . .	56
6.3. Sand . . . . .	62
6.4. Expancel . . . . .	66
6.5. Discussion . . . . .	70
6.6. Further Work . . . . .	71
<b>7. Permeability Measurement Results</b>	<b>73</b>
7.1. Introduction . . . . .	73
7.2. Sugar . . . . .	74
7.3. Sand . . . . .	77
7.4. Expancel . . . . .	80
7.5. Discussion . . . . .	83
7.6. Further Work . . . . .	83
<b>IV Closure</b>	<b>85</b>
<b>8. Thermal Conductivity</b>	<b>87</b>
8.1. Conclusion . . . . .	87
<b>9. Permeability</b>	<b>89</b>
9.1. Conclusion . . . . .	89
<b>Bibliography</b>	<b>91</b>
<b>Equipment and Material References</b>	<b>93</b>
<b>V Appendices</b>	<b>A</b>
<b>A. P&amp;ID</b>	<b>C</b>
A.1. Thermal Conductivity Rig . . . . .	C
A.2. Permeability Rig . . . . .	D
<b>B. Experimental Uncertainties</b>	<b>E</b>
B.1. Basis . . . . .	E
B.2. Single-Sample Analysis . . . . .	E
B.3. t-Distribution and Normal Distribution . . . . .	F
B.4. Overall Uncertainty in a Single Measurement . . . . .	G
<b>C. Measurement Materials</b>	<b>I</b>
C.1. Basis . . . . .	I
C.2. Sugar . . . . .	I
C.3. Sand . . . . .	J
C.4. Expancel 551 DE 40 d42 . . . . .	J
<b>D. Parameters for Permeability Estimation</b>	<b>K</b>

<b>E. MATLAB Scripts</b>	<b>M</b>
E.1. Introduction . . . . .	M
E.2. Thermal Conductivity . . . . .	M
E.3. Permeability . . . . .	M
<b>F. MAPLE: Solution of Partial Derivatives from Uncertainty Calculations</b>	<b>O</b>
F.1. Conductivity . . . . .	O
F.2. Permeability . . . . .	P
F.3. Volume Flow Rotameter . . . . .	Q



## LIST OF FIGURES

2.1. Cylindrical Rig with Centered Heater . . . . .	5
2.2. Design of Thermal Conductivity Rig . . . . .	6
2.3. Components of Thermal Conductivity Test Setup . . . . .	7
2.4. Ideal Temperature Distribution of Thermal Conductivity Test Setup . . . . .	8
2.5. Temperature Distribution without Insulation of Thermal Conductivity Test Setup . . . . .	9
2.6. Heat Flux for Different Insulations, $k_{specimen} = 0.1 \frac{W}{mK}$ . . . . .	10
2.7. Calculated Thermal Conductivity versus Different Conductivities of Insulation . . . . .	11
2.8. Temperature Profiles with Different Outer Wall Materials . . . . .	12
2.9. Temperature Distribution with $k_{specimen} = 0.5 \frac{W}{mK}$ . . . . .	14
2.10. Uncertainty Plots, Case 1 . . . . .	15
2.11. Uncertainty Plots Combined, Case 1 . . . . .	16
2.12. Uncertainty Plots Combined, Case 2 . . . . .	17
3.1. Design of Permeability Test Setup . . . . .	20
3.2. Porous Media . . . . .	20
3.3. Tube Manometer . . . . .	22
3.4. Rotameter . . . . .	22
3.5. Moody Chart . . . . .	24
3.7. $\epsilon$ plotted from $60^\circ$ to $90^\circ$ . . . . .	25
3.8. $\lambda$ value for Polydisperse Beach Sand . . . . .	26
3.9. Estimated Permeability for Polydisperse Beach Sand . . . . .	27
3.11. Permeability Test Setup: Uncertainty Plots . . . . .	31
3.12. Permeability Test Setup: Combined Uncertainty Plots . . . . .	32
4.1. Thermal Conductivity Rig . . . . .	35
4.2. Calibration of Thermocouples, Ice Water . . . . .	37
4.4. Tap Water Cooling . . . . .	40
4.5. Cooling Principle . . . . .	41
4.6. Liquid Nitrogen Coolant Setup . . . . .	41
5.1. Permeability Rig . . . . .	45
5.2. Pressure in Permeability Rig . . . . .	48
6.1. Sugar: Measurement Conditions and Results, April 29 . . . . .	56
6.3. Sugar: Measurement Conditions and Results, May 4 . . . . .	58
6.4. Sugar: Measurement Conditions and Results, May 6 . . . . .	59
6.5. Sugar: Measurement Conditions and Results, May 27 . . . . .	60
6.6. Sugar: Conductivity versus Temperature . . . . .	61
6.7. Sand: Measurement Conditions and Results, May 11 . . . . .	62
6.8. Sand: Measurement Conditions and Results, May 25 . . . . .	63
6.9. Sand: Measurement Conditions and Results, May 31 . . . . .	64
6.10. Sand: Conductivity versus Temperature . . . . .	65
6.11. Expancel: Measurement Conditions and Results, May 26 . . . . .	66

## List of Figures

---

6.12. Expancel: Measurement Conditions and Results, May 28 - 1 . . . . .	67
6.13. Expancel: Measurement Conditions and Results, May 28 - 2 . . . . .	68
6.14. Expancel: Conductivity versus Temperature . . . . .	69
7.1. Permeability Estimation Sugar . . . . .	74
7.2. Sugar: Measurement Results and Uncertainties . . . . .	75
7.3. Sugar: Results and Estimation Plotted Together . . . . .	76
7.4. Permeability Estimation Sand . . . . .	77
7.5. Sand: Measurement Results and Uncertainties . . . . .	78
7.6. Sand: Results and Estimation Plotted Together . . . . .	79
7.7. Permeability Estimation Expancel . . . . .	80
7.8. Expancel: Measurement Results and Uncertainties . . . . .	81
7.9. Expancel: Results and Estimation Plotted Together . . . . .	82
A.1. P&ID Conductivity Rig . . . . .	C
A.2. P&ID Permeability Rig . . . . .	D
B.1. t-Distribution for Several Degrees of Freedom . . . . .	F
D.1. Parameters for Permeability Estimation . . . . .	K



## LIST OF TABLES

2.1. Dimensions of Thermal Conductivity Rig . . . . .	6
2.2. Uncertainties, Case 1 . . . . .	15
2.3. Uncertainties, Case 2 . . . . .	17
3.1. Dimensions of Permeability Rig . . . . .	20
3.3. Assumed Uncertainties . . . . .	30
4.1. Thermal Conductivity Rig - Equipment . . . . .	36
4.2. Standard Deviation Calculation . . . . .	38
4.3. Standard Deviation Calculation . . . . .	39
5.1. Permeability Rig - Equipment . . . . .	46
5.2. Air Flow Rates, Rotameter . . . . .	47
5.3. Uncertainties for a Volume Flow Reading . . . . .	49
6.1. Sugar: Measurement Conditions and Results, April 29 . . . . .	56
6.2. Sugar: Measurement Conditions and Results, May 4 . . . . .	58
6.3. Sugar: Measurement Conditions and Results, May 6 . . . . .	59
6.4. Sugar: Measurement Conditions and Results, May 27 . . . . .	60
6.5. Sugar: 95% Confidence Interval and Individual Uncertainties . . . . .	61
6.6. Sand: Measurement Conditions and Results, May 11 . . . . .	62
6.7. Sand: Measurement Conditions and Results, May 25 . . . . .	63
6.8. Sand: Measurement Conditions and Results, May 31 . . . . .	64
6.9. Sand: 95% Confidence Interval and Individual Uncertainties . . . . .	65
6.10. Expancel: Measurement Conditions and Results, May 26 . . . . .	66
6.11. Expancel: Measurement Conditions and Results, May 28 - 1 . . . . .	67
6.12. Expancel: Measurement Conditions and Results, May 28 - 2 . . . . .	68
6.13. Expancel: 95% Confidence Interval and Individual Uncertainties . . . . .	69
7.1. Uncertainties Permeability Rig . . . . .	73
7.2. Sugar: Measurement Data . . . . .	75
7.3. Sand: Measurement Data . . . . .	78
7.4. Expancel: Measurement Data . . . . .	81
C.1. Sugar: Measured Material Properties . . . . .	I
C.2. Sand: Measured Material Properties . . . . .	J
C.3. Expancel: Material Properties . . . . .	J



# NOMENCLATURE

## Abbreviations

EU	European Union
NTNU	The Norwegian University of Science and Technology
MOF	Metal-Organic Framework
P&ID	Piping and Instrumentation Diagram

## Symbols

$r$	Radial Length [ $m$ ]	$L$	Length [ $m$ ]
$\dot{Q}$	Heat Transfer Rate [ $W$ ]	$\dot{q}$	Heat Flux [ $\frac{W}{m^2}$ ]
$T$	Temperature [ $K$ ] or [ $^{\circ}C$ ]	$h$	Height [ $m$ ]
$D$	Diameter [ $m$ ]	$g$	Gravitational acceleration [ $\frac{m}{s^2}$ ]
$\rho$	Density [ $\frac{kg}{m^3}$ ]	$\mu$	Dynamic Viscosity [ $\frac{kg}{ms}$ ]
$\nu$	Kinematic Viscosity [ $\frac{m^2}{s}$ ]	$A$	Area [ $m^2$ ]
$k$	Thermal Conductivity [ $\frac{W}{mK}$ ]	$\kappa$	Permeability [ $m^2$ ]
$\Phi$	Porosity [1]	$P$	Pressure [ $Pa$ ]
$I$	Current [ $A$ ]	$U$	Voltage [ $V$ ]
$V$	Volume [ $m^3$ ]	$Q$	Volumetric Flow Rate [ $\frac{m^3}{s}$ ] or [ $l/min$ ]
$Re_D$	Reynolds Number [1]	$Re_1 = Re$	Reynolds Number, pore size length scale [1]
$f$	Darcy's Friction Factor [1]	$C_f = \zeta$	Friction Coefficient [1]
$C_d$	Discharge Coefficient [1]	$w_1$	Superficial Velocity [ $\frac{m}{s}$ ]
$R$	Gas Constant [ $\frac{J}{kgK}$ ]	$\tau_w$	Wall Stress [ $Pa$ ]
$\varepsilon$	Free Area Coefficient [1]	$\varepsilon_w$	Wall Roughness [ $m$ ]
$\theta$	Relative Position [ $^{\circ}$ ]	$d_{gr}$	Mean Body Size [ $m$ ]
$\varphi$	Material Parameter [1]	$d_{el}$	$d_{el} = \varphi \cdot d_{gr}$ [1]
$\dot{m}$	Mass Flow Rate [ $\frac{kg}{s}$ ]	$S$	Standard Deviation
$B_{X_i}$	Bias Error	$(U_R)_{0.95}$	95% Confidence Interval
$t_{\alpha}$	Tabulated Values for t-Distribution	$z_{\alpha}$	Tabulated Values for Normal Distribution
$\vec{e}_i$	Unit Vector	$\delta X_i$	Uncertainty of a Parameter

## Superscripts and Subscripts

$ex$	Exit	$in$	Inlet	$r$	Radial Direction
$max$	Maximum	$-$	Average	$\theta$	Angle Direction
$\beta$	Void Fraction	$\sigma$	Solid Fraction	$z$	Height Direction



## INTRODUCTION

### **1.1** Background

Hydrogen is a possible energy storage medium for the transport sector where high energy density can be obtained. Combustion of hydrogen is environmental friendly as the only product is water. There is nevertheless still some challenges to be faced regarding storage; the low density of hydrogen under atmospheric pressure and ambient temperature necessitates the need to develop an efficient storage method. For instance, a light duty vehicle requires between 4 to 10 kilograms of hydrogen to attain a range around 480km, not much in a mass perspective, but when considering that the density at ambient conditions is around  $0.08 \frac{kg}{m^3}$  [3, Table A-16] the numbers are self explanatory.

Today, compressed gas are the preferred method for onboard storage. To obtain a decent energy density it is necessary to compress the gas in the order of 350 to 700 bar. The high pressure carries along safety concerns in the occurrence of an accident and a great energy demand for compression. Another way of storage is liquid tanks which need insulation and a refrigeration unit to avoid evaporation. Hydrogen in liquid form has lower energy content in volume basis than regular fuel which results in bigger storage tanks [5, page 15-16].

None of the current storage methods meet the standards imposed by the United States Department of Energy [4] and must therefore be improved. At the same time, other technologies are under research and development. An alternative method is to store hydrogen in solid state, this can be done with adsorbents where the hydrogen attaches to a surface of a solid. Sorption type materials are characterized by high porosity and surface area.

NTNU participates in a development project of so-called Metal-Organic Framework (MOF) together with Max Planck Institut für Metallforschung and Technische Universität Dresden, both located in Germany. The MOF is a sorption type material intended for hydrogen storage. Research have shown that the thermal effects during filling and discharging have a great influence on the utilization of the storage system. The thermal properties of the MOF need to be characterized for further investigation.

**1.2 Project Description**

Two measurement rigs shall be designed and built to measure thermal conductivity and permeability, respectively. There are many things to consider between a principle design and completion such as dimensioning, material selection, magnitude of the parameters, and measurement inaccuracy. The intention of building the two rigs is to investigate the properties of adsorption hydrogen storage materials; nevertheless, the rigs will be fully capable for measurements on other materials.

This master thesis is a continuation of the project work [1] where several principles for the thermal conductivity rig were investigated. Based on these results, the work will be taken further to develop a rig that fulfills the decided requirements. Adsorption processes produce heat and are more efficient at lower temperatures; therefore, it is necessary to measure the conductivity at these temperatures. It is also required that the rig is capable of measuring the properties for small specimen quantities. Regarding the permeability rig, the work starts from scratch with ambitions of developing a rig capable of measurements for a broad range of materials.

An experimental program will be carried out for both rigs. The results will be compared and discussed, and suggestions for further work will be presented. This report consists of four main parts:

- I. **Design and Prestudy of Test Rigs:** The preparatory work where measurement principles, simulations and estimations, and uncertainties are discussed.
- II. **Test Rigs:** A description of the built rigs where the instrumentation, assembly and usage, and determination of uncertainties are discussed.
- III. **Experimental Results:** The measurement results and suggestions for further work are presented and discussed.
- IV. **Closure:** A summarization and conclusion of the work.

In addition, other relevant information such as the basis for the uncertainty calculations, P&ID's for the rigs, and measurement material properties are attached in the appendix.

---

---

PART I

---

Design and Prestudy of Test Rigs





## THERMAL CONDUCTIVITY RIG

### **2.1** Introduction

The thermal conductivity of porous materials shall be measured in the laboratory. There is no rig in the laboratory that is capable to measure the conductivity for small specimens in the relevant temperature range between  $\div 150^{\circ}\text{C}$  and  $100^{\circ}\text{C}$ .

Based on the project work [1], it was decided to make a cylindrical rig with a centered heater. Radial heat transfer was preferable since heat loss can be disregarded. It is favorable that the rig is as small as possible; less mass will reduce the time for the rig to reach steady state. In addition, some of the specimens to be measured are only available in small amounts. The importance of accurate positioning increases for small dimensions; therefore, it is necessary to evaluate the uncertainties in the measurement. The specimens are assumed to have low conductivities between 0.1 and  $1.0 \frac{\text{W}}{\text{mK}}$ . To make the rig capable of measurements at different temperatures, the side walls will be held at a constant temperature using suitable fluids.

To investigate the heat transfer, several simulations will be carried out in COMSOL. Radial heat transfer requires that the top and bottom are suitably insulated. The temperature should then be constant along the height at a constant radius,  $T(h, r_{\text{constant}}) = T_{\text{constant}}$ .

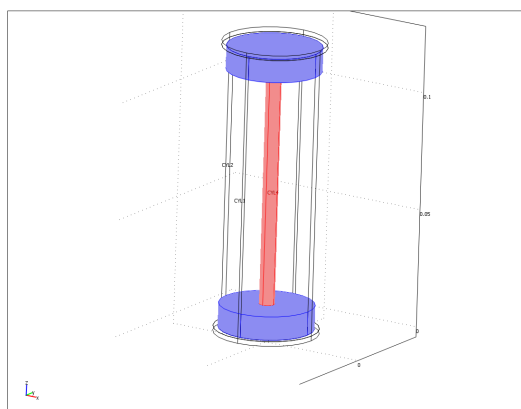


**Figure 2.1.:** Cylindrical Rig with Centered Heater

**2.2 Rig Design and Dimensions**

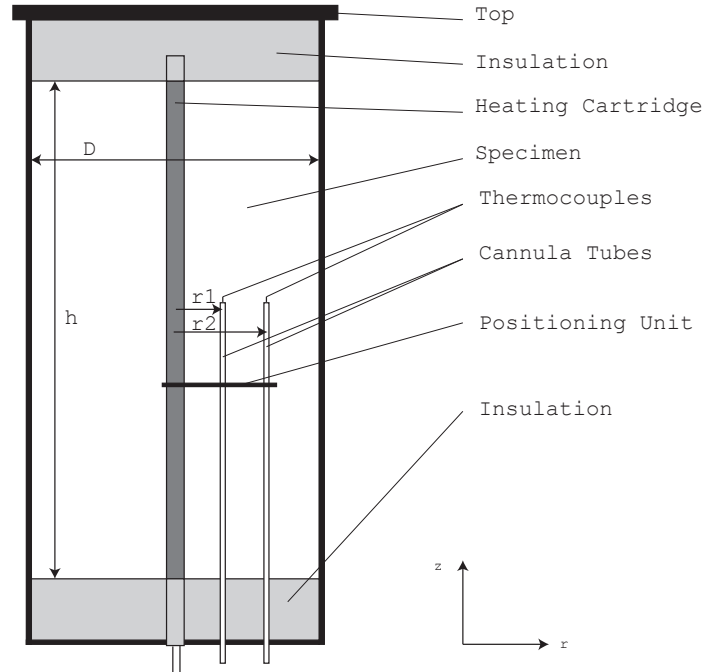


**Figure 2.2.:** Design

The rig should be capable of measurements in the temperature range between  $\pm 150^{\circ}\text{C}$  and  $100^{\circ}\text{C}$  under atmospheric pressure.

D	40mm
h	100mm
r1	8mm
r2	15mm

**Table 2.1.:** Dimensions

Table 2.1 shows the dimensions corresponding to figure 2.2. The wall thickness of the cylinder is 2mm, and the insulation in top and bottom will have a thickness of 10mm. The cannula tubes and positioning unit are intended to be adjustable in the z-direction; they will be adjusted to put the thermocouples correct positioned at  $\frac{h}{2}$ .

The top of the rig is loose, it can be taken away to pour in or remove the specimen. Under measurements, it will be clamped to the rest of the rig. The top consists of a metal surface and insulation.

A heating cartridge with outer diameter 6.5mm and 100mm length will be placed in center of the measurement rig. It is intended to attach some insulation with the same diameter as the element on top and bottom as shown in figure 2.2. The purpose of the insulation is to ensure that the element is centered without letting it be in direct radial contact with something else than the specimen.

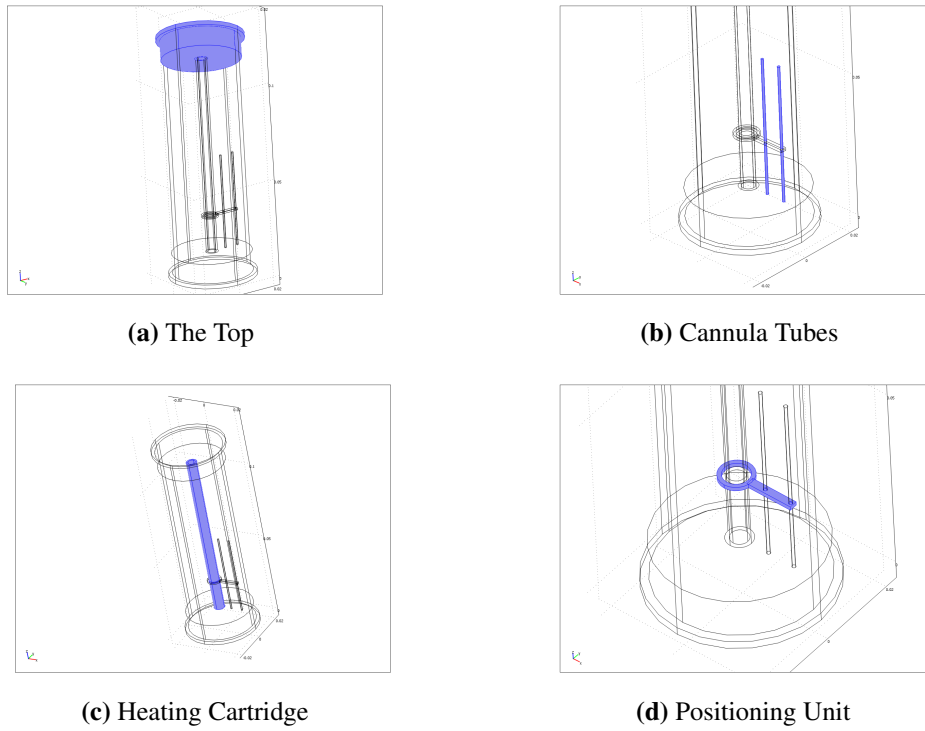


Figure 2.3.: Components

### 2.3 Fourier's Law of Heat Conduction

The conductivity will be calculated using Fourier's law of heat conduction [3, Section 2-1]:

$$\dot{Q}_n = -kA \frac{dT}{dn} \quad (2.1)$$

In three dimensions with cylindrical coordinates, the vector form of  $\dot{Q}_n$  is:

$$\vec{\dot{Q}}_n = \dot{Q}_r \vec{e}_r + \dot{Q}_\theta \vec{e}_\theta + \dot{Q}_z \vec{e}_z \quad (2.2)$$

It is intended to only have radial heat flux in the test rig; hence,  $\dot{Q}_\theta = 0$  and  $\dot{Q}_z = 0$ . The conductivity is solved in radial direction below:

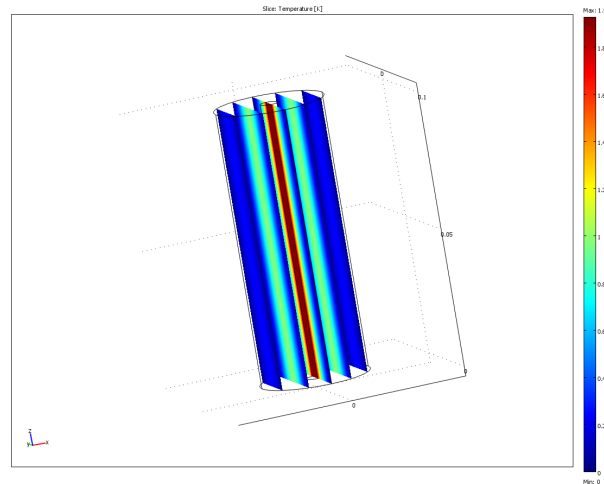
$$k = -\frac{\dot{Q}_r}{2\pi h} \cdot \frac{\ln\left(\frac{r_2}{r_1}\right)}{\Delta T} \quad (2.3)$$

Where  $h$  is the height in z-direction.

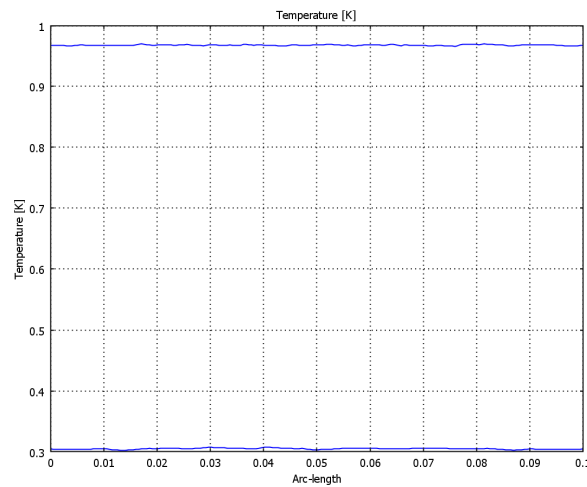
### 2.4 Temperature Distribution and Heat Flow

#### 2.4.1. Basis

As mentioned in the introduction, proper insulation in the top and bottom of the rig is important to achieve radial heat flux. The temperature distributions in a cylinder are shown with and without insulation below.



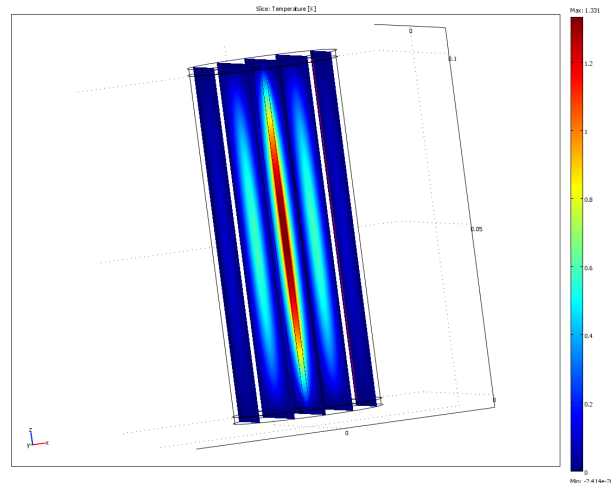
(a) Temperature Distribution Ideal Design



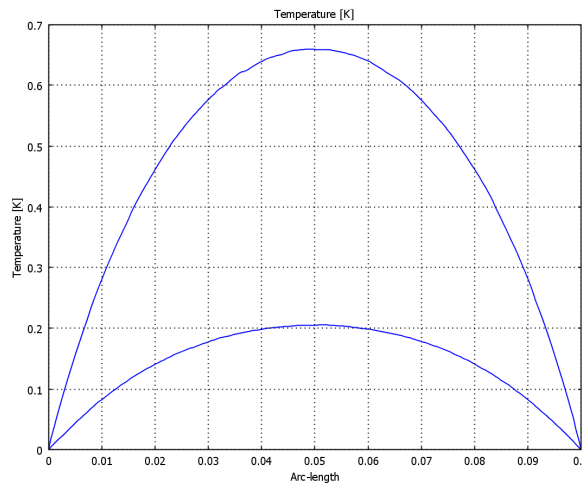
(b) Temperature Plot along  $h$  at  $r_1$  and  $r_2$

**Figure 2.4.:** Ideal Temperature Distribution

This is the ideal case where the heat flux is radial since the top and bottom are perfectly insulated. The temperature at a constant radius is then constant along the height. The next simulation shows the temperature distribution without insulation.



(a) Temperature Distribution without Insulation



(b) Temperature Plot along  $h$  at  $r_1$  and  $r_2$

**Figure 2.5.:** Temperature Distribution without Insulation

### 2.4.2. Simulation Assumptions and Boundary Conditions

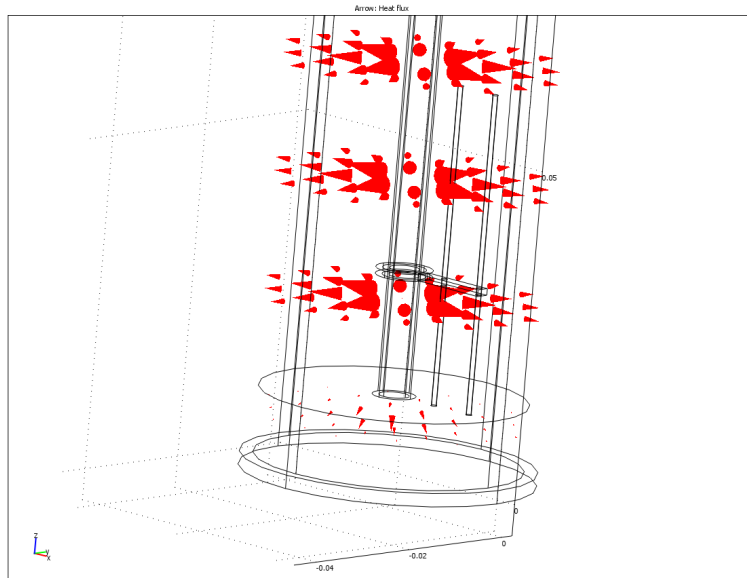
COMSOL Multiphysics 3.4 has been used to simulate the heat flux and temperature distribution. The model has been designed to resemble the rig; however, some modifications and assumptions have been done due to meshing problems and recreation insecurities.

All simulations have been performed with a constant temperature on the outer walls. It is a conservative assumption since the top and bottom will be insulated properly in reality. The heating element has been simulated as a 1mm thick steel cylinder with a constant heat flux on the inner surface. Due to rendering and meshing problems, COMSOL was not able to perform simulations when the cannula tubes were put through the insulation and bottom of the steel cylinder. As shown in figure 2.3, the cannula tubes starts on top of the insulation in the bottom. This means that the influence of steel contact between the outer walls and cannula tubes not will be investigated.

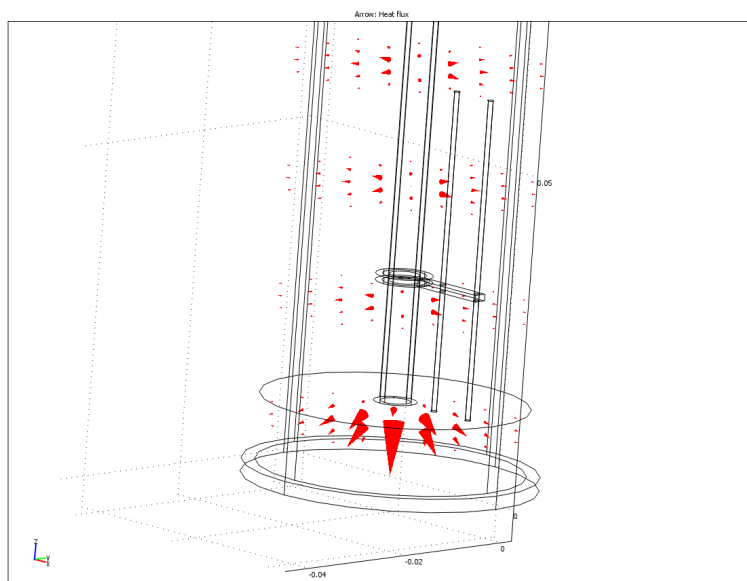
## 2.4. TEMPERATURE DISTRIBUTION AND HEAT FLOW

### 2.4.3. Insulation

It is important that the insulation has lower conductivity than the specimen; otherwise, heat will be transferred axially, and not radial.



(a)  $k_{insulation} = 0.026 \frac{W}{mK}$

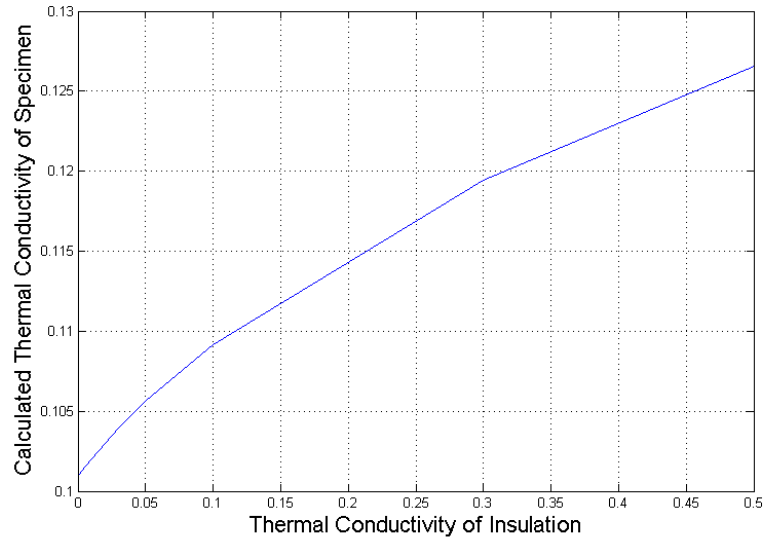


(b)  $k_{insulation} = 0.500 \frac{W}{mK}$

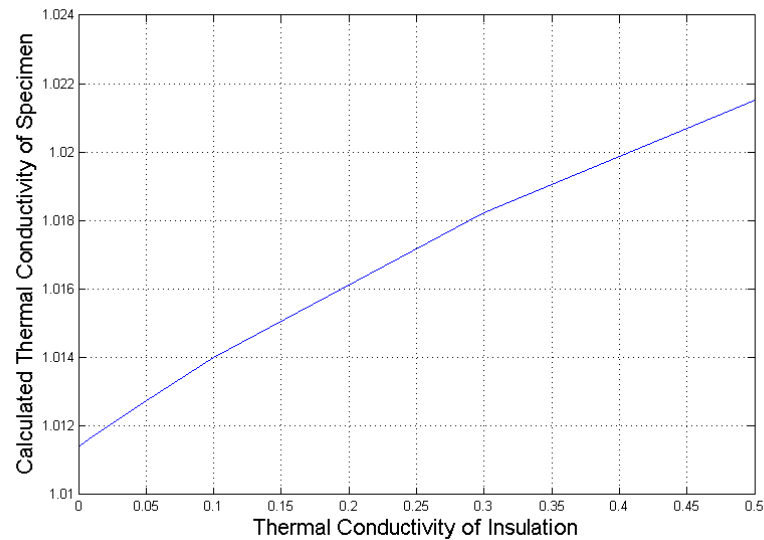
**Figure 2.6.:** Heat Flux for Different Insulations,  $k_{specimen} = 0.1 \frac{W}{mK}$

In order to find the required conductivity for the insulation, simulations have been carried out for specimens with thermal conductivity of  $0.1 \frac{W}{mK}$  and  $1.0 \frac{W}{mK}$  which are expected to be minimum and maximum. For each simulation, the conductivity of the insulation have been decreased and  $T(r_1, \frac{h}{2})$  and  $T(r_2, \frac{h}{2})$  have been used to calculate the conductivity of the specimen using equation 2.3. When the calculated conductivity

of the specimen equals to the one used in simulations, it means that the heat flux is radial. The calculated conductivity of the specimens are plotted against the conductivity of the insulation in figure 2.7. The requirement of proper insulation increases when the specimen has low conductivity. The lower conductivity of the specimen, the more heat will be transferred in axial direction.



(a)  $k_{specimen} = 0.1 \frac{W}{mK}$



(b)  $k_{specimen} = 1.0 \frac{W}{mK}$

**Figure 2.7.:** Calculated Thermal Conductivity versus Different Conductivities of Insulation

Styrofoam HD300 with thermal conductivity  $k = 0.026 \frac{W}{mK}$  [17] seem to be a proper insulation. The heat flux with Styrofoam as insulation is shown in figure 2.6a. The expected measurement error due to insulation can be found in figure 2.7. In the worst case where the specimen has a conductivity of  $k = 0.1 \frac{W}{mK}$ , the error will be around 3%.

## 2.5. EQUIPMENT AND INSTRUMENTATION

### 2.4.4. Outer Walls

Several metals have been considered for the outer walls. Most metals have thermal conductivities that are much higher than the specimen. This means that the temperature profile will be approximately constant through the wall when the temperature on the outer wall is constant. Two temperature plots from center to the outer cylinder wall are shown in figure 2.8 for steel and copper, respectively. Steel was chosen since it was available in the laboratory.

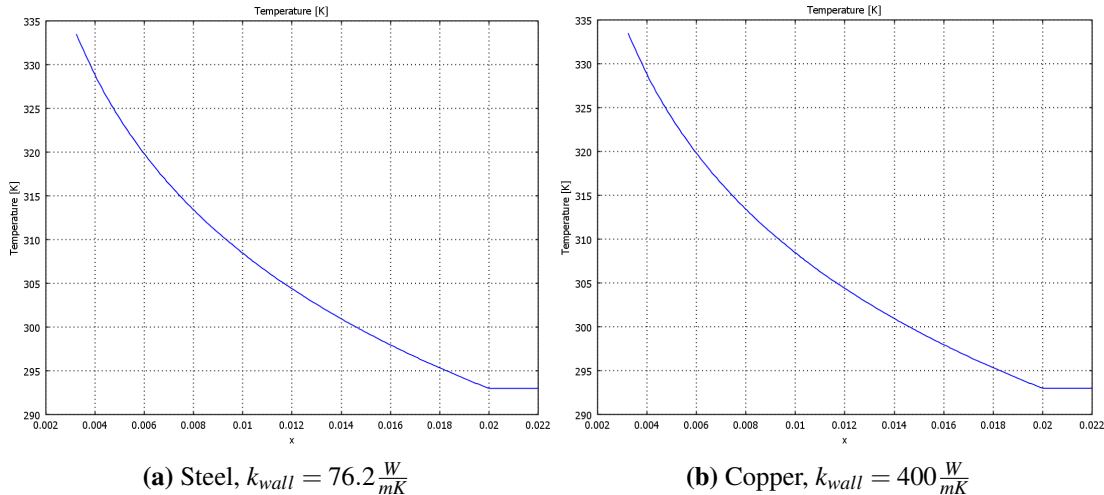


**Figure 2.8.:** Temperature Profiles with Different Outer Wall Materials

## 2.5 Equipment and Instrumentation

### 2.5.1. Thermocouples

The differences between thermocouples and resistance thermometers have been discussed in the project work [1, Section 5.2], and thermocouples were preferred due to its shorter response time, commercial availability in small dimensions, and price. The drawback is higher inaccuracy; however, the deviation from the absolute temperature is not important as long as the two thermocouples are able to give the correct differential temperature. That means that they must be calibrated against each other. Type K thermocouples with 0.25mm diameter will be used in the rig.

### 2.5.2. Power Supply and Heating Cartridge

The power supply and heating cartridge must be adjustable for a range within 0-10W. Simulations have shown that 10W will be more than enough power to obtain a decent temperature profile when  $k_{specimen} = 1.0 \frac{W}{mK}$ . Less power is needed when the specimen has lower conductivity. The power supply should have a display over the output power so it easily can be monitored.



2.5.3. Side Wall Cooling

The side walls must obviously be kept at a lower temperature than the heater to generate radial heat flux. One possibility is to put the side walls of the rig in direct fluid contact, and then regulate the temperature of the fluid. For temperatures around room temperature, this could be done using a standard water bath regulator. What is more difficult is to find suitable fluids for temperatures below 0°C. Other properties such as danger of explosion and fast evaporation rate have to be considered given that the water bath probably has to release some of the gas to the surroundings.

Another possibility is to create a closed system around the rig, it can be done by enclosing the side walls with a tube that leads the fluid around the rig. This solution has been chosen due to the convenience of being able to use tap water as coolant. Use of tap water demands a steady supply of water with constant temperature. For temperatures below 0°C other fluids can be circulated through the tube. If the coolant are explosive as it evaporates, the gas can be connected to a bleed line.

**2.6** Uncertainty Analysis

To identify the resulting influence of uncertainties in the different parameters, a single-sample analysis has been carried out. The result clarifies the needed accuracy of each variable in the conductivity expression. The basis for single-sample analysis is taken from Moffat [7] and further documented in appendix B.2. The thermal conductivity  $k$  depends on the following variables:

$$k = k(\dot{Q}_r, r_1, r_2, h, \Delta T) \quad (2.4)$$

The expected uncertainty can then be written as:

$$\delta k = \left\{ \left( \frac{\partial k}{\partial \dot{Q}_r} \delta \dot{Q}_r \right)^2 + \left( \frac{\partial k}{\partial r_1} \delta r_1 \right)^2 + \left( \frac{\partial k}{\partial r_2} \delta r_2 \right)^2 + \left( \frac{\partial k}{\partial h} \delta h \right)^2 + \left( \frac{\partial k}{\partial \Delta T} \delta \Delta T \right)^2 \right\}^{\frac{1}{2}} \quad (2.5)$$

The partial derivatives has been solved with MAPLE, the solution of  $\delta k$  is also attached in appendix F.1:

$$\frac{\partial k}{\partial \dot{Q}_r} = -\frac{1}{2\pi h} \frac{\ln\left(\frac{r_2}{r_1}\right)}{\Delta T} \quad (2.6)$$

$$\frac{\partial k}{\partial r_1} = \frac{\dot{Q}_r}{2\pi h r_1} \frac{1}{\Delta T} \quad (2.7)$$

$$\frac{\partial k}{\partial r_2} = -\frac{\dot{Q}_r}{2\pi h r_2} \frac{1}{\Delta T} \quad (2.8)$$

$$\frac{\partial k}{\partial h} = \frac{\dot{Q}_r}{2\pi h^2} \frac{\ln\left(\frac{r_2}{r_1}\right)}{\Delta T} \quad (2.9)$$

$$\frac{\partial k}{\partial \Delta T} = \frac{\dot{Q}_r}{2\pi h} \frac{\ln\left(\frac{r_2}{r_1}\right)}{(\Delta T)^2} \quad (2.10)$$

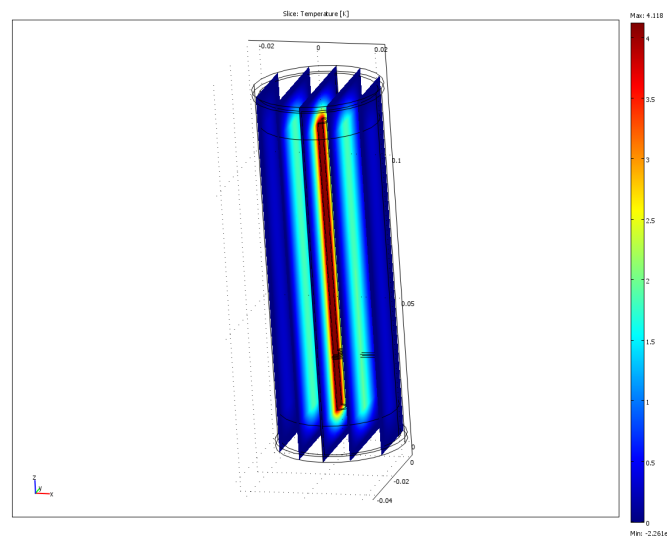
## 2.6. UNCERTAINTY ANALYSIS

### 2.6.1. Two Examples of Uncertainty Calculations

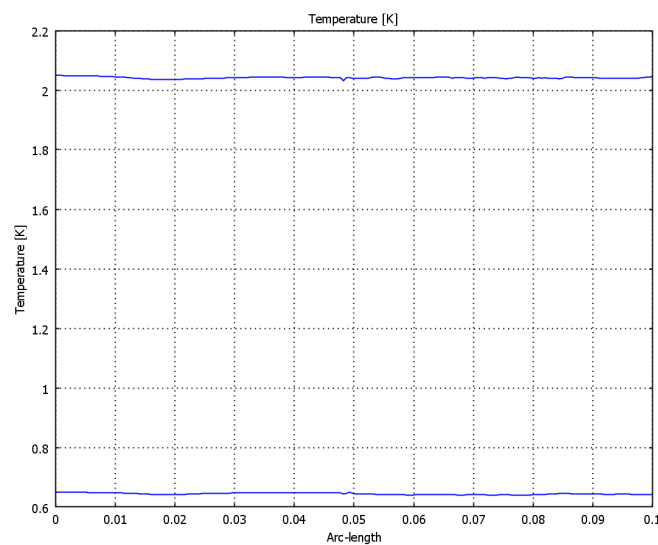
In order to perform an uncertainty calculation using single-sample analysis, it is necessary to have numerical values and defined tolerances for all of the variables. The following calculations are based on simulations in COMSOL and defined tolerances of each parameter.

#### Case 1

Figure 2.9 illustrates the temperature distribution in the rig. The conductivity of the specimen was set to  $k_{specimen} = 0.5 \frac{W}{mK}$  and the heat flux on the inner wall of the heater to  $\dot{q}_r = 500 \frac{W}{m^2}$  which is equal to  $\dot{Q}_r = 0.7069W$ . The temperatures plotted in figure 2.9b are  $T(r_1, \frac{h}{2}) = 2.041237K$  and  $T(r_2, \frac{h}{2}) = 0.642065K$ .



(a) Temperature Distribution  $k_{specimen} = 0.5 \frac{W}{mK}$



(b) Temperature Plot along  $h$  at  $r_1$  and  $r_2$

**Figure 2.9.:** Temperature Distribution with  $k_{specimen} = 0.5 \frac{W}{mK}$

The thermal conductivity of the specimen can be calculated using equation 2.3 which gives the result  $k_{specimen} = 0.5054 \frac{W}{mK}$ . The assumed uncertainties are given in table 2.2:

$\dot{Q}_r$	$0.7069 \pm 0.1W$
$r_1$	$8 \pm 0.5mm$
$r_2$	$15 \pm 0.5mm$
$h$	$100 \pm 5mm$
$\Delta T _{k_{specimen}=0.5 \frac{W}{mK}}$	$1.399172 \pm 0.3K$

Table 2.2.: Uncertainties, Case 1

The uncertainties of each variable are first plotted separately which means that the uncertainty increases linearly. The uncertainties are also plotted combined to illustrate each variables influence when the other uncertainties are set to maximum. The combined uncertainty plots makes it easier to identify which variables that affect the result the most.

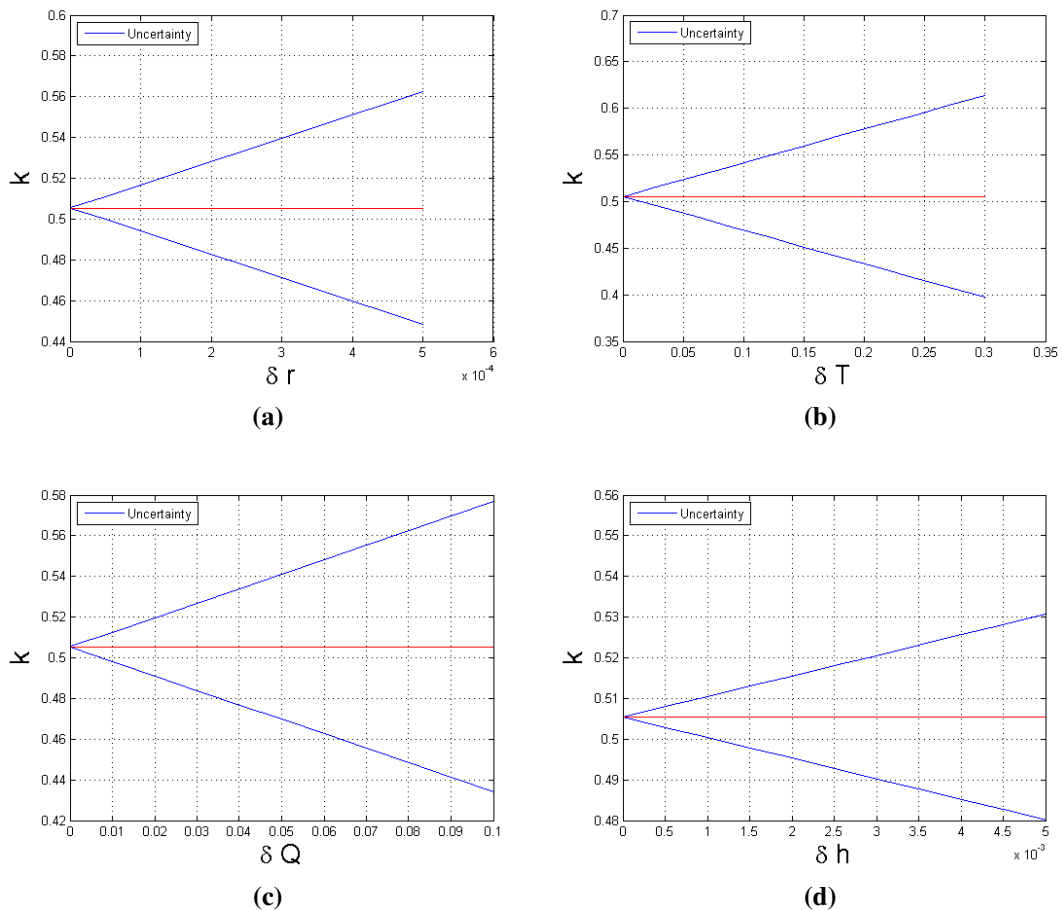
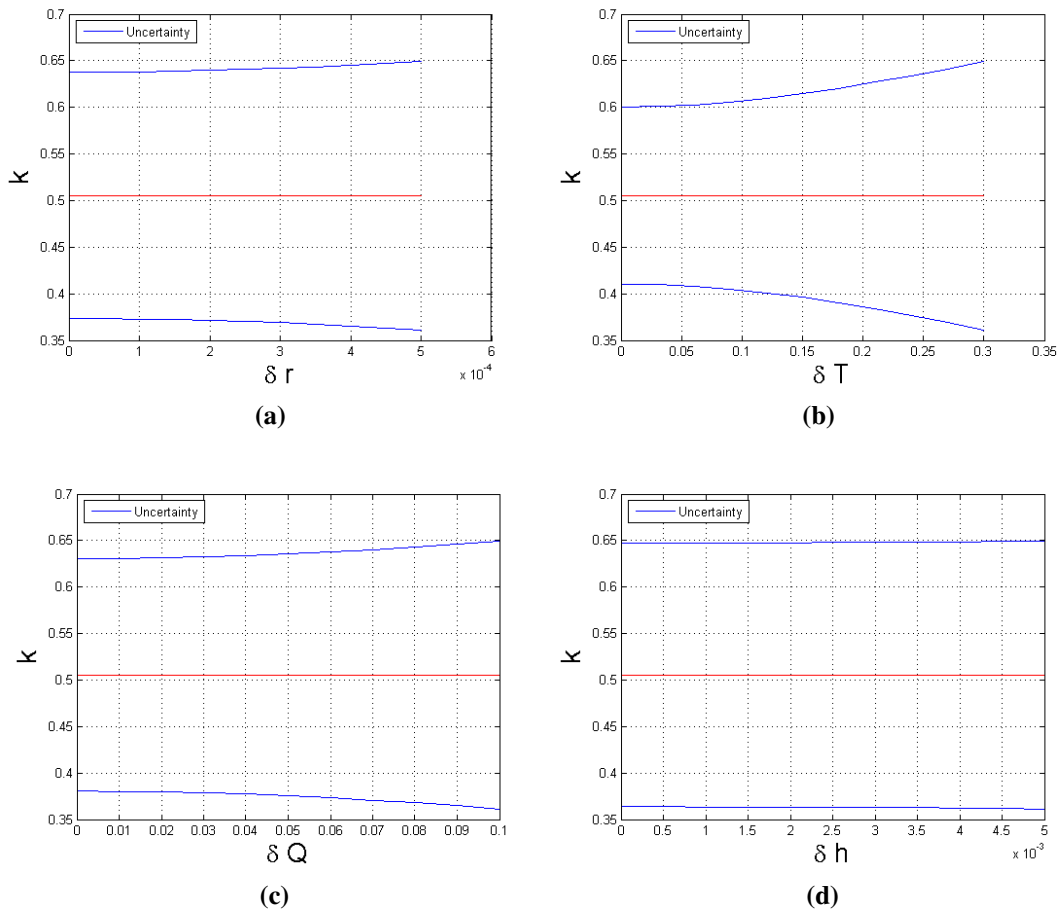


Figure 2.10.: Uncertainty Plots, Case 1

## 2.6. UNCERTAINTY ANALYSIS



**Figure 2.11.:** Uncertainty Plots Combined, Case 1

With all the assumed uncertainties combined, the calculated conductivity can be estimated to be  $k = 0.5054 \pm 0.1140 \frac{W}{mK}$  which equals to an uncertainty of 28.5%. In order to reduce the uncertainty of the specified rig, the heat flux can be increased. The uncertainty of the heat flux will then be relatively smaller, and it will increase the temperature difference between  $T(r_1, \frac{h}{2})$  and  $T(r_2, \frac{h}{2})$ . The new values with an increased heat flux ( $\dot{q}_r = 3000 \frac{W}{m^2}$ ) are shown in table 2.3, and the combined uncertainties are plotted in figure 2.12.

Case 2

$\dot{Q}_r$	$4.2412 \pm 0.1W$
$r_1$	$8 \pm 0.5mm$
$r_2$	$15 \pm 0.5mm$
$h$	$100 \pm 5mm$
$\Delta T _{k_{specimen}=0.5 \frac{W}{mK}}$	$8.395035 \pm 0.3K$

**Table 2.3.:** Uncertainties, Case 2

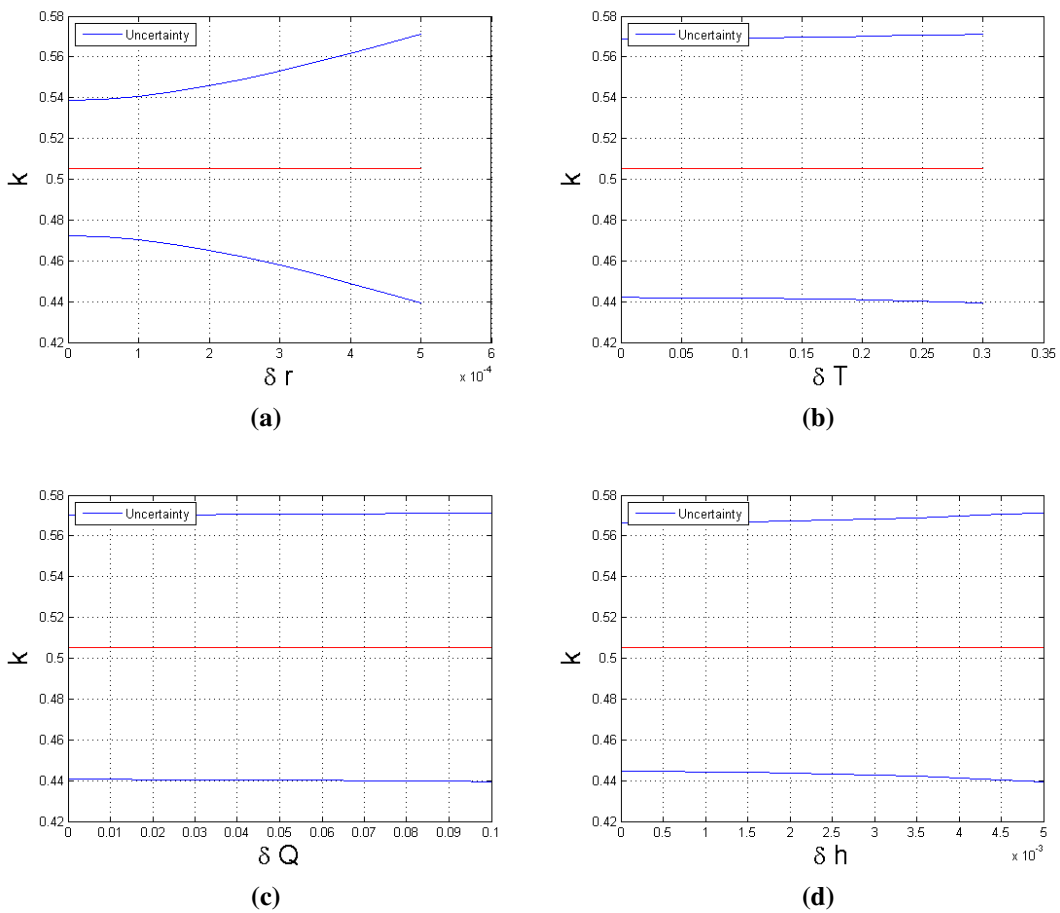


**Figure 2.12.:** Uncertainty Plots Combined, Case 2

Increased heat flux reduces the uncertainty to  $k = 0.5054 \pm 0.0660 \frac{W}{mK}$  which is equal to an uncertainty of 13.05 %. It is clear that accurate positions of the thermocouples are most important in order to achieve a proper result, see figure 2.12a.

The uncertainties presented are based on simulations where each variable have been assumed to have a certain tolerance. First when the rig is built and all the tolerances are properly defined, it will be possible to determine the real uncertainty. The uncertainty will vary between measurements depending on the heat flux as shown above. In the experimental part, every measurement result will be presented with its uncertainty.

### 2.7 Thermal Conductivity Estimation

When the conductivities for the gas and solid phase of a porous material are known, the effective conductivity can be estimated based on the porosity  $\Phi$ . An empirical relation given by A. Bhattacharya, V.V. Calmidi, and R.L. Mahajan can be used [2, Equation (13)]:

$$k_e = A(\Phi k_\beta + (1 - \Phi)k_\sigma) + \frac{1 - A}{\left(\frac{\Phi}{k_\beta} + \frac{1 - \Phi}{k_\sigma}\right)} \quad (2.11)$$

Where  $k_e$  is the effective conductivity and  $A = 0.35$ . This one of several conductivity estimation models, they have all in common that the conductivity of each phase and the porosity must be known.

### 2.8 Discussion

Based on the cylindrical design, a preparatory analysis has been carried out to assess the temperature and heat flow distribution in the rig. Simulations have been performed to investigate the relation between the measured conductivity of the specimen and the insulation. The simulations show that the importance of proper insulation increases when conductivity of the specimen is low. This is because the heat will be transported the easiest way out of the rig, and the easiest way out must always be through the specimen. The insulation material Styrofoam HD300 was selected, and the worst case measurement error was determined to be 3% for specimens with thermal conductivity of  $0.1 \frac{W}{mK}$ .

In addition, a single-sample uncertainty analysis has been performed to show which parameters that affects the conductivity measurement the most. The results show that uncertainties in the positions  $r_1$  and  $r_2$  are most affecting for the conductivity calculations. The uncertainty will vary between measurements, but it should be possible to achieve results with uncertainties below 10% by adjusting the heat. The actual uncertainty of each variable will be determined when the rig is built.

## PERMEABILITY RIG

### **3.1** Introduction

The permeability is a measure of the ability for a porous material to transmit fluids. For a porous storage material, the permeability is an important property. A storage material with high permeability requires a lower gauge pressure for the gas to infiltrate the tank. The permeability can be obtained using Darcy's law (section 3.3) when the pressure loss, fluid velocity and properties are known.

The permeability property is assumed to be independent of which kind of fluid that has been used in the measurement. This means that if the permeability has been measured with air as fluid, the value is valid for other fluids as well. The assumption signifies that the size of the molecules in the fluid are irrelevant. As long as the material has a certain porosity, the assumption should be valid.

The pressure loss through the material is assumed to be much bigger than the wall friction in the pipe:

$$\Delta P_{wall\,friction} \ll \Delta P_{permeability} \quad (3.1)$$

### **3.2** Rig Design

The design is shown in figure 3.1. The rig consists of a transparent cylindrical container which is rotated vertically to obtain an even distribution of the specimen. In order to hold the specimen at the same place, filters will be placed on each side. The diameter is chosen to be the same as for the conductivity test rig. Compressed air from the laboratory will be used as working fluid. To ensure that the air is clean, it is necessary to filtrate the air to remove oil, water, and other particles.

### 3.3. DARCY'S LAW

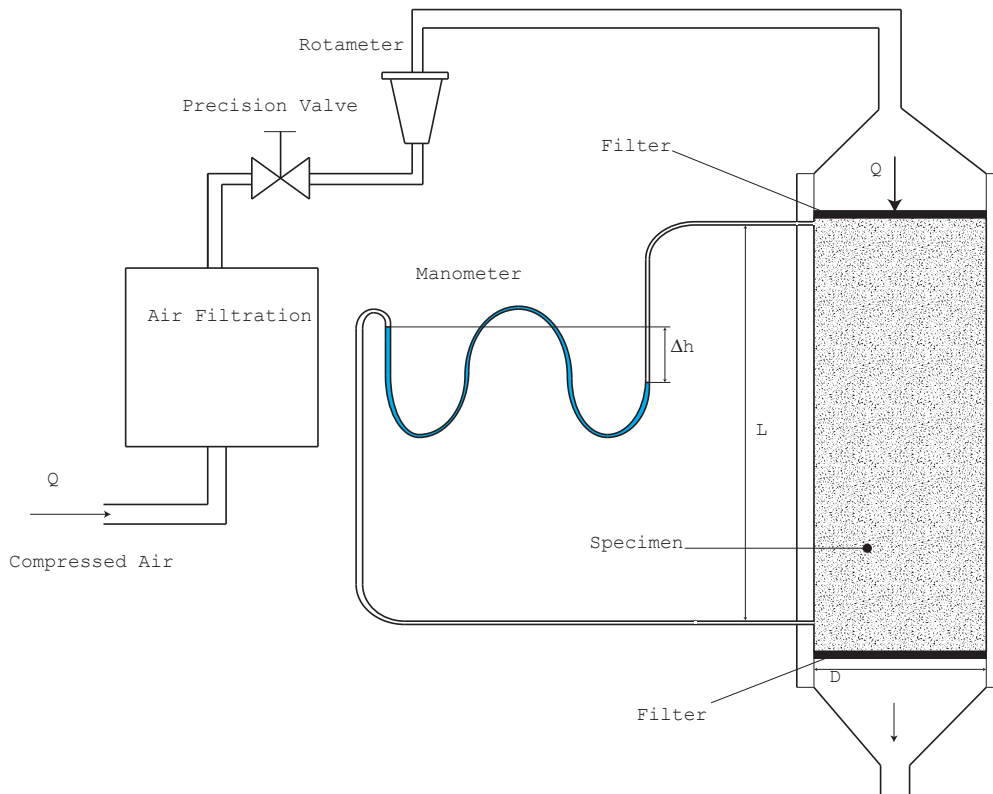


**Figure 3.1.:** Test Setup Design

D	40mm
L	100mm

**Table 3.1.:** Dimensions

### 3.3 Darcy's Law

Consider a porous media consisting of two phases as illustrated in figure 3.2. The porosity is simply the volume fraction of the void space in the control volume.

$$\Phi = \frac{V_{\beta}}{V_{\sigma} + V_{\beta}} \quad (3.2)$$

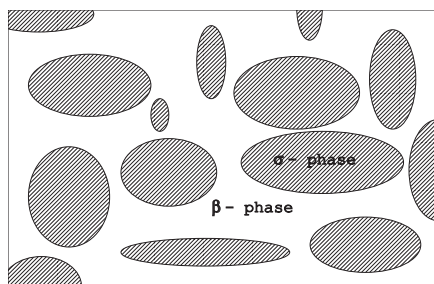


**Figure 3.2.:** Porous Media



Darcy's law has been deviated by Stephen Whitaker in 1986, with the final result as shown below [9, Equation 3.38]:

$$\langle \mathbf{u}_\beta \rangle = -\frac{\kappa}{\mu_\beta} \left[ \nabla \langle P_\beta \rangle^\beta - \rho_\beta \mathbf{g} \right] \quad (3.3)$$

Where  $\mathbf{u}_\beta$  is the velocity and  $\mu_\beta$  the viscosity of a fluid flowing through the porous media. The notation  $\langle \rangle$  is used for phase average, and  $\langle \rangle^\beta$  for intrinsic phase average:

$$\langle \mathbf{u}_\beta \rangle = \frac{1}{V_\beta + V_\sigma} \int_{V_\beta} \mathbf{u}_\beta dV, \quad \langle \mathbf{u}_\beta \rangle^\beta = \frac{1}{V_\beta} \int_{V_\beta} \mathbf{u}_\beta dV, \quad (3.4)$$

The permeability is obtained by measuring the pressure drop and the superficial velocity over the sample.

$$\kappa = -\frac{\langle \mathbf{u}_\beta \rangle \mu_\beta}{\nabla \langle p_\beta \rangle^\beta - \rho_\beta \mathbf{g}} \quad (3.5)$$

It may also be written in terms of volumetric flow:

$$\kappa = \frac{4Q}{\pi D^2} \cdot \frac{\mu}{\frac{\Delta P}{L} - \rho g} \quad (3.6)$$

Darcy's Law is only applicable for slow viscous flow, called creeping flow or Stokes flow. The validity will be shown in section 3.5 where an estimation model for the permeability is introduced.

### **3.4** Equipment and Instrumentation

#### *3.4.1. Filtration*

It is usual that compressed air systems contains traces of oil from the compressor, water, and other particles; therefore, it is necessary to filtrate the air. In addition, filters will be placed on both sides of the specimen to keep it fixed.

#### *3.4.2. Precision Valve*

The compressed air system in the laboratory has an operating pressure between 7 and 8 bar. In order to have accurate control over the pressure and volume flow, it is necessary to use a precision valve with a gauge.

#### *3.4.3. Inclined Tube Manometer*

A tube manometer can be used to measure the differential pressure between two points as illustrated in figure 3.3.

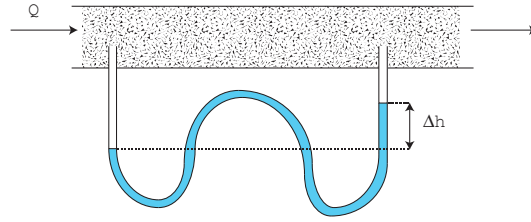


**Figure 3.3.:** Tube Manometer

The difference in height is related to the hydrostatic pressure equation [10, Equation (2.15)]:

$$\nabla P = \rho \mathbf{g} \quad (3.7)$$

$$\Delta P = \rho g \Delta h \quad (3.8)$$

The pressure can be measured more accurate when the manometer is inclined. The pressure loss can also be measured using a dp-cell which tends to be more accurate than a manometer.

#### 3.4.4. Rotameter

The volumetric flow rate will be measured with a rotameter. A rotameter is a relatively simple device, it consists of a float located in a tube with an increasing cross-sectional area or drag coefficient. The position of the float in the z-direction is where the gravitation and drag force are in balance. When the fluid pressure and temperature are known, it is possible to calculate the flow rate.

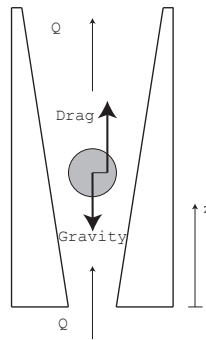


**Figure 3.4.:** Rotameter

There are two forces that must be in balance: the weight of the float  $W = mg$  and the drag force  $D$ . The drag force can be expressed as [10, Equation (7.62)]:

$$D = C_D \frac{1}{2} \rho_{fluid} V^2 A_{float} \quad (3.9)$$

Where  $C_D$  is the drag coefficient and  $A_{float}$  is the frontal area seen from the stream (a circle). The volumetric flow rate can be obtained by setting  $W = D$ , [10, Equation (6.101)]:

$$Q = C_d A_a \left( \frac{2W}{\rho_{fluid} A_{float}} \right)^{\frac{1}{2}} \quad (3.10)$$

Where  $C_d$  is a discharge coefficient for the flow and  $A_a = A_{tube} - A_{float}$ . It is usual that the product  $C_d \cdot A_a$  varies linearly in the z-direction to make the reading equally accurate over the whole scale. In addition, it is possible to change floats in order to increase the flexibility of flow rates. For correct measurements, it is important that the rotameter is oriented vertically.

The density,  $\rho_{fluid}$ , can be calculated with the ideal gas law, [10, Equation (1.10)]:

$$P = \rho RT \quad (3.11)$$

Where  $R$  is the gas constant.

$$\rho = \frac{P}{RT} \quad (3.12)$$

It is clear that the position of the float depends on the density of the flowing fluid; therefore, it is necessary to measure the pressure and temperature. A thermocouple will be used for the temperature, and the precision valve will be equipped with a pressure gauge.

### 3.5 Estimation of Permeability

In order to estimate the permeability, it can be convenient to consider some friction measurement methods for pipes and relate them to flow in porous media. The formulas used in this section are taken from White [10] and Idelchik [6].

The Reynolds number [10, Equation (1.24)] can be used to determine whether a flow is laminar or turbulent which is important for the pressure loss.

$$Re_D = \frac{\rho V D}{\mu} \quad (3.13)$$

Darcy's friction factor [10, Equation (6.11)] is often used as a measure for the friction. The friction coefficient  $C_f$  is another commonly used variable:

$$f = \frac{8\tau_w}{\rho V^2} = 4C_f = 4\zeta \quad (3.14)$$

Where  $\tau_w$  is the wall stress and  $V$  the velocity.

The friction varies linearly with the Reynolds number for laminar flow. For turbulent flow, it is more complicated. The roughness of the wall,  $\epsilon_w$ , does also have to be considered. The friction factor for turbulent flows can be found using the Colebrook formula [10, Equation (6.48)] which is the accepted design formula for turbulent friction. The formula was later plotted by Moody, and is now called the Moody chart, see figure 3.5.

### 3.5. ESTIMATION OF PERMEABILITY

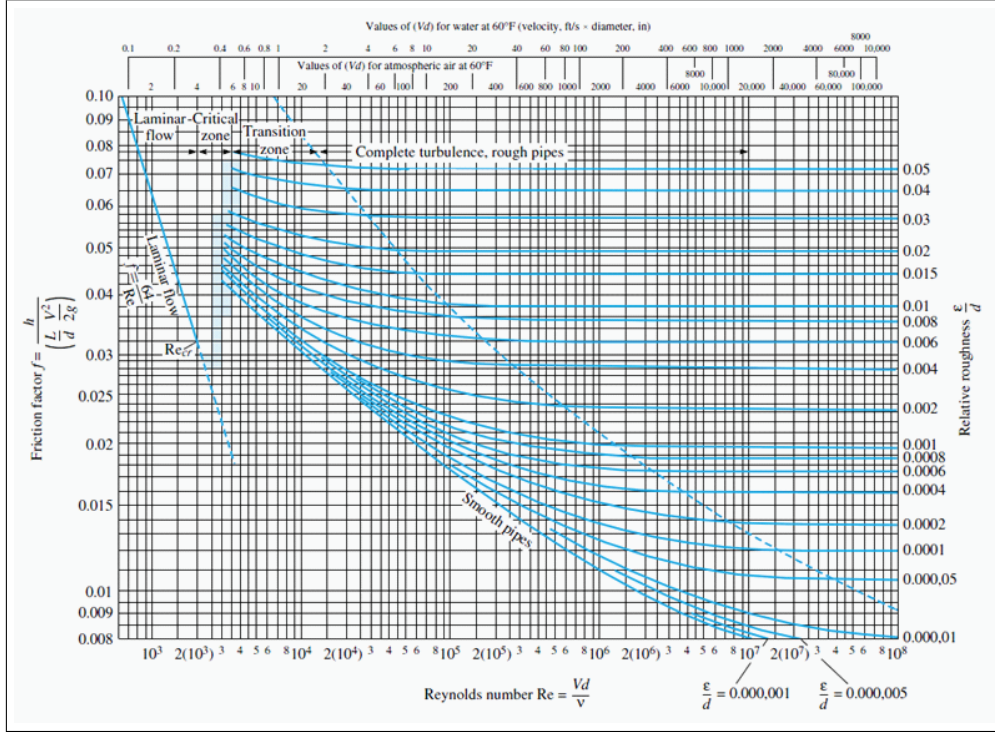


Figure 3.5.: Moody Chart, [10, Fig.6.13 in White]

$$\frac{1}{f^{\frac{1}{2}}} = -2.0 \log \left( \frac{\epsilon_w/D}{3.7} + \frac{2.51}{Re_D f^{\frac{1}{2}}} \right) \quad (3.15)$$

Note how the friction factor varies along with the Reynolds number in the Moody chart. The principals are the same for flow in a porous material; however, the formulas for the friction factor are more complex. The following empirical equations are taken from Handbook of Hydraulic Resistance, written by I.E. Idelchik [6, Chapter 8]. They are applicable for a bed of spherical or lumpy irregular-shape bodies as illustrated in figure 3.6.

$$\zeta = \frac{2\Delta P}{\rho w_1^2} = \lambda \frac{L}{d_{el}} + \Delta\zeta_t = \frac{1}{4}f \quad (3.16)$$

$$\Delta\zeta_t = 2 \frac{T_{ex} - T_{in}}{T_m}, \quad T_m = \frac{T_{in} + T_{ex}}{2} \quad (3.17)$$

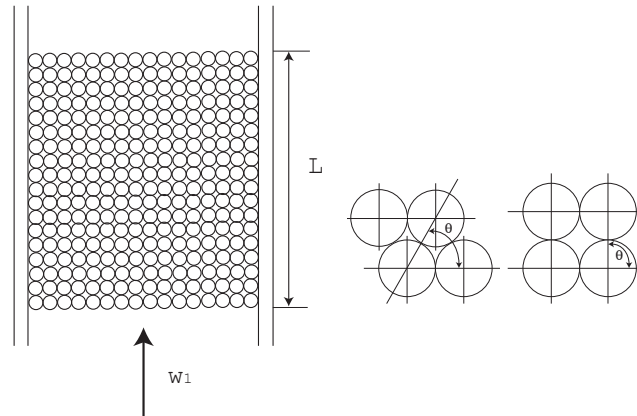
$$\lambda = \frac{360(1-\epsilon)^2}{\epsilon^3 Re_1} + \frac{B'(1-\epsilon)}{\epsilon^3} = \frac{A_1}{Re_1} + B_1 \quad (3.18)$$

$$\epsilon = 1 - \frac{\pi}{6(1-\cos\theta)\sqrt{1+2\cos\theta}} \quad (3.19)$$

$$Re_1 = \frac{w_1 d_{el}}{v} \quad (3.20)$$

Where  $d_{el} = \phi_1 d_{gr}$ .  $d_{gr}$  is the mean size diameter of the body.  $d_{gr}$ ,  $\phi_1$  and  $\epsilon$  are tabulated for several materials (attached in appendix D).  $B' = 1.8$  for bodies with smooth surface, and  $B' = 4.0$  for bodies with rough surface.  $w_1$  is the superficial

velocity of the fluid, and  $\nu = \frac{\mu}{\rho}$  the kinematic viscosity. The angle  $\theta$  describes the relative position between the bodies as illustrated in figure 3.6b, it is used to calculate  $\epsilon$  which is the free area coefficient. The term  $\Delta\zeta_t$  treats the effects of density changes in the working fluid. When  $\Delta\zeta_t > 0$ , it means that the fluid has been heated and therefore expanded, this will lead to an acceleration of the fluid and increase the friction.  $Re_1$  is the Reynolds number based on a pore size length scale.



(a) Packed Material in Tube (b) Relative Position,  $60^\circ$  to  $90^\circ$

**Figure 3.6.:** Packing of Spherical Bodies

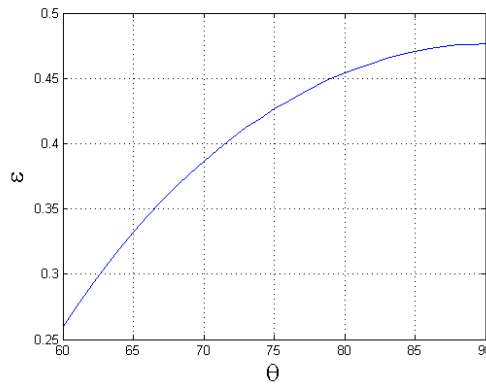


**Figure 3.7.:**  $\epsilon$  plotted from  $60^\circ$  to  $90^\circ$

To illustrate the similarity to the Moody chart,  $\lambda$  (equation 3.18) has been plotted for different Reynolds numbers (figure 3.8). This is the most general way to present how the friction varies for a specified material. The friction coefficient or factor can easily be calculated when the length of the bed  $L$ , the mean body size  $d_{gr}$ , and the relative position  $\theta$  are known. In addition, one may consider the term  $\Delta\zeta_t$  that treats the effect of density changes of the working fluid.

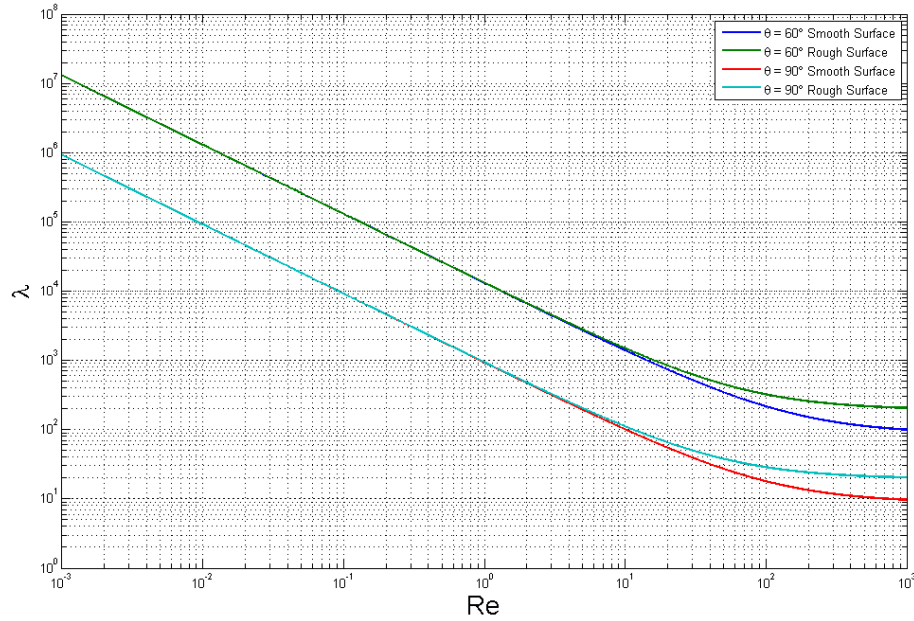


**Figure 3.8.:**  $\lambda$  value for Polydisperse Beach Sand

The linear part of the plot can be considered as the laminar part of the flow regime. That means that when  $Re_1 < 1$ , it is the first term in equation (3.18),  $\frac{A_1}{Re_1}$ , that is of magnitude. In comparison, the friction factor for a laminar flow in the Moody chart is  $f = \frac{64}{Re_D}$ . Another similarity is that the roughness is neglectable for laminar flow.  $\lambda$  is plotted for two relative positions,  $60^\circ$  and  $90^\circ$ , which are the minimum and maximum angle used by Idelchik.

Darcy's law from section 3.3 can be rewritten in terms of the pressure gradient:

$$\frac{\Delta P}{L} = \frac{4Q}{\pi D^2} \cdot \frac{\mu}{\kappa} \quad (3.21)$$

The gravitational influence is neglected since it not is considered by Idelchik. Next, equation (3.16) is rewritten in terms of the pressure gradient and with constant temperature:

$$\frac{\Delta P}{L} = \frac{\rho w_1^2}{2} \cdot \frac{\lambda}{d_{el}} \quad (3.22)$$

The two equations gives a new expression for the permeability:

$$\kappa = \frac{2\mu}{\rho} \frac{d_{el}}{\lambda w_1} \quad (3.23)$$

As long as the flow is in the laminar regime, the velocity  $w_1$  will practically be cancelled out by  $\lambda$ . That means that the permeability will have an approximate constant value independent of the velocity in this flow regime. This supports the validity of Darcy's Law which only is applicable for creeping flow. The permeability for the polydisperse beach sand are plotted in figure 3.9, observe that the permeability is approximately constant for  $Re_1 < 1$ .

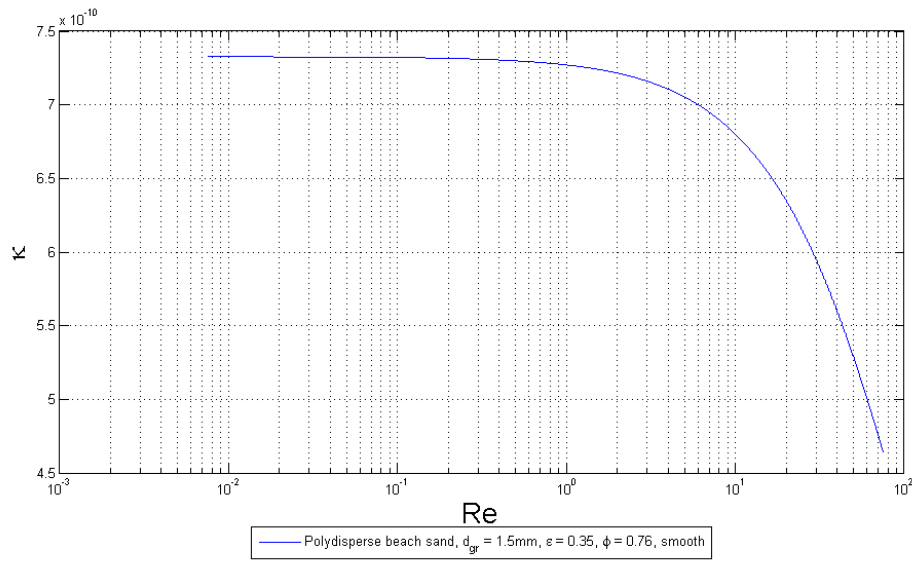


**Figure 3.9.:** Estimated Permeability for Polydisperse Beach Sand

When the average diameter and packing properties of the material are known, the permeability can be estimated. In addition, the Reynolds number can be used to find the maximum flow rate:

$$Q_{max} = \frac{Re_{max} \cdot v}{d_{el}} \cdot A \quad (3.24)$$

Where  $A$  is the area of the cross section and  $Re_{max}$  the maximum Reynolds number in the laminar flow regime.

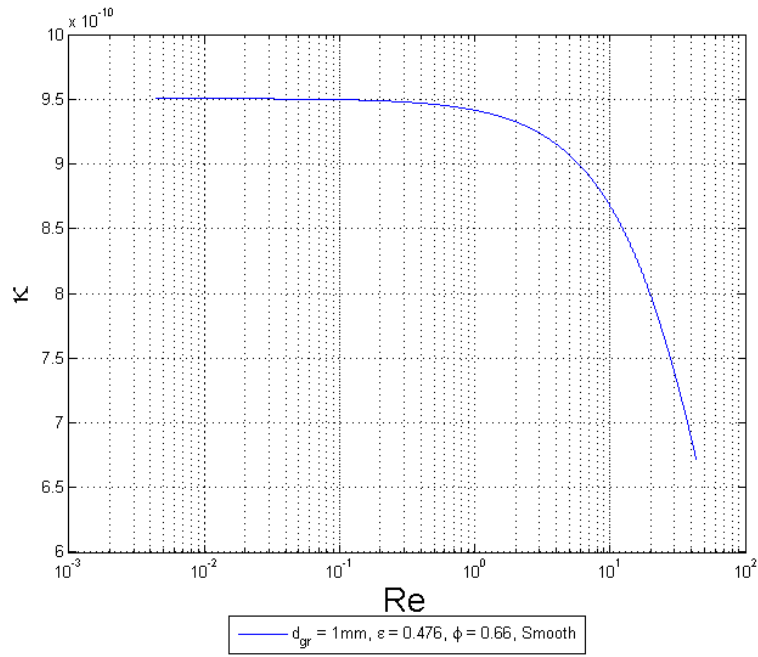
### 3.6 Estimation of Pressure Loss

It is convenient to have a certain since of the magnitude of the pressure loss under selection of measurement instruments. The maximum and minimum pressure loss can be estimated when the materials are assumed to have a diameter between  $10\mu m$  and  $1000\mu m$ .

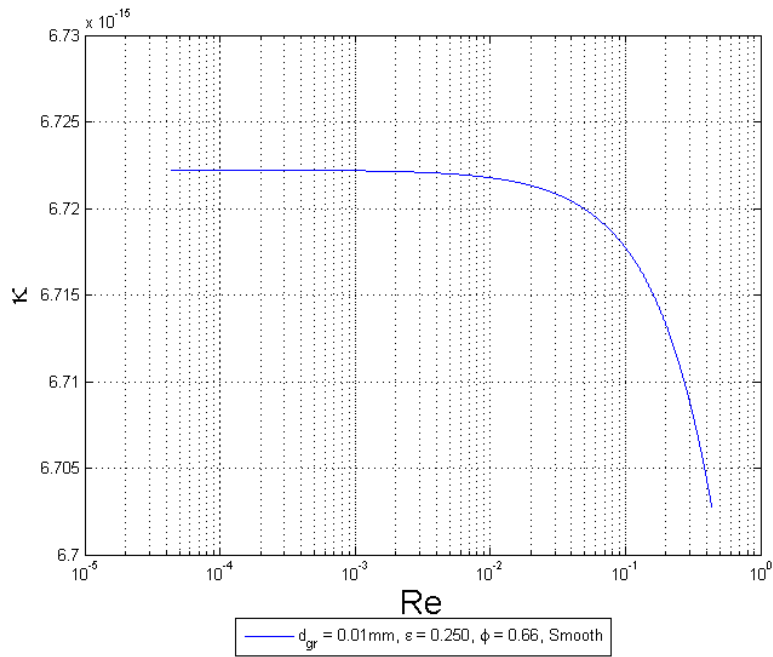
$$\Delta P = w_1 \cdot \frac{\mu L}{\kappa} = \frac{Re_{max} \cdot v}{d_{el}} \cdot \frac{\mu L}{\kappa} = \frac{Re_{max} \cdot \mu^2 L}{\rho d_{el} \kappa} \quad (3.25)$$

The velocity  $w_1$  has been substituted with the maximum allowed flow criteria from section 3.5. The estimated permeability for two materials are plotted in figure 3.10. In order to find the minimum and maximum pressure loss, the relative position has been set to  $90^\circ$  and  $60^\circ$ , respectively, in the two cases. The coefficient of the body shape has been set to  $\varphi = 0.66$ , based on an average of the tabulated values in appendix D.

### 3.6. ESTIMATION OF PRESSURE LOSS



(a)  $d_{gr} = 1000\mu\text{m}$



(b)  $d_{gr} = 10\mu\text{m}$

**Figure 3.10.:** Estimated Permeability

The permeability were estimated to be  $\kappa_{(a)} = 9.5 \cdot 10^{-10}m^2$  and  $\kappa_{(b)} = 6.722 \cdot 10^{-15}m^2$  for  $Re_{max} = 10^{-1}$  and  $Re_{max} = 10^{-3}$ , respectively. The pressure losses are calculated in table 3.2.



	$\mu$		$1.825 \cdot 10^{-5} Pa \cdot s$
	$\rho$		$1.204 \frac{kg}{m^3}$
	$d_{gr} = 1000 \mu m$		$d_{gr} = 10 \mu m$
$\kappa$	$9.5 \cdot 10^{-10} m^2$	$\kappa$	$6.722 \cdot 10^{-15} m^2$
$Re_{max}$	$10^{-1}$	$Re_{max}$	$10^{-3}$
$d_{el} = \varphi \cdot d_{gr}$	$0.66 \cdot 10^{-3} m$	$d_{el} = \varphi \cdot d_{gr}$	$0.66 \cdot 10^{-5} m$
$\Delta P$	<b>4.41 Pa</b>	$\Delta P$	<b>623529 Pa</b>
$w_1$	$0.0024 \frac{m}{s}$	$w_1$	$0.0024 \frac{m}{s}$
$Q$	$0.1734 \frac{l}{min}$	$Q$	$0.1734 \frac{l}{min}$

Table 3.2.: Pressure Loss Estimation

The two pressure loss estimations above are hopefully extreme results on each side of the scale, but it is clear that a great variance can be expected for different diameters and packing. In case (a) with the largest diameter, it might be necessary to use a longer pipe to increase the pressure loss. In case (b) it would be necessary to decrease the velocity  $w_1$  which affects the Reynolds number.

For correct permeability measurements, it is necessary to have some knowledge about the material properties such as average diameter and packing angle in order to adjust the volumetric flow rate correct. It might be necessary to use several manometers or dp-cells with different range to measure the pressure loss.

### 3.7 Uncertainty Analysis

The following variables are considered to fluctuate during measurements:

$$\kappa = \kappa(Q, \Delta P, \mu, L, \rho) \quad (3.26)$$

The expected uncertainty can be found by using single-sample analysis, the basis is taken from Moffat [7] and is documented in appendix B.2:

$$\delta \kappa = \left\{ \left( \frac{\partial \kappa}{\partial Q} \delta Q \right)^2 + \left( \frac{\partial \kappa}{\partial \Delta P} \delta \Delta P \right)^2 + \left( \frac{\partial \kappa}{\partial \mu} \delta \mu \right)^2 + \left( \frac{\partial \kappa}{\partial L} \delta L \right)^2 + \left( \frac{\partial \kappa}{\partial \rho} \delta \rho \right)^2 \right\}^{\frac{1}{2}} \quad (3.27)$$

The partial derivatives are solved below:

$$\frac{\partial \kappa}{\partial Q} = \frac{4}{\pi D^2} \cdot \frac{\mu}{\frac{\Delta P}{L} - \rho g} \quad (3.28)$$

$$\frac{\partial \kappa}{\partial \Delta P} = -\frac{4Q}{\pi D^2} \cdot \frac{\mu}{\left(\frac{\Delta P}{L} - \rho g\right)^2 \cdot L} \quad (3.29)$$

$$\frac{\partial \kappa}{\partial \mu} = \frac{4Q}{\pi D^2} \cdot \frac{1}{\frac{\Delta P}{L} - \rho g} \quad (3.30)$$

$$\frac{\partial \kappa}{\partial L} = \frac{4Q}{\pi D^2} \cdot \frac{\mu \cdot \Delta P}{\left(\frac{\Delta P}{L} - \rho g\right)^2 L^2} \quad (3.31)$$

$$\frac{\partial \kappa}{\partial \rho} = \frac{4Q}{\pi D^2} \cdot \frac{\mu g}{\left(\frac{\Delta P}{L} - \rho g\right)^2} \quad (3.32)$$

Several of the variables above will not be measured directly. The state of the air in terms of pressure and temperature determines the density  $\rho$  (equation 3.12). The density is important for the rotameter which measures the flow rate, and it is also used to calculate the hydrostatic pressure contribution since the pipe is vertical.

A rough estimate shows that the hydrostatic pressure contribution will have minimal influence on the result. If the pressure of the air is 1 atm, and the temperature is 20°C, the density is  $\rho = 1.204 \frac{kg}{m^3}$  [3, Table A-15]. Depending on the measured pressure loss  $\Delta P$ , the hydrostatic contribution is most likely to be significantly lower.

$$\rho g \ll \frac{\Delta P}{L} \quad (3.33)$$

The hydrostatic contribution is obviously greater when heavier fluids than air is used.

The viscosity is only dependent of the temperature,  $\mu = \mu(T)$ ; therefore, a thermocouple will be used for the measurement. Table values from Çengel shows that the viscosity for air vary between  $\mu(T = 10^\circ C) = 1.778 \cdot 10^{-5} \frac{kg}{m \cdot s}$  and  $\mu(T = 50^\circ) = 1.963 \cdot 10^{-5} \frac{kg}{m \cdot s}$  [3, Table A-15].

The length  $L$  of the pipe has been set to 100mm. An uncertainty of  $\pm 5mm$  is realistic when considering that the two holes for the differential pressure measurement must have a certain diameter.

### 3.7.1. Example of an Uncertainty Calculation

The volumetric flow rate  $Q$  and expected differential pressure  $\Delta P$  are dependent of the sample material. In order to demonstrate an uncertainty calculation, the polydisperse beach sand has been used. The permeability can be retrieved from figure 3.9 to be  $\kappa = 7.3 \cdot 10^{-10} m^2$  for Reynolds numbers  $Re_1 < 1$ .  $Re_{max}$  has been used to estimate the pressure loss and the resulting volumetric flow.

$Q$	$1.0028 \pm 0.1 \frac{l}{min} = (1.6713 \pm 0.1667) \cdot 10^{-5} \frac{m^3}{s}$
$\Delta P$	$33.2 \pm 5 Pa$
$\mu$	$(1.825 \pm 0.1) \cdot 10^{-5} Pa \cdot s$
$L$	$100 \pm 5 mm$

**Table 3.3.:** Assumed Uncertainties

The uncertainties of each variable are first plotted separately which means that the uncertainty increases linearly. The uncertainties are also plotted combined to illustrate each variables influence when the other uncertainties are set to maximum. The combined uncertainty plots makes it easier to identify which variables that affect the result the most.

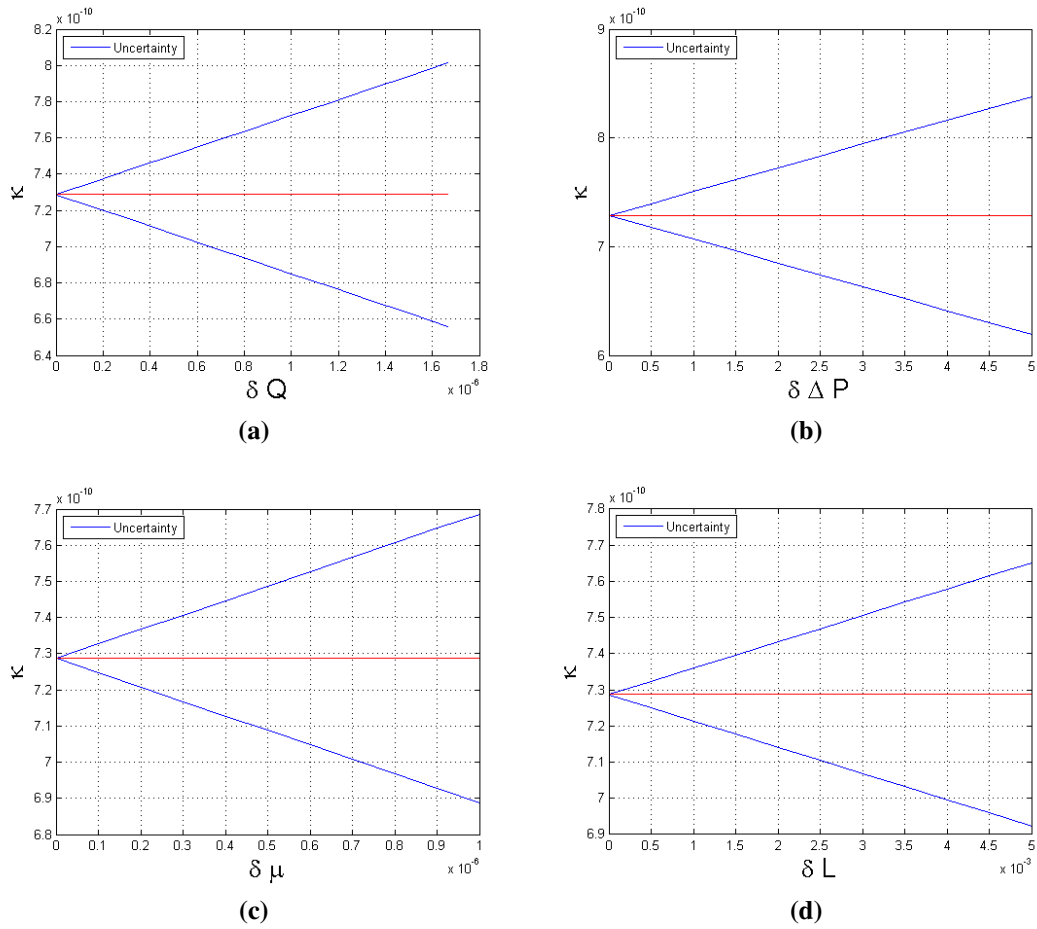
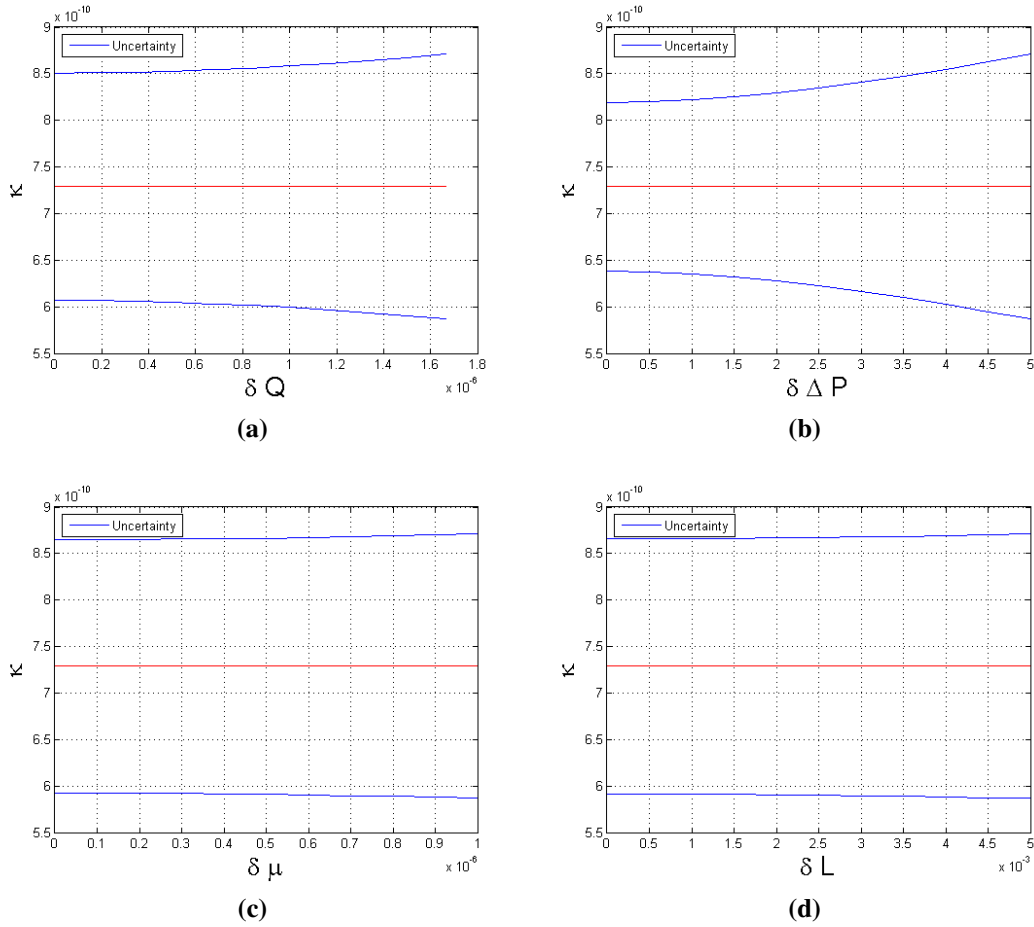


Figure 3.11.: Uncertainty Plots

$\delta p$  has not been considered since the empirical model not considers it. In addition, the hydrostatic contribution has been shown to be significantly less than the pressure loss from the flow through the specimen. The uncertainty of the density is more important for the rotameter, see section 3.4.4, and will be calculated separately in section 5.3.4.



**Figure 3.12.:** Combined Uncertainty Plots

In this case, the uncertainty was  $\kappa = (7.29 \pm 1.42) \cdot 10^{-10} m^2$  which almost is 20%. Figure 3.12b shows that the pressure loss uncertainty is the most affecting parameter. For measurements with higher pressure losses, the uncertainty will decrease.

### 3.8 Discussion

Based on the principles of Darcy’s law, a test rig for permeability measurements has been developed. Required equipment and instrumentation to measure the different parameters have been accounted for. With Darcy’s law as the only reference, there was too many unknowns in order to make any proper estimates of the magnitude of the parameters. Therefore, a set of empirical formulas were used to estimate the permeability for different body diameters, and the corresponding flow rate and pressure loss. The estimations indicate that the permeability will be measured as a constant value in the laminar flow regime which states the validity of Darcy’s law for creeping flow.

An example of a single-sample uncertainty analysis has been given; however, the uncertainties  $\delta Q$  and  $\delta \Delta P$  are not properly defined and need to be determined.

The pressure loss due to wall friction has not been considered, but it is reasonable to assume that its magnitude is much lower than the pressure loss through the material.

---

---

PART II

---

Test Rigs



## THERMAL CONDUCTIVITY RIG, COMPLETION

### **4.1** Introduction

This chapter deals with the practical details regarding the conductivity rig. The preparatory work is documented in chapter 2, and the P&ID for the rig is attached in appendix A.1.

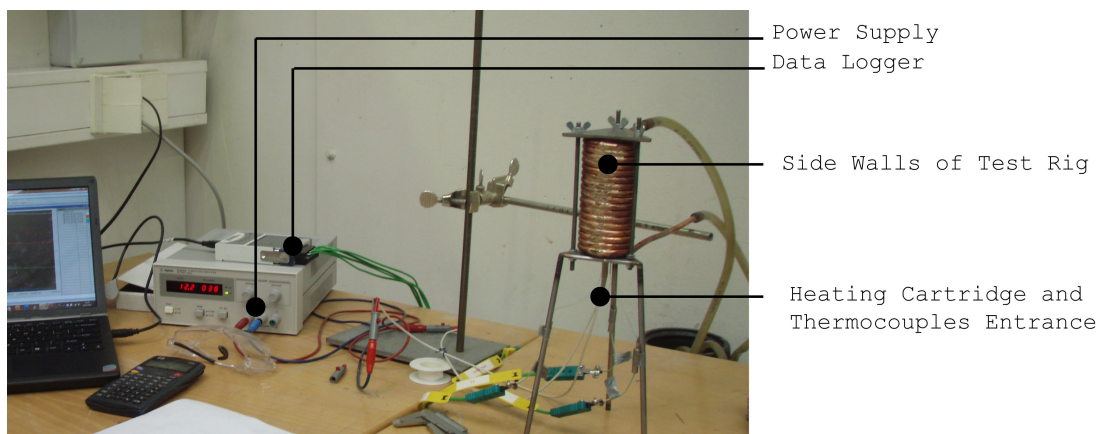


**Figure 4.1.:** Thermal Conductivity Rig

There are some differences between the prestudy design and the actual rig. The top and bottom in the actual rig have been made triangular in order to hold the rig together as shown in figure 4.1. The heater will be centered with a positioning unit to keep it centered during the filling. A thin layer of Teflon has been placed between the cylinder and the top and bottom to avoid direct steel contact. The positioning unit for the cannula tubes is also made of Teflon. The side wall of the rig is enclosed by a copper tube.

In addition to the two planned thermocouples, a third will be placed at the heater. This makes it possible to calculate the conductivity three times in a measurement which can be helpful for verification of the results.

The uncertainty  $\delta X_i$  of each variable will be determined.

**4.2 Equipment and Instrumentation**

The equipment listed below are the main components of the rig. In addition, some other equipment for the side wall cooling have been used which are described in section 4.5.

Component	Supplier	Price	Specifications
Heating Cartridge	Norske Backer avd. Moss	500 NOK	Ø6.5mm L100mm 160W 230V
4 Thermocouples	Max Sievert A/S	800 NOK	Type K Ø0.25mm L150mm, [18]
Power Supply	Elfa Elektronikk AS	3000 NOK	Angilent E3612A, 0-60V 0-0.5A, [16]
Data Logger	NTNU (borrowed)	-	NI USB-9162 and NI9211, 4 channels, [14] and [15]

**Table 4.1.:** Equipment

More information for some of the equipment can be found on the data sheets referred to in the specifications.

**4.3 Evaluation of Data**

*4.3.1. Data Logging*

The temperature measurements are logged digitally with LABVIEW, and the results will be exported to Excel and MATLAB for treatment. The heat flux are read from the display of the power supply, and the positions are measured manually.

*4.3.2. Smoothing of Temperature Measurements*

In order to reduce the temperature fluctuations, all the temperatures used have been smoothed:

$$\bar{T} = \frac{1}{2n + 1} \sum_{i=-n}^n T_i \quad (4.1)$$

In this report, all temperature measurements have been smoothed using  $n = 10$  which means that each measurement has been averaged with the 10 previous and next measurements.

*4.3.3. Multiple Measurements*

To ensure correct results, it is necessary to do multiple measurements and compare the results. The t-Distribution (documented in appendix B.3) can be used to calculate a confidence interval for the similar measurements. Use of the t-Distribution assumes that each sample is independent and the selection is normally distributed.



## 4.4 Calibration and Determination of Uncertainties

### 4.4.1. Thermocouples

The thermocouples need to be calibrated against each other and absolute temperature. There are four thermocouples bought in for the rig, they have been put in ice water for calibration.

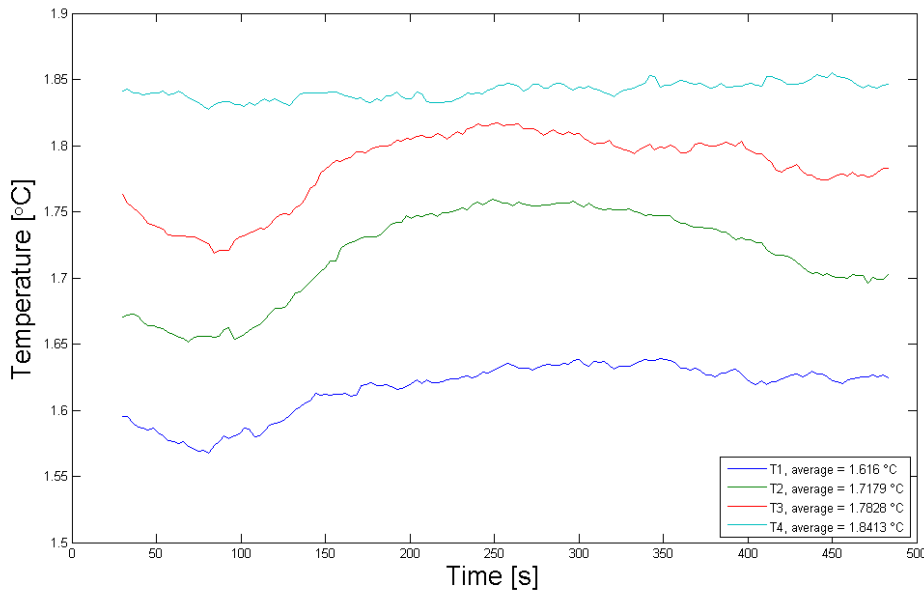


**Figure 4.2.:** Calibration of Thermocouples, Ice Water

In lack of many calibration points, the calibration results are assumed to be valid over a wide temperature range.

### Overall Uncertainty

The method for overall uncertainty is taken from Moffat [7] and documented in appendix B.4. The two sources of errors, *bias* and *precision errors*, are combined in a root-sum-square expression.

First, the precision error is considered. For a 95% confidence interval with many sampling points ( $n > 30$ ), a normal distribution can be assumed. The standard deviations shown in table 4.2 are calculated from the calibration in ice water ( $n = 152$ ), and are meant to illustrate the magnitude of the precision error. Thermocouple 2, 3, and 4 have been used in the rig.

$\Delta\bar{T}_{2-3}$	$\Delta\bar{T}_{2-4}$	$\Delta\bar{T}_{3-4}$
$\div 0.0649K$	$\div 0.1234K$	$\div 0.0585K$
$S_{2-3}$	$S_{2-4}$	$S_{3-4}$
0.0098K	0.0333K	0.0263K
$t_{0.025} \cdot S_{2-3} / \sqrt{n}$	$t_{0.025} \cdot S_{2-4} / \sqrt{n}$	$t_{0.025} \cdot S_{3-4} / \sqrt{n}$
$0.019 / \sqrt{n}$	$0.065 / \sqrt{n}$	$0.052 / \sqrt{n}$

**Table 4.2.:** Standard Deviation Calculation

Equation B.4 has been used to calculate the standard deviation  $S$ . Depending on the number of samples  $n$ , the confidence interval for the precision error is likely to be very small. The value  $t_{0.025} = 1.960$  [8, Table A.4] has been used for the calculation.

Secondly, the bias error should be considered. The main bias error regarding temperature measurement is the deviation from the calibration point. This error will obviously be corrected before calculating the conductivity. This states the paradox of bias errors; if a fixed error is known, it will be corrected. Therefore, it might seem strange that the bias error ever should have a value other than zero. Nevertheless, it has been set to  $\pm 0.1K$  in order to compensate for general inaccuracy in the thermocouples.

The 95% confidence interval for the temperature is then (equation B.9):

$$(U_R)_{0.95} = \left\{ (0.1K)^2 + \left( t_{\alpha=0.025} \cdot \frac{S}{\sqrt{n}} \right)^2 \right\}^{\frac{1}{2}} \quad (4.2)$$

The precision error is considered neglectable in comparison to the bias error. The overall uncertainty for  $\delta\Delta T$  will hereby be:

$$\delta\Delta T = \pm 0.1K \quad (4.3)$$

#### 4.4.2. Power Supply

The power supply has been compared to a multimeter in the laboratory. The plots in figure 4.3 show that they correspond within a tolerable accuracy.

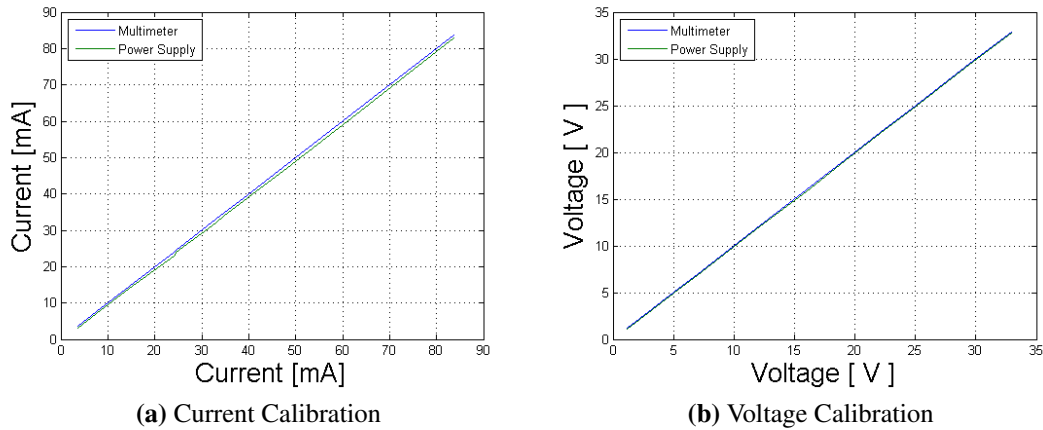


**Figure 4.3.:** Power Supply Readings

The curves show a deviation between 0.5 to 1.1mA for the current, and maximum 0.1V for the voltage. It indicates that the power supply delivers proper readings; however, neither of the devices have been calibrated against an absolute reference. Therefore, it has been chosen to use the power supply readings with an uncertainty of  $\pm 1.0\text{mA}$  and  $\pm 0.1\text{V}$  for the current and voltage, respectively.

$$\delta\dot{Q}_r = (I + 1.0\text{mA}) \cdot (U + 0.1\text{V}) - I \cdot U \quad (4.4)$$

#### 4.4.3. Radial Position

The radial position is measured with a slide caliper as illustrated in figure 4.9a. To ensure that the measurements are correct, multiple slide calipers have been used, both digital and analog. The overall uncertainty is calculated similarly as for the temperature measurements.

$r_2$	$r_3$
7.35	14.35
7.21	14.25
7.25	14.15
7.73	13.91
7.61	13.81
7.63	13.85
7.79	14.03
$S_2$	$S_3$
0.06	0.04
$t_{0.025} \cdot S_2 / \sqrt{n}$	$t_{0.025} \cdot S_3 / \sqrt{n}$
0.05	0.04

**Table 4.3.:** Standard Deviation Calculation

Table 4.3 shows several measurements of the radial position. The 95% confidence interval for the precision error is calculated with  $t_{0.025} = 2.447$  [8, Table A.4]. In addition to the precision error, the bias error has been set to 0.2mm in order to compensate for reading inaccuracy in the slide caliper. The overall uncertainty is then (equation B.9):

$$\delta r = (U_R)_{0.95} = \left\{ (0.2\text{mm})^2 + (t_{\alpha=0.025} \cdot 0.06\text{mm} / \sqrt{7})^2 \right\}^{\frac{1}{2}} = 0.21\text{mm} \quad (4.5)$$

It is the assumed bias error that mainly affects the magnitude of the uncertainty.

#### 4.4.4. Height of Heating Cartridge

The height of the heating cartridge is measured to be exactly 100mm as specified; however, it is hard to determine if the heat production starts and ends completely on the top and bottom of the cartridge. The uncertainty is hereby set to  $\delta h = \pm 5\text{mm}$ . It might be strange to assume that the heat production can take place over a longer length than the cartridge itself, but in this way loss in the wires and error due to some axial heat transfer (section 2.4.3) get compensated for.

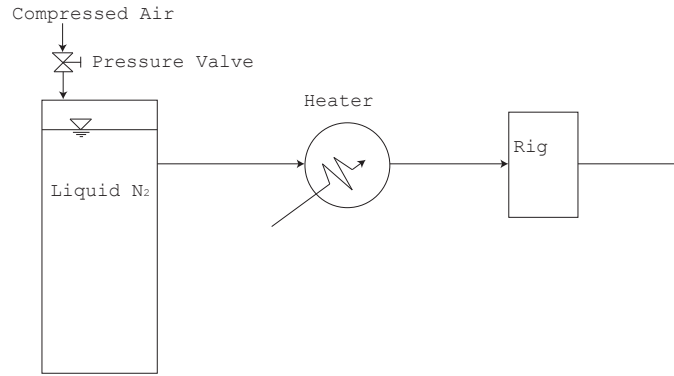
##### 4.5 Side Wall Cooling

For measurements above  $10^{\circ}\text{C}$  it is convenient to use tap water as coolant. The tap water in the laboratory has a range between roughly  $10^{\circ}\text{C}$  and  $60^{\circ}\text{C}$ . A thermocouple has been placed at the inlet of the rig to monitor the temperature. Experience has shown that it takes time to reach a steady temperature; moreover, some fluctuations will occur during a measurement. The water goes through a bottle in front of the rig with the purpose of removing the smallest temperature fluctuations.



**Figure 4.4.:** Tap Water Cooling

For measurements below  $0^{\circ}\text{C}$  it is necessary to use another coolant than water. Liquid nitrogen has been considered to be a natural choice due to its availability and non-explosive properties. With a boiling point of  $77.2\text{K}$  [3, Table A-2] it should be possible to reach low temperatures. The principle is illustrated schematically in figure 4.5. A pressure valve connected between a tank with liquid nitrogen and the compressed air supply in the laboratory controls the mass flow of nitrogen. The nitrogen is then transported through a heater which can be adjusted to reach the desired coolant temperature. The heater consists of a hot-wire that is fastened around the tube and a power supply. The power supply has a regulator which was intended to make it possible to deliver a specified coolant temperature; however, the attempts were unsuccessful due to instabilities in the regulator. Therefore, the power supply will be set to deliver constant power which will lead to a steady temperature. It is possible to adjust the power.



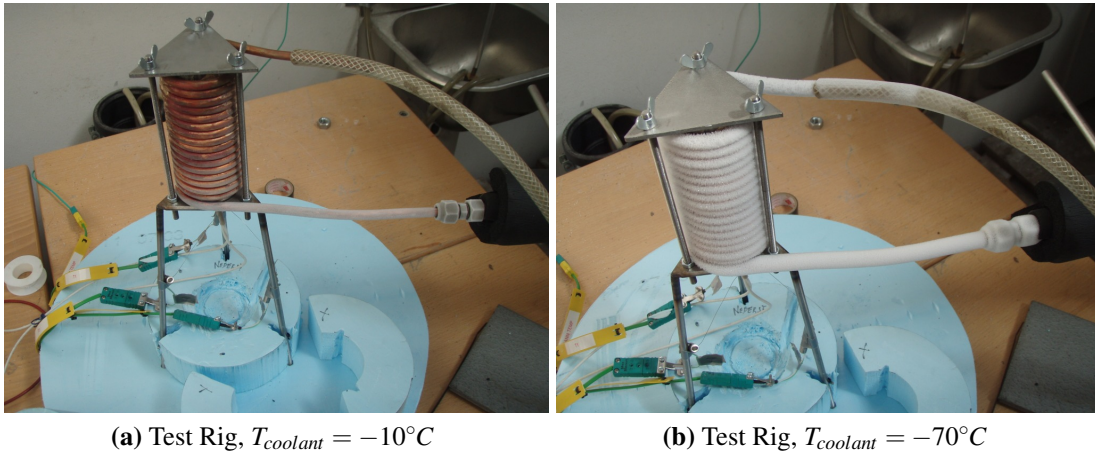
**Figure 4.5.:** Cooling Principle

Figure 4.6 shows the setup in reality. The test rig will be insulated further with Styrofoam and Armaflex under low temperature measurements. During the heating process, the liquid nitrogen will evaporate. After the test rig, the nitrogen is released out to the surroundings.



**Figure 4.6.:** Liquid Nitrogen Coolant Setup

#### 4.5. SIDE WALL COOLING



**Figure 4.7.:** Test Rig at Low Temperatures

The importance of outer insulation increases for lower temperatures. The pipe between the heater and test rig is insulated with Armaflex. The test rig is insulated with Styrofoam and Armaflex as shown in figure 4.8.

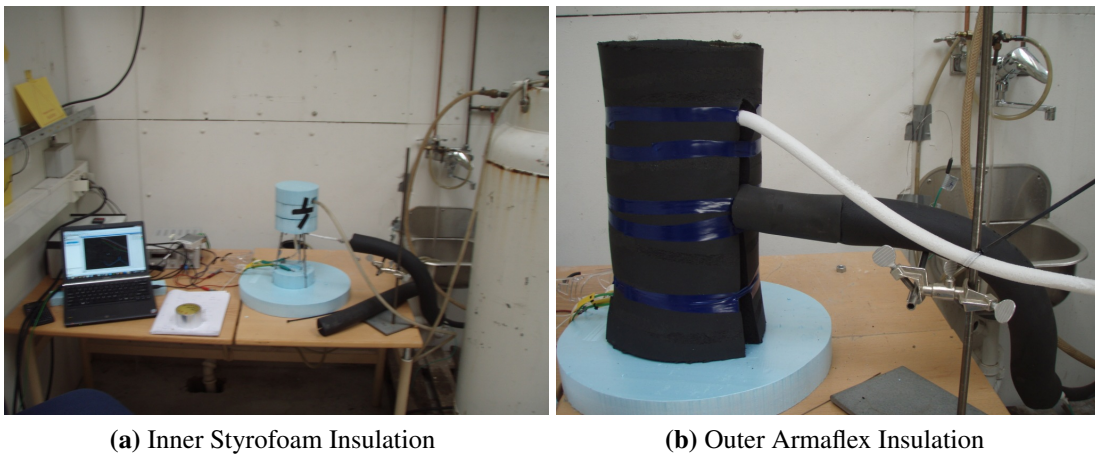


**Figure 4.8.:** Test Rig at Low Temperatures, Insulated

**4.6** Assembly

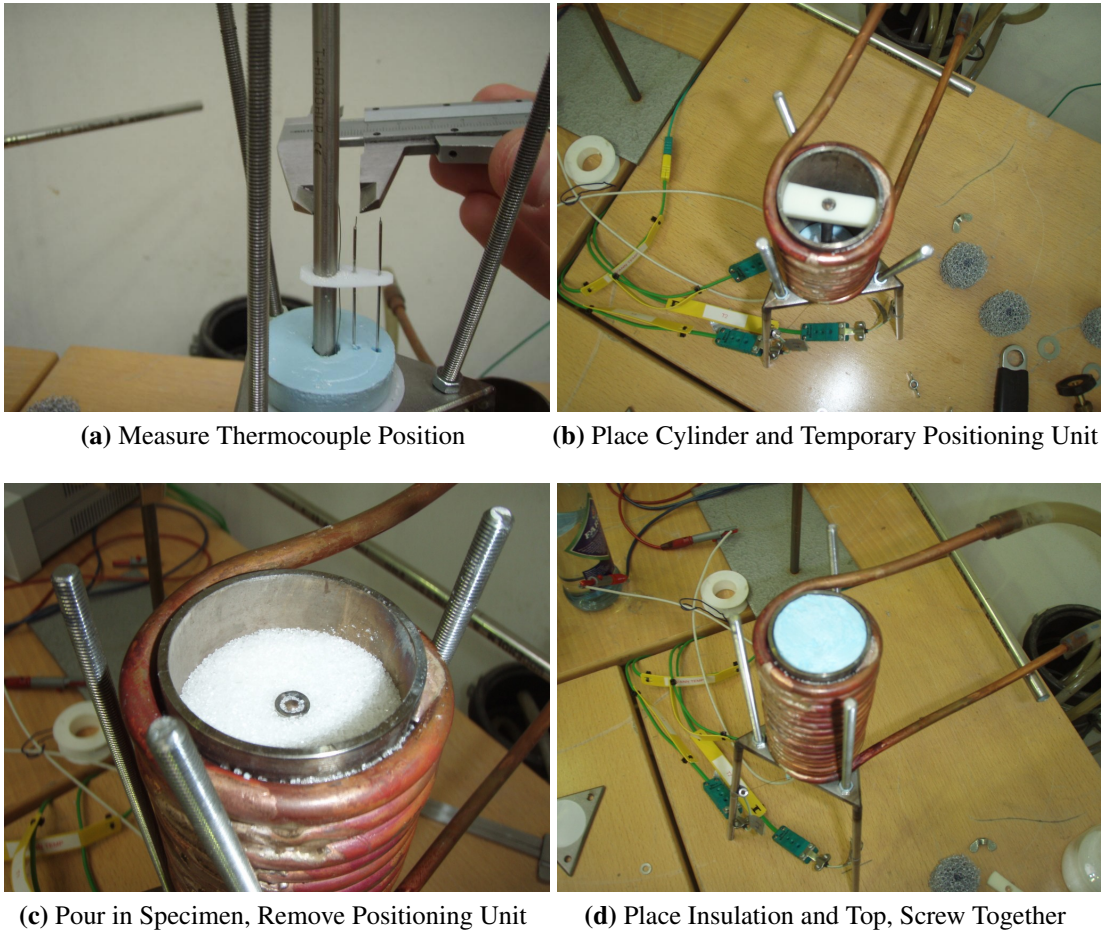


**Figure 4.9.:** Usage of Thermal Conductivity Rig

The side wall temperature must be held constant in order to reach steady state. It is important that the heater is placed in the center; therefore, a positioning unit will be placed on top during filling (see figure 4.9b) to keep the heater centered. This is considered to be a better solution than the one presented in the prestudy since the heater will be centered during the filling. When the cylinder is loaded with the specimen, the positioning unit will be removed since the specimen itself keeps the heater centered.

**4.7** Discussion

Based on calibration and overall uncertainty estimation, the assumed uncertainties  $\delta X_i$  from the prestudy have been further determined. It is important to mention that the overall uncertainty is based on the assumption that the mean of the measurement is the correct value. According to Moffat [7] is the best estimate of a variable the mean plus or minus the uncertainty  $(U_R)_{0.95}$ . The uncertainty will be calculated using equation 2.5 and presented with each conductivity measurement. Note that all variables are assumed to be normally distributed and independent.

#### 4.7. DISCUSSION

---

It should also be mentioned that the error due to some axial heat flux which was discussed in section 2.4.3 are assumed to be taken account for in the uncertainty of the height and heat flux.

Further developments are presented after the measurement results in section 6.6



## PERMEABILITY RIG, COMPLETION

### **5.1** Introduction

This chapter deals with the practical details regarding the permeability rig. The preparatory work is documented in chapter 3, and the P&ID for the rig is attached in appendix A.2.

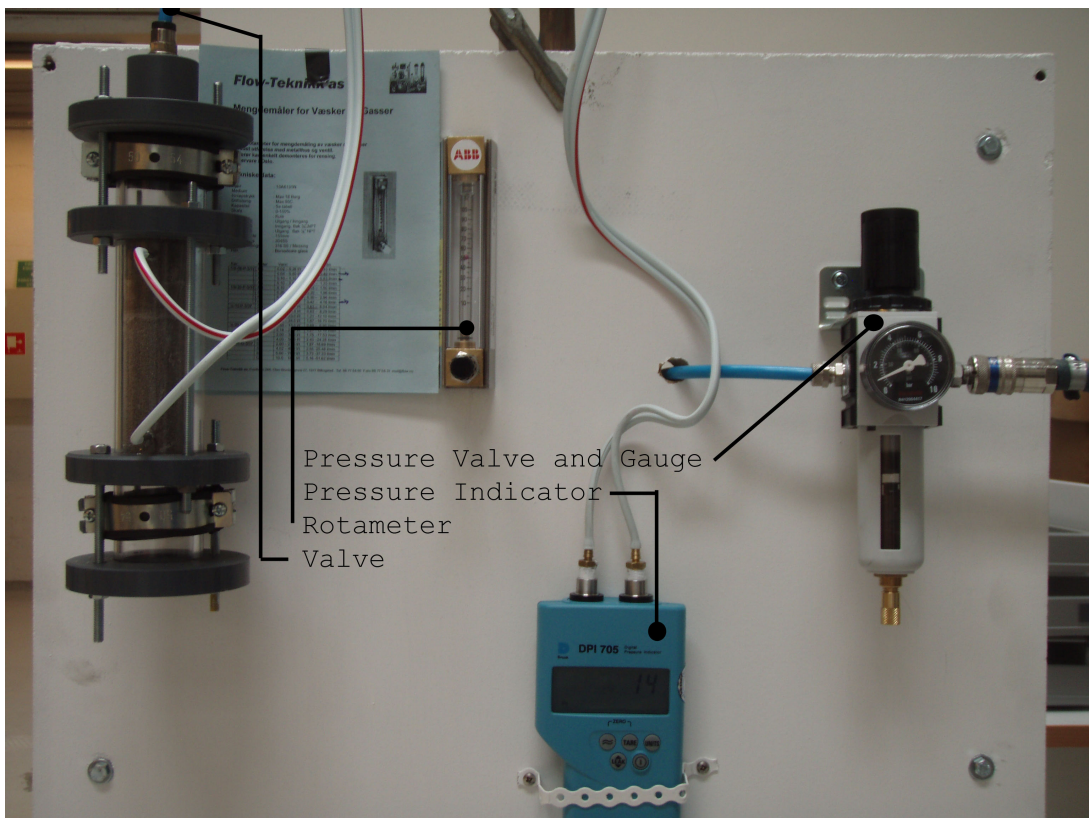


**Figure 5.1.:** Permeability Rig

Unfortunately, time has not allowed the rig to be properly calibrated. The uncertainty  $\delta X_i$  of each variable will be further investigated.

**5.2 Equipment and Instrumentation**

The equipment below are the main components of the rig.

Component	Supplier	Price	Specifications
Precision Valve and Gauge	Bosch Rexroth AS	500 NOK	Bosch Rexroth R412004417 Operating Range: 0-8 bar display: 0-10 bar, [11]
Rotameter	Flow-Teknikk AS	4000 NOK	ABB A6131C-3B. Two Tubes: 0.05-0.49 l/min, 0.42-4.16 l/min
Filter	-	-	Fineness < 30 $\mu\text{m}$
Pressure Indicator	NTNU (borrowed)	-	GE Druck DPI 705 0 - 70mbar, $\delta\Delta P = \pm 7\text{Pa}$ , [13]

**Table 5.1.:** Equipment

More information for some of the equipment can be found on the data sheets referred to in the specifications.

**5.3 Evaluation of Data and Estimation of Uncertainties**

*5.3.1. Data Logging*

All inputs for the permeability calculation will be read manually and treated in MATLAB. The necessary information for a measurement point are:

- Flow rate [%] and which tube that was used
- Pressure loss [Pa]
- Gauge pressure [bar]
- Temperature [ $^{\circ}\text{C}$ ]

*5.3.2. Pressure Valve and Gauge*

The pressure valve and gauge is the connection between the compressed air in the laboratory and the permeability rig. The valve is equipped with a filter that removes oil, water, and dust particles. The valve is adjustable for small changes which is important in order to control the volume flow. The gauge pressure is readable with an accuracy of  $\pm 0.1\text{bar}$ .

*5.3.3. Pressure Indicator*

A digital pressure indicator (dp-cell) with a measurement range between 0 and 7000Pa has been borrowed for the measurements, it has a 0.1% full scale accuracy ( $\pm 7\text{Pa}$ ). The instrument will be reset in front of a measurement which means that the small

hydrostatic contribution of the air can be fully neglected (also discussed in section 3.7). In addition, the indicator is equipped with a thermometer that will be used to monitor the temperature of the air.

#### 5.3.4. Rotameter

The limits of flow rate can be adjusted by change of float or tube. It has a linear scale from 0 to 100 %. In order to make the rotameter able to measure flow rates for other pressures and temperatures than specified, it is necessary to know the density of the fluid. Equation 3.10 shows that the flow rate is proportional with the inverse square root of the fluids density:

$$Q \propto \rho_{fluid}^{-\frac{1}{2}} \quad (5.1)$$

$$Q_{min} = C_{min} \cdot \rho_{fluid}^{-\frac{1}{2}} \quad , \quad Q_{max} = C_{max} \cdot \rho_{fluid}^{-\frac{1}{2}} \quad (5.2)$$

In order to find the flow rate it is therefore necessary to measure the pressure and temperature. The floats given range for minimum and maximum flow at a temperature of 20°C and atmospheric pressure are used as a reference to find the constants  $C_{min}$  and  $C_{max}$ . Some other values are calculated in table 5.2.

P = 1 atm , T = 20°C (reference)	0.05 - 0.49 l/min	0.0036 - 0.0354 kg/h
P = 2 atm , T = 20°C	0.035 - 0.347 l/min	0.0051 - 0.0501 kg/h
P = 3 atm , T = 20°C	0.029 - 0.283 l/min	0.0063 - 0.0614 kg/h

**Table 5.2.:** Air Flow Rates, Rotameter

The flow rates under different pressures are given as actual volume flow and mass flow. Note that the mass flow increases under higher pressures even if the actual volume flow decreases. The valve between the container and rotameter can be used to obtain higher pressures through the rotameter and subsequently expand the air upstream of the specimen. This results in a extended flow range for the rotameter. The mass flow through the rotameter is:

$$\dot{m} = \rho_{fluid} \cdot \left[ Q_{min} + (Q_{max} - Q_{min}) \cdot \frac{X}{100} \right] \quad (5.3)$$

Where  $X$  is the read value on the rotameter between 0 and 100 and  $\rho_{fluid}$  the density of the fluid ( $\rho_2$  in figure 5.2).

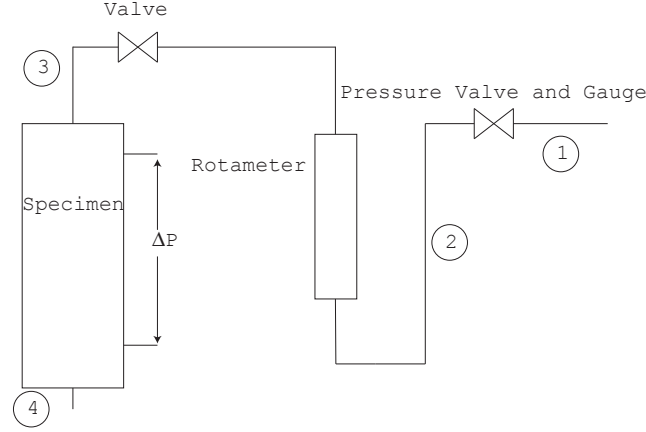


**Figure 5.2.:** Pressure in Permeability Rig

The actual flow is calculated from the average density through the specimen:

$$\bar{\rho} = \frac{P_3 + P_4}{2} \cdot \frac{1}{R \cdot \bar{T}} \quad (5.4)$$

Where  $P_4 = 1\text{atm}$  and  $P_3 = P_4 + \Delta P$ .

$$Q = \frac{\dot{m}}{\bar{\rho}} \quad (5.5)$$

To estimate the uncertainty of a volume flow reading, single-sample analysis taken from Moffat [7] (appendix B.2) has been used. First, it is convenient to rewrite the expression for volume flow, the notations for pressures and densities correspond with figure 5.2.

$$Q = \frac{\rho_2^{\frac{1}{2}}}{\bar{\rho}} \cdot \left[ C_{min} + (C_{max} - C_{min}) \cdot \frac{X}{100} \right] \quad (5.6)$$

$$Q = \left( \frac{P_4 + \Delta P + P_{gauge}}{R \cdot T_2} \right)^{\frac{1}{2}} \cdot \frac{2R \cdot \bar{T}}{P_4 + \Delta P + P_4} \cdot \left[ C_{min} + (C_{max} - C_{min}) \cdot \frac{X}{100} \right] \quad (5.7)$$

Where  $P_{gauge}$  is the gauge pressure read from the pressure valve. The rig is assumed to operate isothermal,  $T_2 = \bar{T} = T$ .

$$Q = \frac{\sqrt{(P_4 + \Delta P + P_{gauge}) \cdot R \cdot T}}{P_4 + \frac{\Delta P}{2}} \cdot \left[ C_{min} + (C_{max} - C_{min}) \cdot \frac{X}{100} \right] \quad (5.8)$$

A single sample volume flow reading is with that dependent on the following variables:

$$Q = Q(P_4, \Delta P, P_{gauge}, R, T, X) \quad (5.9)$$

$$\delta Q = \left\{ \left( \frac{\partial Q}{\partial P_4} \delta P_4 \right)^2 + \left( \frac{\partial Q}{\partial \Delta P} \delta \Delta P \right)^2 + \left( \frac{\partial Q}{\partial P_{gauge}} \delta P_{gauge} \right)^2 + \left( \frac{\partial Q}{\partial R} \delta R \right)^2 + \left( \frac{\partial Q}{\partial T} \delta T \right)^2 + \left( \frac{\partial Q}{\partial X} \delta X \right)^2 \right\}^{\frac{1}{2}} \quad (5.10)$$

The partial derivatives has been solved using MAPLE and the solution is attached in appendix F.3. Clearly, the uncertainty depends on each single sample; therefore, it will be calculated in front of every permeability uncertainty calculation. The tolerances are defined below:

$\delta P_4$	$\delta \Delta P$	$\delta P_{gauge}$	$\delta R$	$\delta T$	$\delta X$
$\pm 1000 \text{ Pa}$	$\pm 7 \text{ Pa}$	$0, P_{gauge} = 0$ $\pm 10^4 \text{ Pa}, P_{gauge} > 0$	$\pm 15 \frac{\text{J}}{\text{kgK}}$	$\pm 3 \text{ K}$	$\pm 3$

**Table 5.3.:** Uncertainties for a Volume Flow Reading

$\delta P_4$  has been set to  $\pm 1000 \text{ Pa}$  to account for variations in the atmospheric pressure,  $\delta R$  to  $\pm 15 \frac{\text{J}}{\text{kgK}}$  for variations in the humidity of the air, and the reading insecurity  $\delta X$  of the rotameter to  $\pm 3$ .

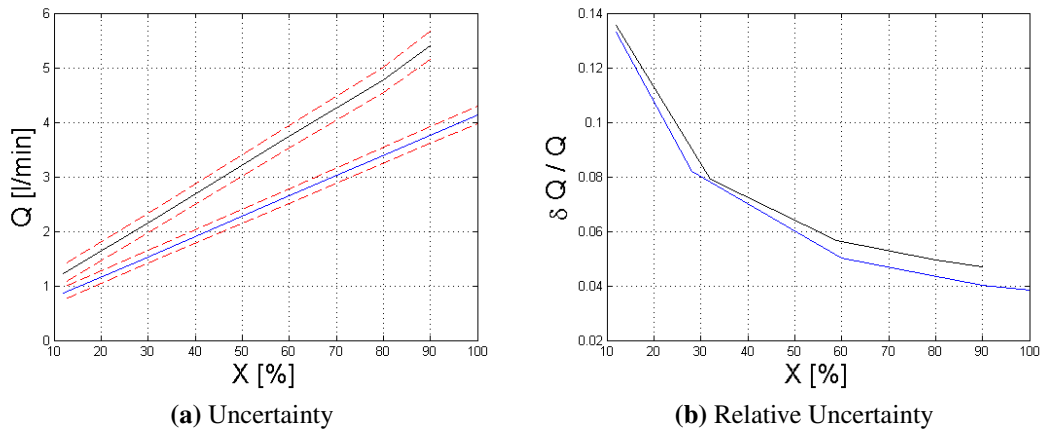


**Figure 5.3.:** Uncertainty for Volume Flow for  $P_{gauge} = 0 \text{ bar}$  and  $P_{gauge} = 1 \text{ bar}$

Note that the temperature has been assumed to be constant through the rig. The uncertainty  $\delta Q$  will be used in the calculation of  $\delta \kappa$ .

### 5.3.5. Measurement of Viscosity

As mentioned in section 3.7, the viscosity is only dependent on temperature,  $\mu = \mu(T)$ . For air in room temperature, the uncertainty of the viscosity will be set to  $\delta \mu = \pm 0.025 \cdot 10^{-5} \frac{\text{kg}}{\text{ms}}$  based on the three values  $\mu(15^\circ \text{C}) = 1.802 \cdot 10^{-5} \frac{\text{kg}}{\text{ms}}$ ,  $\mu(20^\circ \text{C}) = 1.825 \cdot 10^{-5} \frac{\text{kg}}{\text{ms}}$ , and  $\mu(25^\circ \text{C}) = 1.849 \cdot 10^{-5} \frac{\text{kg}}{\text{ms}}$  from Çengel [3, Table A-15].

### 5.3.6. Length

Since the two holes for measurement of pressure loss have a certain diameter, it is reasonable to assume that there is an uncertainty in the length between the points. The two holes in the container have a diameter of approximately 1 mm; therefore, the uncertainty of the length has been sent to  $\delta L = 2 \text{ mm}$ .

## 5.4. ASSEMBLY

### 5.4 Assembly



(a) Open the Top



(b) Pour in Specimen



(c) Place Filter and Top



(d) Screw Together

**Figure 5.4.:** Assembly of Permeability Rig

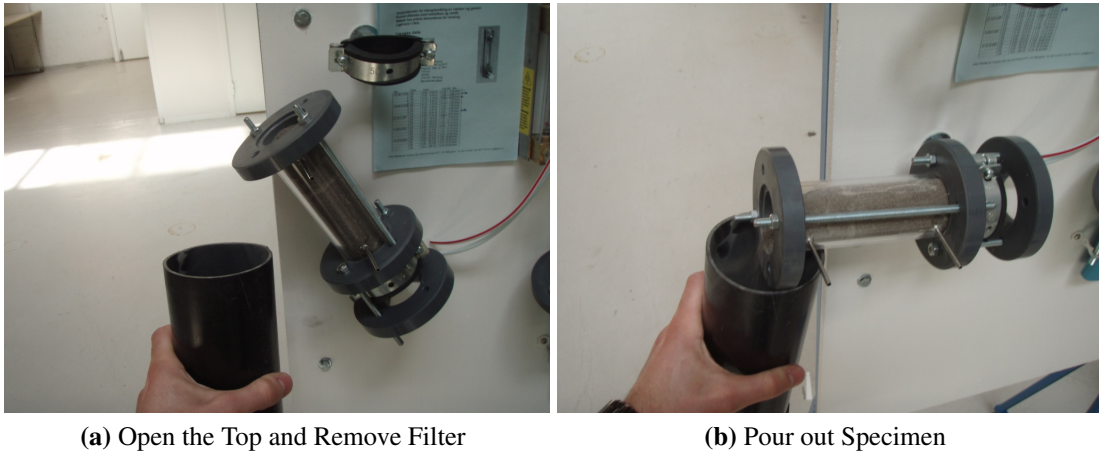


Figure 5.5.: Disassembly of Permeability Rig

### 5.5 Preparation and Accomplishment of a Measurement

In front of a measurement, the pressure loss should be estimated by using the procedure described in section 3.6. The empirical formulas in section 3.5 are dependent on several parameters which may be difficult to obtain for a material; therefore, it is important to remember that the estimation may differ strongly from the measurement result. The parameters for several materials are attached in appendix D, these may be used as guiding under an estimation.

Under a measurement, the precision valve will be used to adjust the volume flow. At each sampling point, the necessary information will be noted (section 5.3.1). The rotameter allows for measurements in the range between 0.05 and 4.16 l/min. It is also possible to increase the range by increasing the gauge pressure.

For each sampling point, the uncertainty will be calculated in addition to the permeability. Since the hydrostatic pressure not will affect the result, equation 3.6 reduces to:

$$\kappa = \frac{4Q\mu L}{\pi D^2 \Delta P} \quad (5.11)$$

For the uncertainty calculation, this means that the permeability is dependent on the following variables:

$$\kappa = \kappa(Q, \Delta P, \mu, L) \quad (5.12)$$

The uncertainty is calculated using single-sample analysis taken from Moffat [7] as described in appendix B.2, the derivatives has been solved with MAPLE and the solution is attached in appendix F.2.

### 5.6 Discussion

The uncertainties of the rig has been further investigated where  $\delta Q$  has been determined based on single-sample analysis. The pressure loss,  $\delta \Delta P$ , has been found in product specifications.  $\delta \mu$  and  $\delta L$  are based on table values and assumptions, respectively. Unfortunately, time has not allowed the rig to be properly calibrated which means that there may be unknown deviations that affects the result. The temperature will only be measured in the dp-cell which not is representative for the temperature

## 5.6. DISCUSSION

---

in the flow. This is an improvement point, but for now the rig have been assumed to operate isothermal at room temperature.

The rig is capable of measurements for flow rates at minimum 0.05 l/min, a gauge pressure up to 8 bar, and maximum pressure loss of 7000Pa. The hydrostatic pressure contribution has been removed from the permeability expression since the pressure indicator will be reset in front of a measurement.

Further developments are presented after the measurement results in section 7.6.



---

---

PART III

---

Experimental Results



## THERMAL CONDUCTIVITY MEASUREMENT RESULTS

### **6.1** Introduction

The thermal conductivity have been measured for the materials listed below. More information regarding the materials are found in appendix C.

- Sugar
- Sand
- Expancel

The materials have been selected in cooperation with the Department. Due to delays, the storage powder for hydrogen was not available for measurements. It turned out to be difficult to find materials where the exact properties were known; therefore, it was not possible to estimate the conductivity properly. The measurements in this chapter is therefore to be considered as a test of the rig, data reduction, and an examination of the measurement accuracy. The rigs ability for measurements in high and low temperatures will also be tested. The temperature range depends on the stability of the tap water, and how low temperatures that will be achievable using nitrogen as coolant.

In one measurement, the conductivity will be calculated three times since there are three thermocouples in the rig. The uncertainties that were determined in section 4.4 are used for each individual calculation. They are assumed to be applicable around the mean of each variable.

The conductivity has also been plotted against the temperature. In this case, the average conductivity has been calculated based on the measurements at the current temperature. The method for multiple measurements has been used to calculate a confidence interval around the mean (appendix B.3). This method requires that each measurement is independent which not is the case for the following measurements. However, in lack of multiple independent measurements at the same temperature it has been neglected to demonstrate the principle.

**6.2** Sugar

6.2.1. Individual Measurements

April 29 - Measurement Sugar

Date	April 29	Specimen	Sugar
Filename	0429.xlsx	Density	$\rho = 1020 \frac{kg}{m^3}$
Thermocouple Position	$r_1 = 3.38mm$ $r_2 = 7.73mm$ $r_3 = 13.91mm$	Thermocouple Deviation	$T_1 = +1.7179K$ $T_2 = +1.7828K$ $T_3 = +1.8413K$
Cooling Method	Tap Water	Side Wall Temperature	$T_{wall} = 13.4 - 8.8^\circ C$
Power Supply	$U = 12.7V$ $I = 39mA$ $Q = 0.50W$	Uncertainties	$\delta Q_r = \pm 0.017W$ $\delta r = \pm 0.21mm$ $\delta h = \pm 5mm$ $\delta \Delta T = \pm 0.1K$
Steady State Temperatures	$T_1 = 19.079^\circ C$ $T_2 = 14.280^\circ C$ $T_3 = 10.857^\circ C$	Thermal Conductivity	$k(T_{1-2}) = 0.137 \pm 0.014 \frac{W}{mK}$ $k(T_{2-3}) = 0.136 \pm 0.012 \frac{W}{mK}$ $k(T_{1-3}) = 0.137 \pm 0.011 \frac{W}{mK}$

**Table 6.1.:** Sugar: Measurement Conditions and Results, April 29

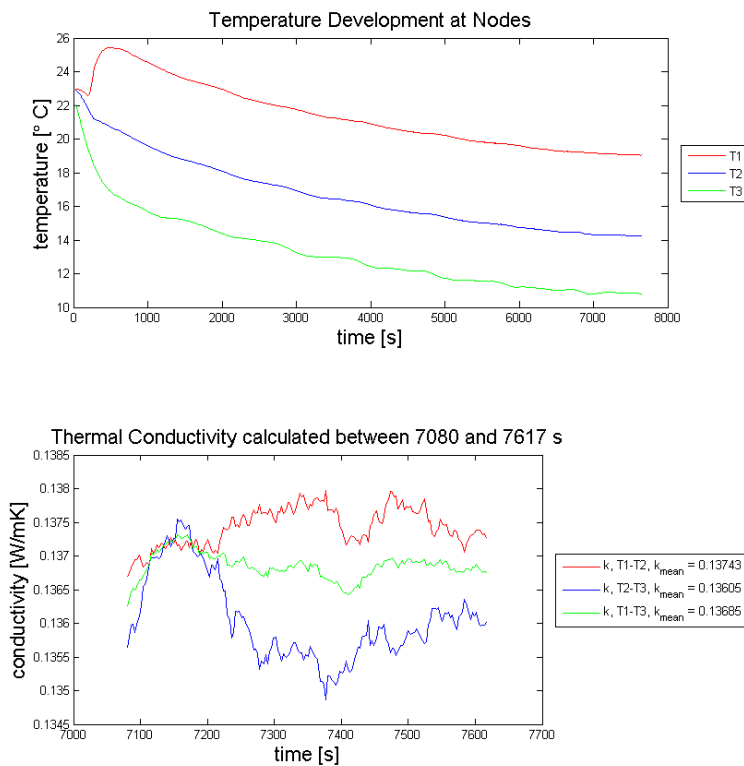


**Figure 6.1.:** Sugar: Measurement Conditions and Results, April 29

Due to variations in the temperature from the tap water, it was difficult to obtain steady state. The last 10 minutes of the measurement are considered to be steady state.

To show the influence of each variable using the determined uncertainties, they have been plotted for  $k(T_{2-3})$ :

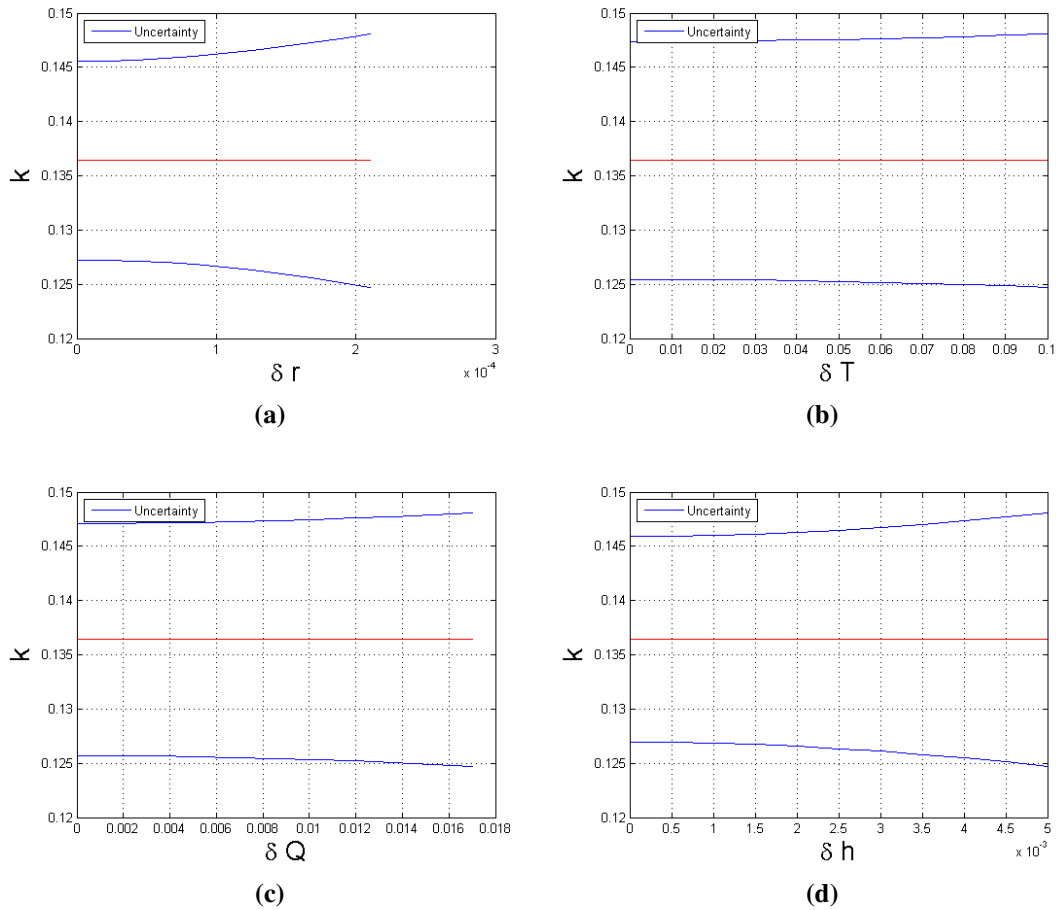


Figure 6.2.: Uncertainty Plots Combined

The influence of each variable are approximately the same in every measurement and will therefore only be plotted for this measurement. The plots show that the uncertainty of positioning  $\delta r$  followed by the height  $\delta h$  are of greatest magnitude.

May 4 - Measurement Sugar

Date	May 4	Specimen	Sugar
Filename	0504.x1s.x	Density	$\rho = 1020 \frac{kg}{m^3}$
Thermocouple Position	$r_1 = 3.38mm$ $r_2 = 8.01mm$ $r_3 = 13.81mm$	Thermocouple Deviation	$T_1 = +1.7179K$ $T_2 = +1.7828K$ $T_3 = +1.8413K$
Cooling Method	Tap Water	Side Wall Temperature	$T_{wall} = 46 - 50^\circ C$
Power Supply	$U = 13.3V$ $I = 41mA$ $Q = 0.5453W$	Uncertainties	$\delta Q_r = \pm 0.018W$ $\delta r = \pm 0.21mm$ $\delta h = \pm 5mm$ $\delta \Delta T = \pm 0.1K$
Steady State Temperatures	$T_1 = 56.675^\circ C$ $T_2 = 51.616^\circ C$ $T_3 = 48.417^\circ C$	Thermal Conductivity	$k(T_{1-2}) = 0.148 \pm 0.015 \frac{W}{mK}$ $k(T_{2-3}) = 0.148 \pm 0.013 \frac{W}{mK}$ $k(T_{1-3}) = 0.148 \pm 0.011 \frac{W}{mK}$

Table 6.2.: Sugar: Measurement Conditions and Results, May 4

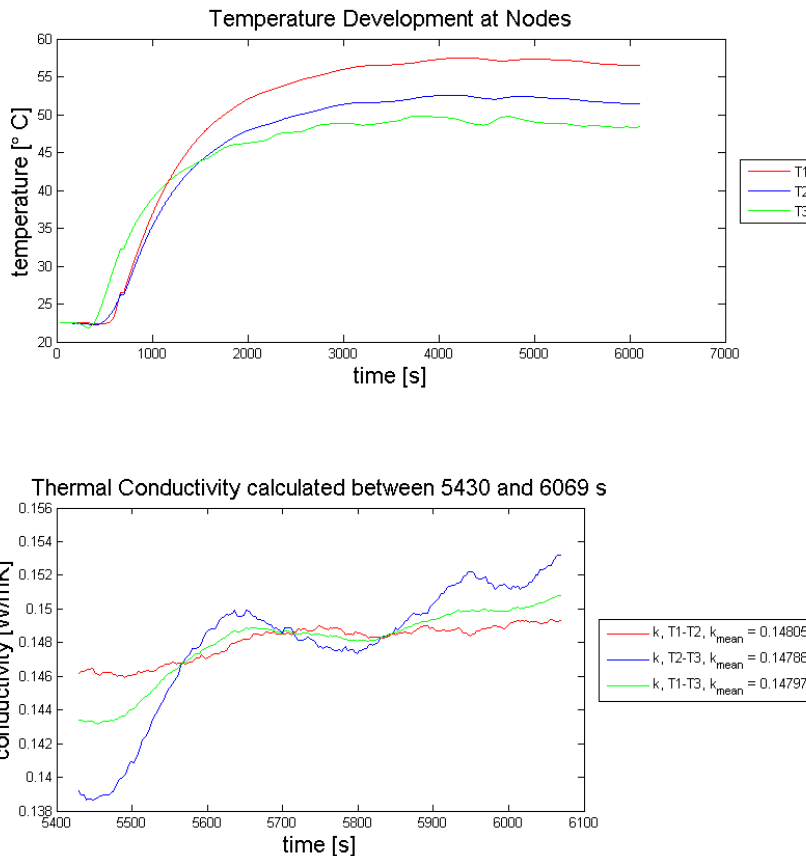


Figure 6.3.: Sugar: Measurement Conditions and Results, May 4

The temperature of the water supply stabilized after approximately 5000 seconds. If the water had delivered a steady temperature, the rig would have reached steady state after approximately 3000 seconds. The three conductivity calculations corresponds satisfactory.

May 6 - Measurement Sugar

Date	May 6	Specimen	Sugar
Filename	0506.xlsx	Density	$\rho = 1020 \frac{kg}{m^3}$
Thermocouple Position	$r_1 = 3.38mm$ $r_2 = 8.21mm$ $r_3 = 13.85mm$	Thermocouple Deviation	$T_1 = +1.7179K$ $T_2 = +1.7828K$ $T_3 = +1.8413K$
Cooling Method	Tap Water	Side Wall Temperature	$T_{wall} = 61 - 65^\circ C$
Power Supply	$U = 13.3V$ $I = 42mA$ $Q = 0.5586W$	Uncertainties	$\delta Q_r = \pm 0.018W$ $\delta r = \pm 0.21mm$ $\delta h = \pm 5mm$ $\delta \Delta T = \pm 0.1K$
Steady State Temperatures	$T_1 = 70.482^\circ C$ $T_2 = 65.803^\circ C$ $T_3 = 63.115^\circ C$	Thermal Conductivity	$k(T_{1-2}) = 0.169 \pm 0.017 \frac{W}{mK}$ $k(T_{2-3}) = 0.173 \pm 0.016 \frac{W}{mK}$ $k(T_{1-3}) = 0.170 \pm 0.013 \frac{W}{mK}$

Table 6.3.: Sugar: Measurement Conditions and Results, May 6

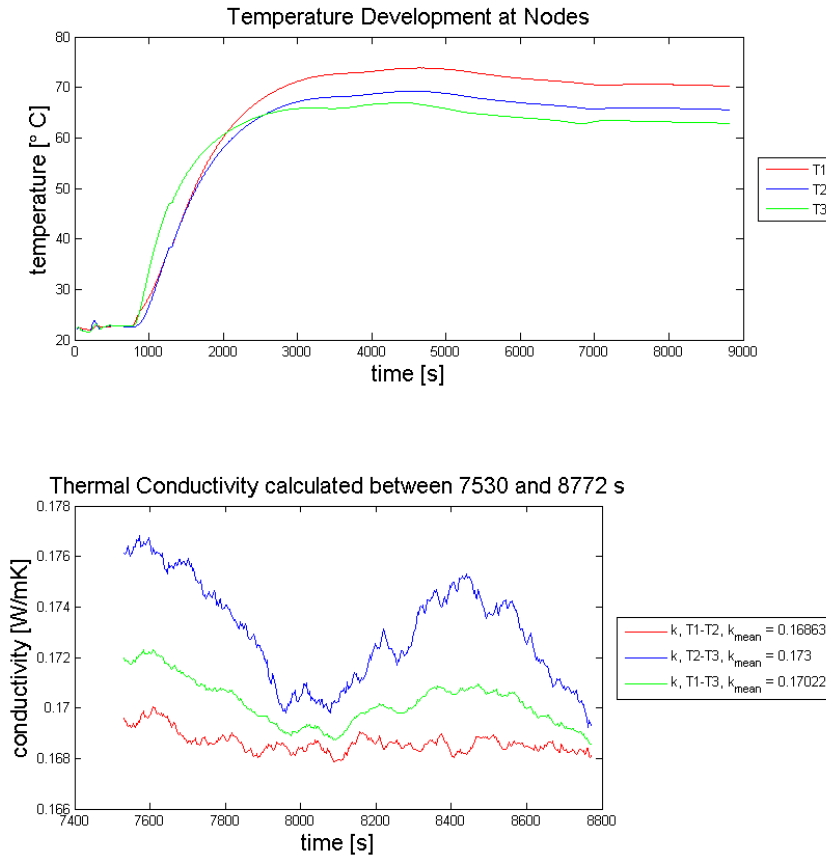


Figure 6.4.: Sugar: Measurement Conditions and Results, May 6

Instabilities in the water supply lead to a far-reaching process of obtaining steady state. The three conductivity calculations are displaced from each other which can indicate that the position of  $T_2$  is above the measured value.

May 27 - Measurement Sugar

Date	May 27	Specimen	Sugar
Filename	0527.x1sx	Density	$\rho = 1020 \frac{kg}{m^3}$
Thermocouple Position	$r_1 = 3.38mm$ $r_2 = 6.11mm$ $r_3 = 13.91mm$	Thermocouple Deviation	$T_1 = +1.7179K$ $T_2 = +1.7828K$ $T_3 = +1.8413K$
Cooling Method	Nitrogen	Side Wall Temperature	$T_{wall} = \div 147 - \div 145^\circ C$
Power Supply	$U = 12.0V$ $I = 38mA$ $Q = 0.456W$	Uncertainties	$\delta Q_r = \pm 0.016W$ $\delta r = \pm 0.21mm$ $\delta h = \pm 5mm$ $\delta \Delta T = \pm 0.1K$
Steady State Temperatures	$T_1 = \div 131.383^\circ C$ $T_2 = \div 135.915^\circ C$ $T_3 = \div 142.571^\circ C$	Thermal Conductivity	$k(T_{1-2}) = 0.095 \pm 0.013 \frac{W}{mK}$ $k(T_{2-3}) = 0.090 \pm 0.007 \frac{W}{mK}$ $k(T_{1-3}) = 0.092 \pm 0.007 \frac{W}{mK}$

Table 6.4.: Sugar: Measurement Conditions and Results, May 27

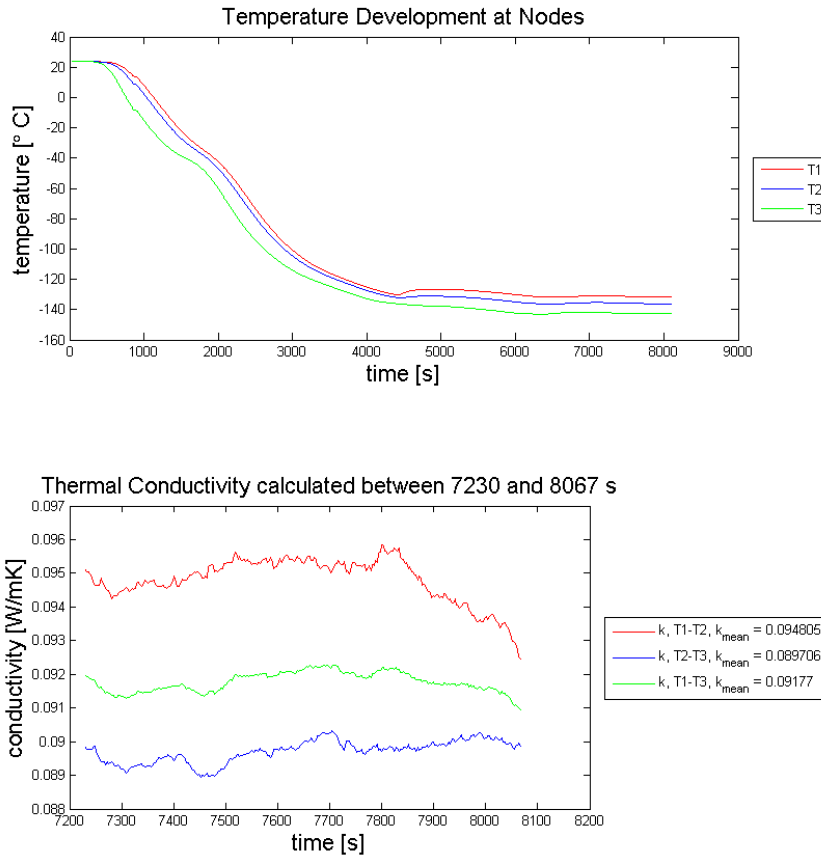


Figure 6.5.: Sugar: Measurement Conditions and Results, May 27

It took approximately 2 hours to obtain a stable coolant temperature. Once again, the three calculations are displaced from each other. In this case, it can indicate that the position of  $T_2$  is below the measured value. Water condensates and freezes on the rig at lower temperatures, it is not known how this affects the measurement.



6.2.2. Overall Result

The confidence interval has been calculated around the mean of each measurement with  $t_{0.025} = 4.303$  when  $n = 3$  [8, Table A.4]. Note that the three calculations not are independent.

$T_{avg} = \div 137.0^{\circ}C$	$0.086081 < 0.092333 < 0.098585$	$\delta\bar{k} = 0.009$
$T_{avg} = 15.0^{\circ}C$	$0.13523 < 0.13667 < 0.1381$	$\delta\bar{k} = 0.012$
$T_{avg} = 52.5^{\circ}C$	$0.148 < 0.148 < 0.148$	$\delta\bar{k} = 0.013$
$T_{avg} = 66.8^{\circ}C$	$0.1655 < 0.17067 < 0.17584$	$\delta\bar{k} = 0.015$

**Table 6.5.:** Sugar: 95% Confidence Interval around the Mean and Average of Individual Uncertainties

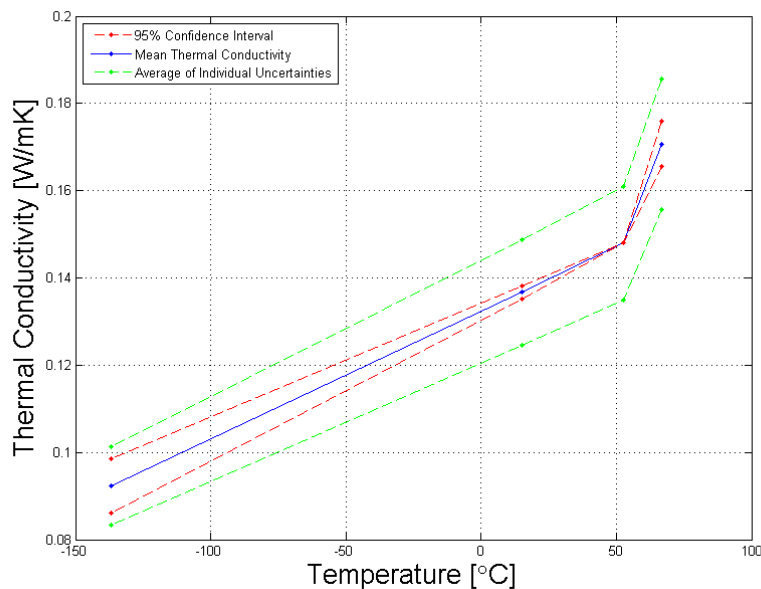


**Figure 6.6.:** Sugar: Conductivity versus Temperature

The plot is based on four measurements where the three first form a linear trend. The fourth measurement rises somehow higher than what may be expected. Anyway, without more measurements or reference data, it is hard to determine if one or several of the results are wrong. A rough estimate based on the conductivity of solid sugar and the porosity indicates that the conductivity should be  $0.174 \frac{W}{mK}$  at  $27^{\circ}C$  (appendix C.2),  $0.04 \frac{W}{mK}$  above the measured value.

The average of the individual uncertainties show that the conductivity may differ 10% from the mean. The size of the confidence interval illustrates if the three calculations in one measurement differ from each other.

**6.3 Sand**

6.3.1. Individual Measurements

May 11 - Measurement Sand

Date	May 11	Specimen	Sand
Filename	0511.xlsx	Density	$\rho = 2209 \frac{kg}{m^3}$
Thermocouple Position	$r_1 = 3.38mm$ $r_2 = 7.81mm$ $r_3 = 14.03mm$	Thermocouple Deviation	$T_1 = +1.7179K$ $T_2 = +1.7828K$ $T_3 = +1.8413K$
Cooling Method	Tap Water	Side Wall Temperature	$T_{wall} = 5 - 6^\circ C$
Power Supply	$U = 18.4V$ $I = 57.5mA$ $Q = 1.058W$	Uncertainties	$\delta Q_r = \pm 0.024W$ $\delta r = \pm 0.21mm$ $\delta h = \pm 5mm$ $\delta \Delta T = \pm 0.1K$
Steady State Temperatures	$T_1 = 17.087^\circ C$ $T_2 = 11.760^\circ C$ $T_3 = 8.0201^\circ C$	Thermal Conductivity	$k(T_{1-2}) = 0.265 \pm 0.026 \frac{W}{mK}$ $k(T_{2-3}) = 0.264 \pm 0.021 \frac{W}{mK}$ $k(T_{1-3}) = 0.264 \pm 0.019 \frac{W}{mK}$

**Table 6.6.:** Sand: Measurement Conditions and Results, May 11

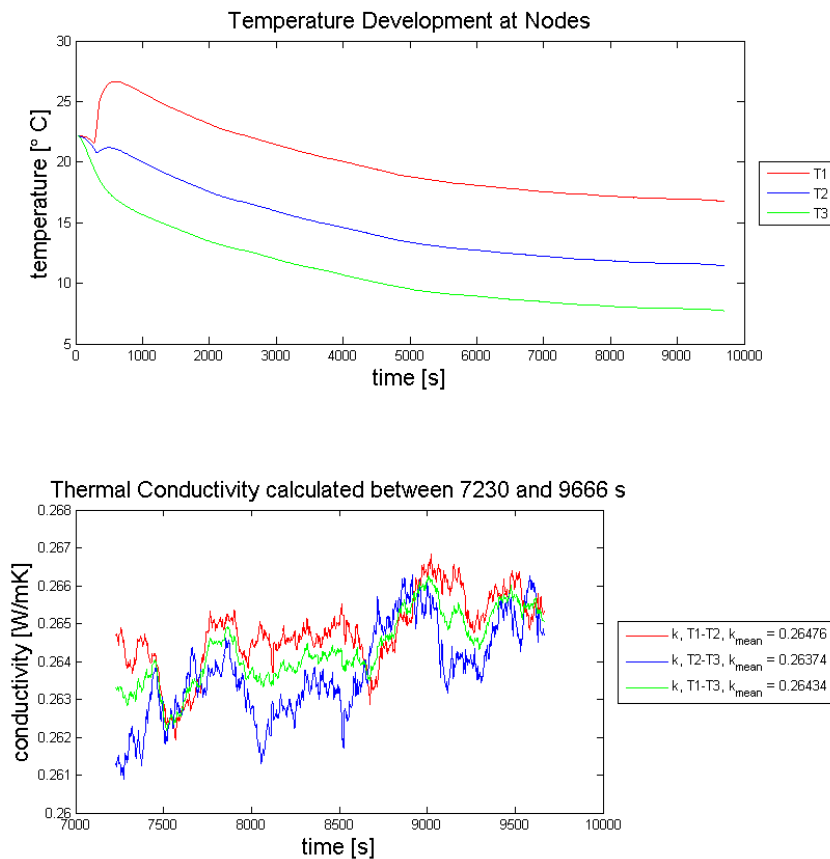


**Figure 6.7.:** Sand: Measurement Conditions and Results, May 11

After a long time to stabilize the tap water, the results turned out to be satisfactory.

May 25 - Measurement Sand

Date	May 25	Specimen	Sand
Filename	0525.xlsx	Density	$\rho = 2209 \frac{kg}{m^3}$
Thermocouple Position	$r_1 = 3.38mm$ $r_2 = 7.11mm$ $r_3 = 14.11mm$	Thermocouple Deviation	$T_1 = +1.7179K$ $T_2 = +1.7828K$ $T_3 = +1.8413K$
Cooling Method	Nitrogen	Side Wall Temperature	$T_{wall} = \div 72.0 - \div 74.5^\circ C$
Power Supply	$U = 17.5V$ $I = 55.0mA$ $Q = 0.9625W$	Uncertainties	$\delta Q_r = \pm 0.023W$ $\delta r = \pm 0.21mm$ $\delta h = \pm 5mm$ $\delta \Delta T = \pm 0.1K$
Steady State Temperatures	$T_1 = \div 55.502^\circ C$ $T_2 = \div 61.077^\circ C$ $T_3 = \div 66.372^\circ C$	Thermal Conductivity	$k(T_{1-2}) = 0.204 \pm 0.022 \frac{W}{mK}$ $k(T_{2-3}) = 0.198 \pm 0.015 \frac{W}{mK}$ $k(T_{1-3}) = 0.201 \pm 0.015 \frac{W}{mK}$

Table 6.7.: Sand: Measurement Conditions and Results, May 25

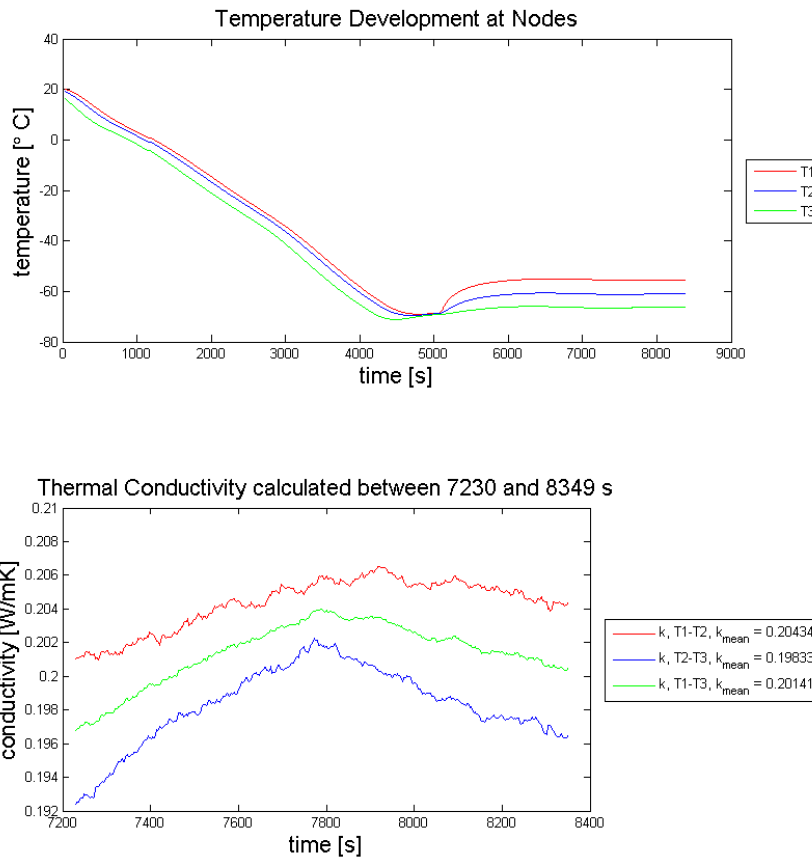


Figure 6.8.: Sand: Measurement Conditions and Results, May 25

The results indicate that the position of  $T_2$  is below the measured value. Water condensates and freezes on the rig at lower temperatures, it is not known how this affects the measurement.

## May 31 - Measurement Sand

Date	May 31	Specimen	Sand
Filename	0531.xlsx	Density	$\rho = 2209 \frac{kg}{m^3}$
Thermocouple Position	$r_1 = 3.38mm$ $r_2 = 8.25mm$ $r_3 = 13.91mm$	Thermocouple Deviation	$T_1 = +1.7179K$ $T_2 = +1.7828K$ $T_3 = +1.8413K$
Cooling Method	Tap Water	Side Wall Temperature	$T_{wall} = 57.0 - 59.5^\circ C$
Power Supply	$U = 19.2V$ $I = 59.0mA$ $Q = 1.1328W$	Uncertainties	$\delta Q_r = \pm 0.025W$ $\delta r = \pm 0.21mm$ $\delta h = \pm 5mm$ $\delta \Delta T = \pm 0.1K$
Steady State Temperatures	$T_1 = 71.481^\circ C$ $T_2 = 66.214^\circ C$ $T_3 = 63.092^\circ C$	Thermal Conductivity	$k(T_{1-2}) = 0.305 \pm 0.029 \frac{W}{mK}$ $k(T_{2-3}) = 0.302 \pm 0.026 \frac{W}{mK}$ $k(T_{1-3}) = 0.304 \pm 0.022 \frac{W}{mK}$

Table 6.8.: Sand: Measurement Conditions and Results, May 31

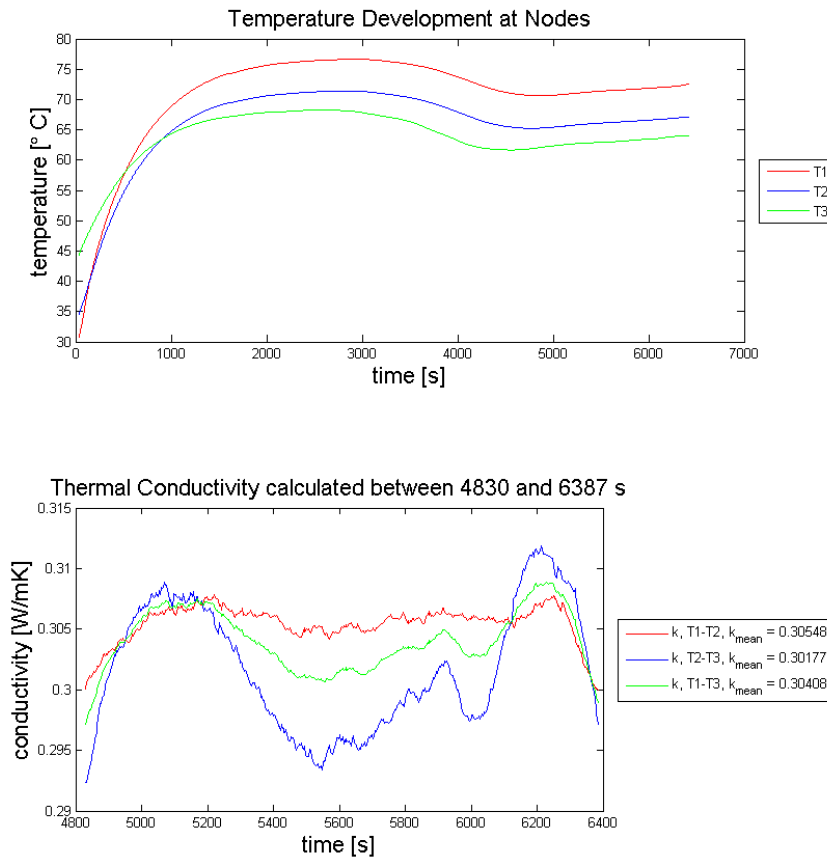


Figure 6.9.: Sand: Measurement Conditions and Results, May 31

Note that the calculation of  $k(T_{2-3})$  fluctuates more than the two other calculations, this is because  $k(T_{2-3})$  is most sensitive for temperature fluctuations on the side wall.

6.3.2. Overall Result

The confidence interval has been calculated around the mean of each measurement with  $t_{0.025} = 4.303$  when  $n = 3$  [8, Table A.4]. Note that the three calculations not are independent.

$T_{avg} = \div 60.9^{\circ}C$	$0.19355 < 0.201 < 0.20845$	$\delta\bar{k} = 0.017$
$T_{avg} = 12.3^{\circ}C$	$0.2629 < 0.26433 < 0.26577$	$\delta\bar{k} = 0.022$
$T_{avg} = 67.3^{\circ}C$	$0.29987 < 0.30367 < 0.30746$	$\delta\bar{k} = 0.026$

**Table 6.9.:** Sand: 95% Confidence Interval around the Mean and Average of Individual Uncertainties

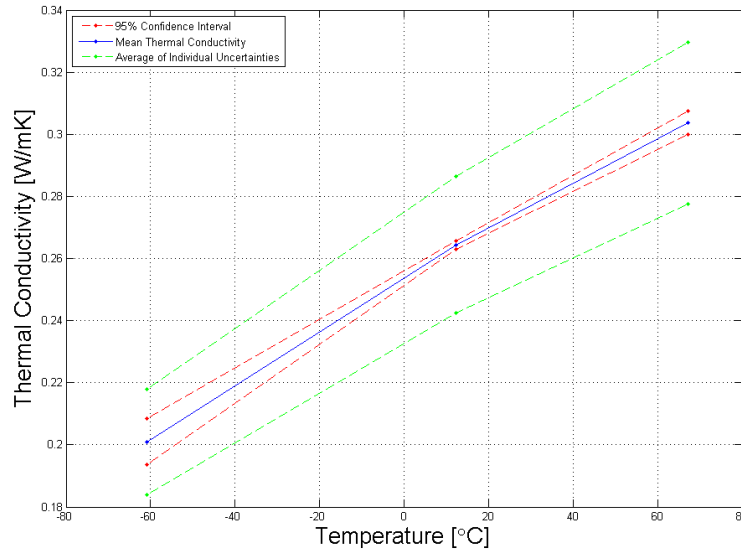


**Figure 6.10.:** Sand: Conductivity versus Temperature

The three results indicates a linear trend. Unfortunately, the conductivity of solid sand was not found; therefore, it was not possible to estimate the conductivity. Table values from Çengel shows that sand has a conductivity between  $0.2 - 1.0 \frac{W}{mK}$ , the measured values are within these limits.

The average of the individual uncertainties show that the conductivity may differ up to 10% from the mean. The confidence interval shows that the three calculations in each measurement corresponds satisfactory.

**6.4 Expancel**

6.4.1. Individual Measurements

May 26 - Measurement Expancel

Date	May 26	Specimen	Expancel
Filename	0526.xlsx	Density	$\rho = 42 \frac{kg}{m^3}$
Thermocouple Position	$r_1 = 3.38mm$ $r_2 = 7.21mm$ $r_3 = 13.91mm$	Thermocouple Deviation	$T_1 = +1.7179K$ $T_2 = +1.7828K$ $T_3 = +1.8413K$
Cooling Method	Nitrogen	Side Wall Temperature	$T_{wall} = \div 113.0 - \div 117.0^{\circ}C$
Power Supply	$U = 9.7V$ $I = 30.0mA$ $Q = 0.291W$	Uncertainties	$\delta \dot{Q}_r = \pm 0.013W$ $\delta r = \pm 0.21mm$ $\delta h = \pm 5mm$ $\delta \Delta T = \pm 0.1K$
Steady State Temperatures	$T_1 = \div 74.843^{\circ}C$ $T_2 = \div 89.835^{\circ}C$ $T_3 = \div 103.418^{\circ}C$	Thermal Conductivity	$k(T_{1-2}) = 0.023 \pm 0.003 \frac{W}{mK}$ $k(T_{2-3}) = 0.022 \pm 0.002 \frac{W}{mK}$ $k(T_{1-3}) = 0.023 \pm 0.002 \frac{W}{mK}$

**Table 6.10.:** Expancel: Measurement Conditions and Results, May 26

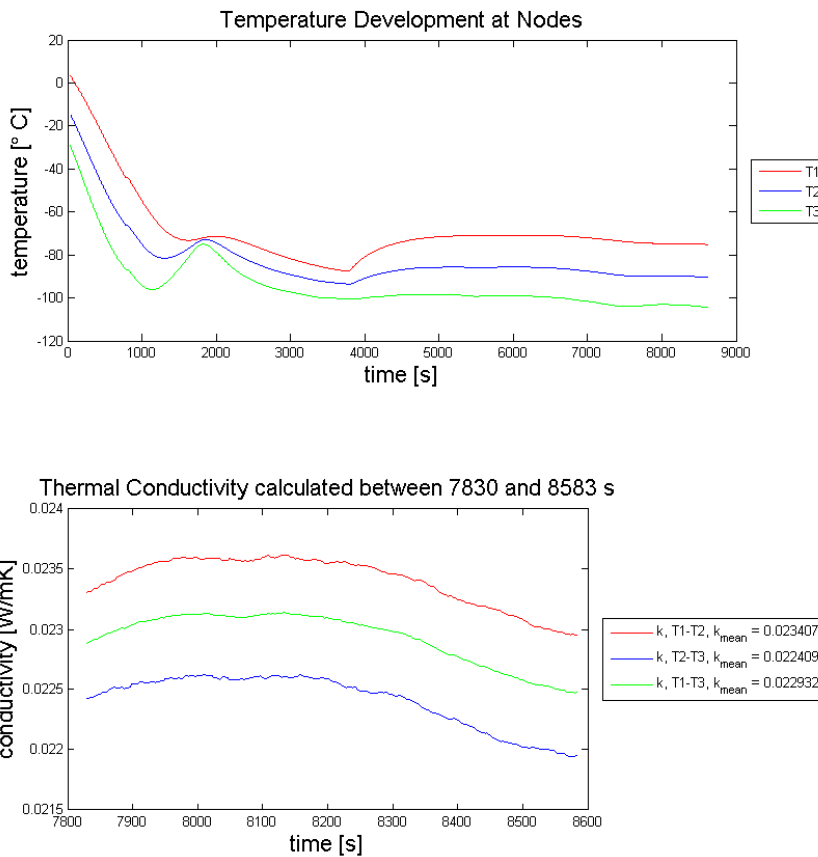


**Figure 6.11.:** Expancel: Measurement Conditions and Results, May 26

The coolant temperature was stabilized after approximately 6000 seconds. The results indicate that the position of  $T_2$  is below the measured value. Water condensates and freezes on the rig at lower temperatures, it is not known how this affects the measurement.

May 28 - Measurement Expancel - 1

Date	May 28	Specimen	Expancel
Filename	0528_1.xlsx	Density	$\rho = 42 \frac{kg}{m^3}$
Thermocouple Position	$r_1 = 3.38mm$ $r_2 = 8.09mm$ $r_3 = 13.91mm$	Thermocouple Deviation	$T_1 = +1.7179K$ $T_2 = +1.7828K$ $T_3 = +1.8413K$
Cooling Method	Tap Water	Side Wall Temperature	$T_{wall} = 11.8 - 12.5^\circ C$
Power Supply	$U = 7.3V$ $I = 22.0mA$ $Q = 0.1606W$	Uncertainties	$\delta Q_r = \pm 0.010W$ $\delta r = \pm 0.21mm$ $\delta h = \pm 5mm$ $\delta \Delta T = \pm 0.1K$
Steady State Temperatures	$T_1 = 19.909^\circ C$ $T_2 = 14.560^\circ C$ $T_3 = 11.314^\circ C$	Thermal Conductivity	$k(T_{1-2}) = 0.042 \pm 0.005 \frac{W}{mK}$ $k(T_{2-3}) = 0.043 \pm 0.004 \frac{W}{mK}$ $k(T_{1-3}) = 0.042 \pm 0.004 \frac{W}{mK}$

Table 6.11.: Expancel: Measurement Conditions and Results, May 28 - 1

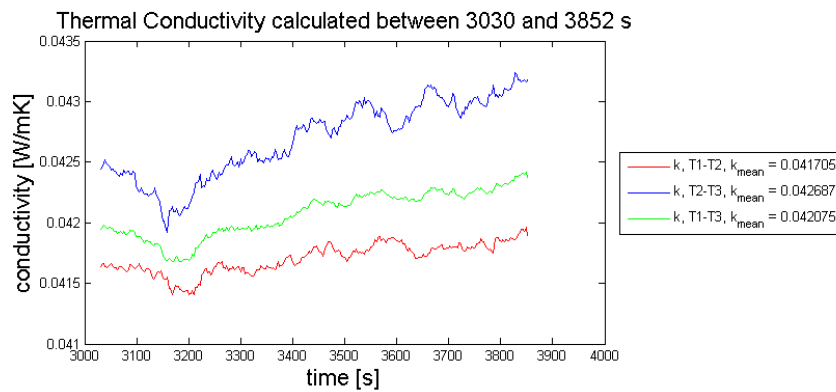
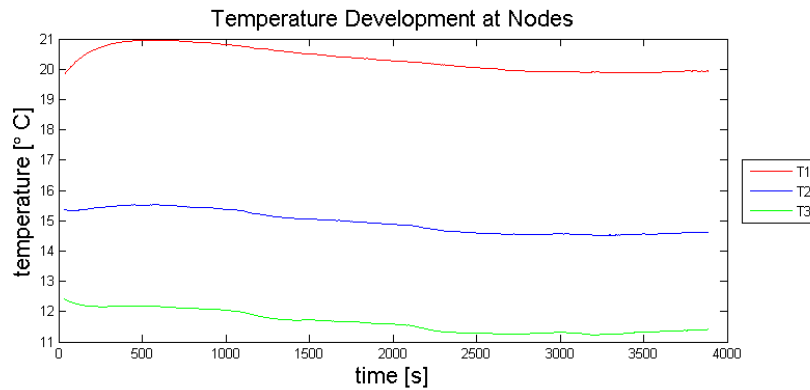


Figure 6.12.: Expancel: Measurement Conditions and Results, May 28 - 1

The tap water stabilized quickly, and the measurement was done within one hour. The results indicate that the position of  $T_2$  was above the measured value.

May 28 - Measurement Expancel - 2

Date Filename	May 28 0528_2.xlsx	Specimen Density	Expancel $\rho = 42 \frac{kg}{m^3}$
Thermocouple Position	$r_1 = 3.38mm$ $r_2 = 8.09mm$ $r_3 = 13.91mm$	Thermocouple Deviation	$T_1 = +1.7179K$ $T_2 = +1.7828K$ $T_3 = +1.8413K$
Cooling Method	Tap Water	Side Wall Temperature	$T_{wall} = 52.0 - 54.0^\circ C$
Power Supply	$U = 7.3V$ $I = 22.0mA$ $Q = 0.1606W$	Uncertainties	$\delta Q_r = \pm 0.010W$ $\delta r = \pm 0.21mm$ $\delta h = \pm 5mm$ $\delta \Delta T = \pm 0.1K$
Steady State Temperatures	$T_1 = 56.409^\circ C$ $T_2 = 53.414^\circ C$ $T_3 = 52.064^\circ C$	Thermal Conductivity	$k(T_{1-2}) = 0.075 \pm 0.009 \frac{W}{mK}$ $k(T_{2-3}) = 0.103 \pm 0.013 \frac{W}{mK}$ $k(T_{1-3}) = 0.084 \pm 0.008 \frac{W}{mK}$

Table 6.12.: Expancel: Measurement Conditions and Results, May 28 - 2

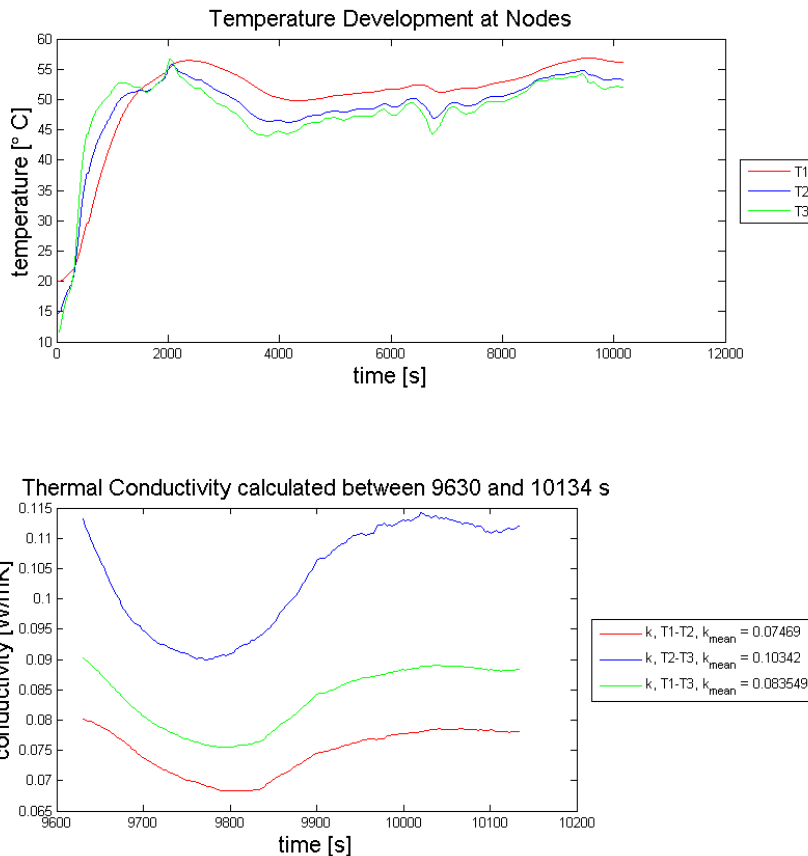


Figure 6.13.: Expancel: Measurement Conditions and Results, May 28 - 2

The measurement was carried out without emptying and refilling the rig from the previous measurement, the positions are therefore the same. Once again, the results indicate that the position of  $T_2$  was above the measured value. The temperature of the tap water would not stabilize properly which in particular affects the calculation of  $k(T_{2-3})$ .



6.4.2. Overall Result

The confidence interval has been calculated around the mean of each measurement with  $t_{0.025} = 4.303$  when  $n = 3$  [8, Table A.4]. Note that the three calculations not are independent.

$$\begin{array}{l|l|l}
 T_{avg} = \div 89.4^{\circ}C & 0.021232 < 0.022667 < 0.024101 & \delta\bar{k} = 0.0023 \\
 T_{avg} = 15.3^{\circ}C & 0.040899 < 0.042333 < 0.043768 & \delta\bar{k} = 0.0043 \\
 T_{avg} = 54.0^{\circ}C & 0.051821 < 0.087333 < 0.12285 & \delta\bar{k} = 0.010
 \end{array}$$

**Table 6.13.:** Expancel: 95% Confidence Interval around the Mean and Average of Individual Uncertainties

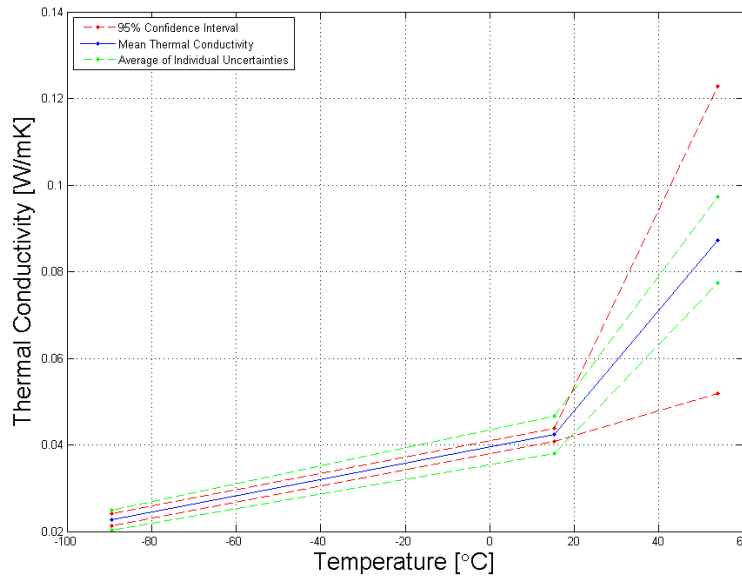


**Figure 6.14.:** Expancel: Conductivity versus Temperature

The confidence interval indicates that the reliability of the calculation at  $54^{\circ}C$  is low which was explained by fluctuations in the hot water supply. The average of the individual uncertainties are around 10% for these measurements as well, the error is however likely to be greater in this case. Expancel has a conductivity below the lower limit of the rig which means that more heat will be transported axially.

**6.5 Discussion**

The rig has delivered results for all the materials that were tested in a wide temperature range. All the results indicates that the conductivity for a material increase along with the temperature. Based on the uncertainties that were determined in section 4.4, each individual measurement has an uncertainty around 10%. The temperatures have been calculated as the average of the measurements under steady state; in addition, the measurements have been smoothed out using equation 4.1 to remove fluctuations. According to Moffat (appendix B.4) is the best estimation of a variable the mean plus or minus the uncertainty interval. This statement has been used in the uncertainty analysis; moreover, the uncertainty intervals are assumed to be equal in all measurements and are calculated from the calibration of the thermocouples.

For each material, the overall result has been presented with the average of the individual uncertainties and a 95% confidence interval of the mean conductivity. The purpose of the confidence interval is mainly to illustrate how the data should be treated when multiple independent measurements are present. This means that several measurements should be carried out at the same temperature to use this method correct. The confidence interval results presented are not independent since they are all from one measurement.

All of the measurements have in common that the calculated conductivity between  $T_1$  and  $T_3$  is in the middle of the three calculations. This can be an indicator of a wrong position measurement of  $T_2$ . Note that small deviations in the positioning affects the results since the diameter of the rig is very small.

In the prestudy, the lowest conductivity for the specimen was set to  $0.1 \frac{W}{mK}$  with Styrofoam as insulation. Therefore, the results for expancel are not considered to be reliable since heat will be transported axially as well as radial.

The measurements have been performed using a coolant fluid to deliver constant temperature at the side wall of the rig. Tap water was used for measurements above  $10^\circ C$ , and nitrogen for colder temperatures. The temperature range of the measurements were between  $\div 137$  and  $67.3^\circ C$  at the most. For both coolant liquids, it turned out to be a far-reaching process to obtain a constant temperature. Regarding the tap water, it all depended on the water supply that had a tendency to fluctuate and interfere with the steady state process in the rig. The bottle connected between the rig and tap water (see figure 4.4) turned out to have little effect in leveling out the fluctuations. It might work better if the bottle had a larger volume. Anyway, a more stable water cooling solution is considered to be the major improvement point of the rig. The nitrogen supply was easier to regulate as the mass flow and temperature from the tank were constant. A constant cooling temperature was reached when the temperature of the heater and nitrogen fell in balance. At low temperatures, water condensates and freezes on the rig, it is not known how this affects the specimen inside the rig.

The importance of outer insulation increase for measurements at temperatures under room temperature as heat may enter the rig. The rig has been insulated properly with Styrofoam and Armaflex (see figure 4.8) to avoid this; however, it should be investigated with COMSOL or a similar program to ensure that there is no leaks. For measurements at higher temperatures, the risk of axial heat transportation increase, this should also be investigated.

## 6.6 Further Work

- To make the rig more flexible of measurements at different temperatures, the side wall cooling should be developed further. The tap water is not able to deliver constant temperature over longer time periods and makes it a far-reaching process to obtain steady state in the rig.
- The thermocouples have only been calibrated in ice-water, they should be calibrated at other temperatures as well such as boiling water and nitrogen. The results should be used to create a calibration curve.
- Under measurements of the hydrogen storage material, several measurements should be carried out at the same temperature. The t-Distribution from appendix B.3 should be used to calculate a 95% confidence interval.
- The test rig is only capable of measurements under atmospheric pressure. To perform measurements under other pressures, the rig must be sealed and connected to a compressor. The maximum pressure that the rig can handle should be determined.
- The temperature at the heating cartridge and side wall have been assumed to be equal over the whole surface. This need to be verified and can be done using several thermocouples or a thermal imaging camera. Further investigation may reduce the uncertainty of  $\delta h$  and  $\delta \dot{Q}_r$ . As mentioned in the discussion, heat leaks should be investigated further in COMSOL.



## PERMEABILITY MEASUREMENT RESULTS

### 7.1 Introduction

The permeability has been measured on the materials listed below, the materials are described further in appendix C.

- Sugar
- Sand
- Expancel

In front of a measurement, the permeability has been estimated based on the mean body diameter size,  $d_{gr}$ , and the tabulated values for  $\varphi$  and  $\varepsilon$  found in appendix D. The laminar flow range has been calculated; however, the measurements have been run over the whole flow range of the rotameter as long as the pressure loss not has exceeded its maximum (7000Pa). Measurements with pressure loss beneath 15Pa have been neglected. The single-sample uncertainty has been calculated for each sampling point.

The calculated permeability, the average, and the individual uncertainty have been plotted against the actual volume flow. The relative uncertainty ( $\frac{\delta\kappa}{\kappa}$ ) has been plotted underneath to indicate the reliability of the measurements. In addition, the permeability has been plotted against the Reynolds number defined by Idelchik (equation 3.20), and the parameters  $\varepsilon$  and  $\varphi$  have been modified to match the measurements. The uncertainties listed in table 7.1 have been used in all of the measurements.

The permeability and the uncertainty has been calculated based on the average measurements where the relative uncertainty  $\frac{\delta\kappa}{\kappa}$  are below 15%.

$\delta Q$	$\delta\Delta P$	$\delta\mu$	$\delta L$
Section 5.3.4	$\pm 7\text{Pa}$	$0.025 \cdot 10^{-5} \frac{\text{kg}}{\text{ms}}$	$\pm 2\text{mm}$

**Table 7.1.:** Uncertainties Permeability Rig

## 7.2 Sugar

### 7.2.1. Estimation

The mean size diameter of the body has been measured using a slide caliper to be  $d_{gr} = 0.90\text{mm}$ , ten measurements were done on ten bodies. The permeability has been estimated using  $\phi$  and  $\varepsilon$  from polydisperse beach sand (appendix D) and the method from section 3.5.

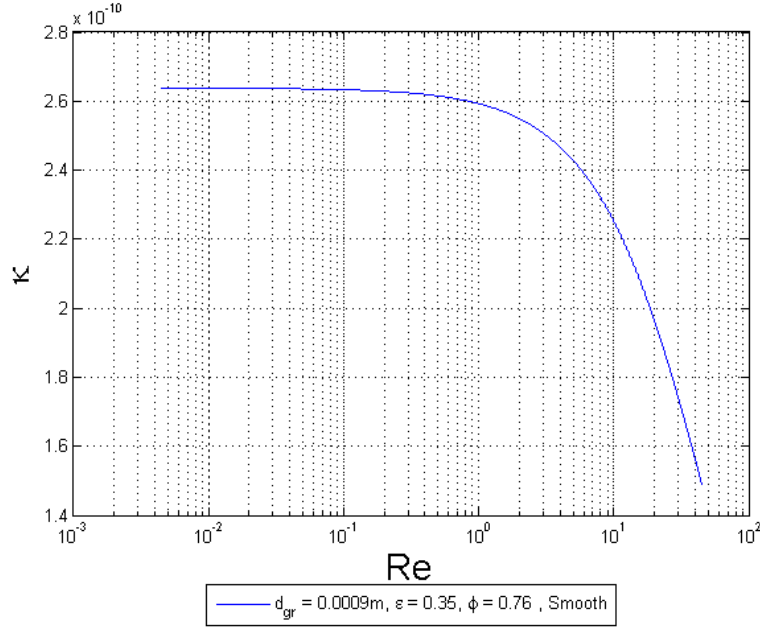


**Figure 7.1.:** Permeability Estimation Sugar

The pressure loss at  $Re = 10^{-1}$  can then be estimated with equation 3.25 to be:

$$\Delta P = \frac{Re \cdot \mu^2 L}{\rho d_{el} \kappa} = \frac{0.1 \cdot (1.825 \cdot 10^{-5} \text{Pa} \cdot \text{s})^2 \cdot 0.1 \text{m}}{1.204 \frac{\text{kg}}{\text{m}^3} \cdot 0.76 \cdot (0.9 \cdot 10^{-3} \text{m}) \cdot 2.65 \cdot 10^{-10} \text{m}^2} = 15.3 \text{Pa} \quad (7.1)$$

There are many parameters in this estimation that may differ, but at least the order of magnitude of the pressure loss is determined. Likewise, the maximum volume flow for laminar flow can be approximated (equation 3.24):

$$Q_{max} = \frac{10^{-1} \cdot (1.52 \cdot 10^{-5} \frac{\text{m}^2}{\text{s}})}{0.76 \cdot (0.9 \cdot 10^{-3} \text{m})} \cdot \frac{\pi}{4} \cdot (0.04 \text{m})^2 = 2.79 \cdot 10^{-6} \frac{\text{m}^3}{\text{s}} = 0.167 \frac{\text{l}}{\text{min}} \quad (7.2)$$

7.2.2. June 2 - Measurement Sugar

Q [l/min]	$\Delta P$ [Pa]	Q [l/min]	$\Delta P$ [Pa]
0.3561	25.0	2.9075	240.0
0.3780	28.0	3.1549	269.0
0.4087	31.0	3.3898	293.0
0.4743	41.0	3.7605	335.0
0.9757	72.0	4.1313	371.0
1.3474	112.0	4.5661	407.0
1.6818	145.0	5.6613	552.0
2.2128	197.0	5.9021	554.0
2.3134	190.0	6.8581	668.0

Table 7.2.: Sugar: Measurement Data

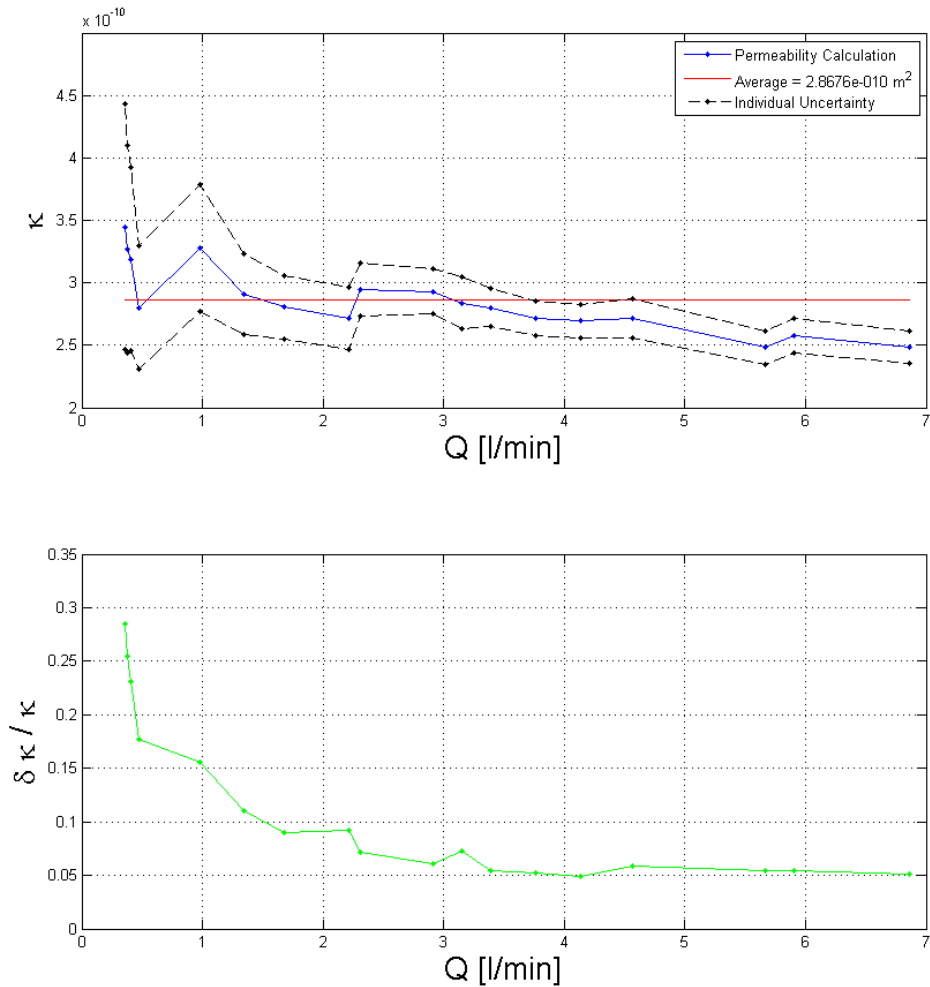
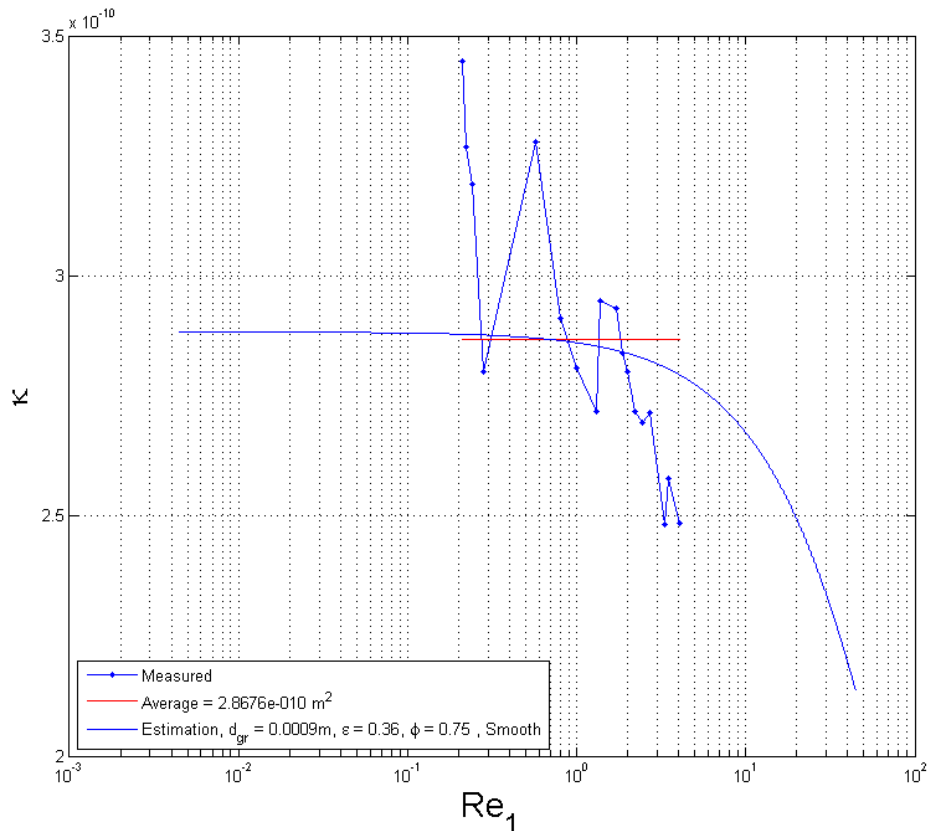


Figure 7.2.: Sugar: Measurement Results and Uncertainties

The average permeability based on the measurements between 1 and 6.8 l/min is  $\kappa = (2.80 \pm 0.2) \cdot 10^{-10} m^2$ . However, the measurements with sufficient pressure loss were

at much higher flow rates than the limit estimated for laminar flow. It indicates that the measurements are taken outside the validity range of Darcy's Law which also is visible in the decreasing plots. The length of the rig should be extended to increase the pressure loss at low flow rates.



**Figure 7.3.:** Sugar: Results and Estimation Plotted Together

The parameters have been set to  $\epsilon = 0.36$  and  $\phi = 0.75$  to match the average. The measurements indicate that the permeability sinks for higher Reynolds numbers; however, few and inaccurate measurements in the lower range makes it difficult to achieve a constant value for the permeability. It is therefore hard to determine if the measurements and estimation follow the same tendency.



### 7.3 Sand

#### 7.3.1. Estimation

The mean size diameter of the body has been measured using a slide caliper to be  $d_{gr} = 0.71\text{mm}$ , ten measurements where done on ten bodies. The permeability has been estimated using  $\phi$  and  $\epsilon$  from polydisperse beach sand (appendix D) and the method from section 3.5.

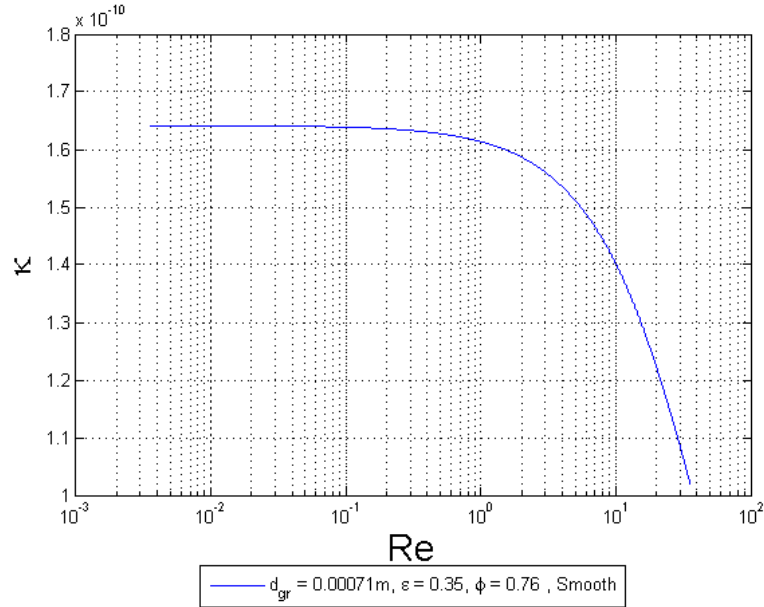


**Figure 7.4.:** Permeability Estimation Sand

The pressure loss at  $Re = 10^{-1}$  can then be estimated with equation 3.25 to be:

$$\Delta P = \frac{Re \cdot \mu^2 L}{\rho d_{el} \kappa} = \frac{0.1 \cdot (1.825 \cdot 10^{-5} \text{ Pa} \cdot \text{s})^2 \cdot 0.1 \text{ m}}{1.204 \frac{\text{kg}}{\text{m}^3} \cdot 0.76 \cdot (0.71 \cdot 10^{-3} \text{ m}) \cdot 1.65 \cdot 10^{-10} \text{ m}^2} = 31.1 \text{ Pa} \quad (7.3)$$

The corresponding volume flow is:

$$Q_{max} = \frac{10^{-1} \cdot (1.52 \cdot 10^{-5} \frac{\text{m}^2}{\text{s}})}{0.76 \cdot (0.71 \cdot 10^{-3} \text{ m})} \cdot \frac{\pi}{4} \cdot (0.04 \text{ m})^2 = 3.54 \cdot 10^{-6} \frac{\text{m}^3}{\text{s}} = 0.213 \frac{\text{l}}{\text{min}} \quad (7.4)$$

### 7.3. SAND

#### 7.3.2. May 27 - Measurement Sand

Q [l/min]	$\Delta P$ [Pa]	Q [l/min]	$\Delta P$ [Pa]
0.4831	17.0	2.6493	88.0
0.4835	17.0	3.6058	133.0
0.5538	22.0	3.6813	129.0
0.6871	31.0	3.7643	135.0
0.7877	35.0	4.1357	155.0
0.8643	24.0	4.7808	180.0
1.2182	45.0	5.4088	211.0
1.4594	50.0	5.5916	211.0
1.8109	67.0	6.4875	257.0
2.2665	81.0		

**Table 7.3.:** Sand: Measurement Data

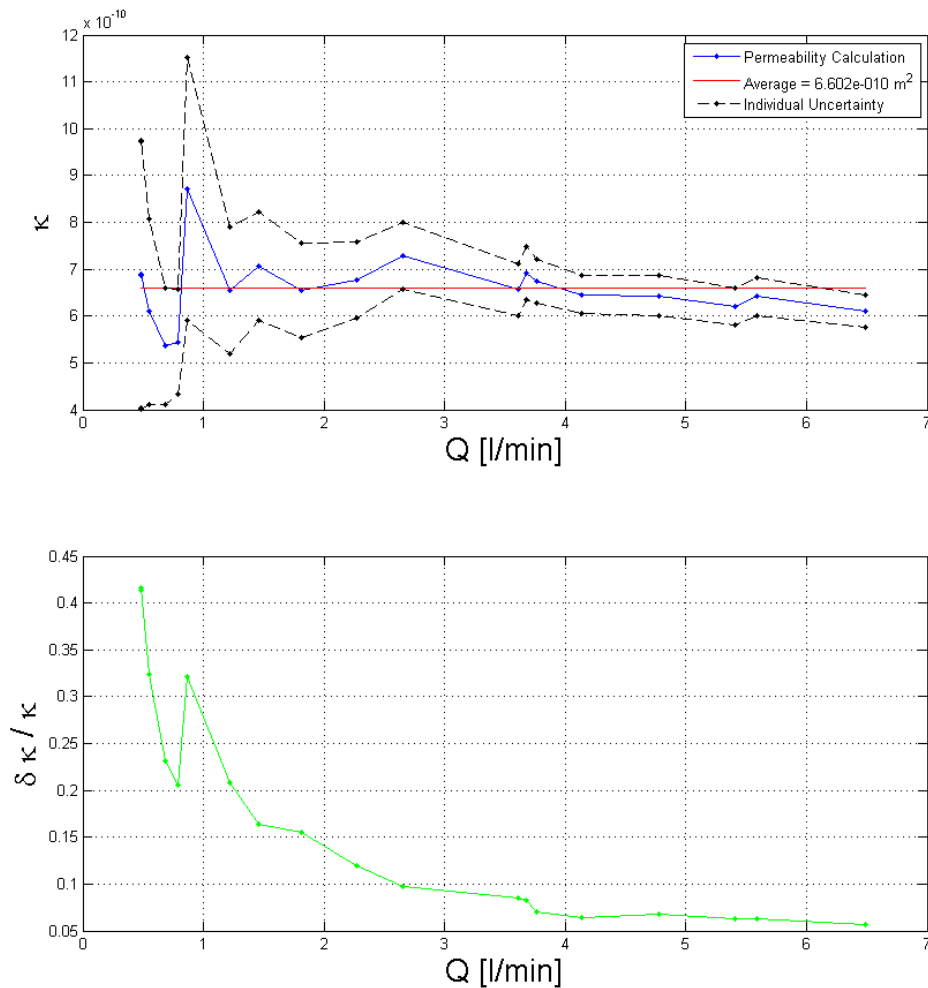


**Figure 7.5.:** Sand: Measurement Results and Uncertainties

The uncertainties in the measurements below 2 l/min are above 15%. The average permeability based on the measurements between 2 and 6.5l/min is  $\kappa = (6.60 \pm 0.52) \cdot 10^{-10} m^2$ . However, the measurements with sufficient pressure loss were at much higher flow rates than the estimated limit for laminar flow. The permeability seems nevertheless to remain constant for flow rates below 4 l/min.

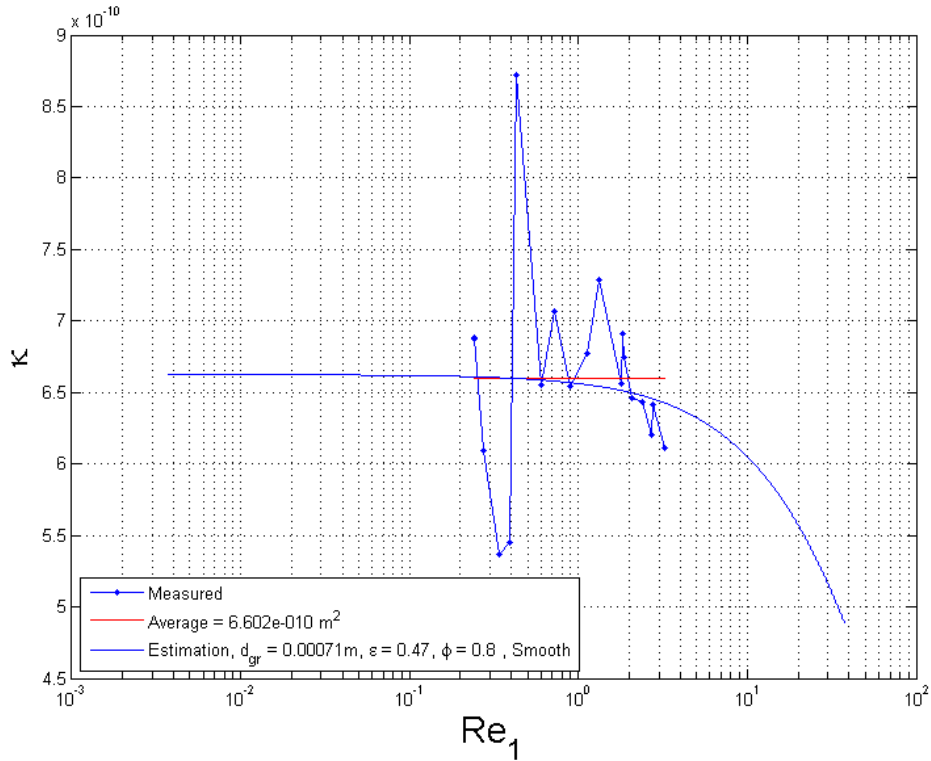


Figure 7.6.: Sand: Results and Estimation Plotted Together

The parameters have been modified to match the results better, they are in fact quite similar with the properties of bank sand in appendix D. Note that the uncertainty in the first six measurements are above 20% which can be an explanation for the deviations in the beginning. Measurements over a wider flow range are necessary to determine if the estimation and results corresponds.

## 7.4 Expancel

### 7.4.1. Estimation

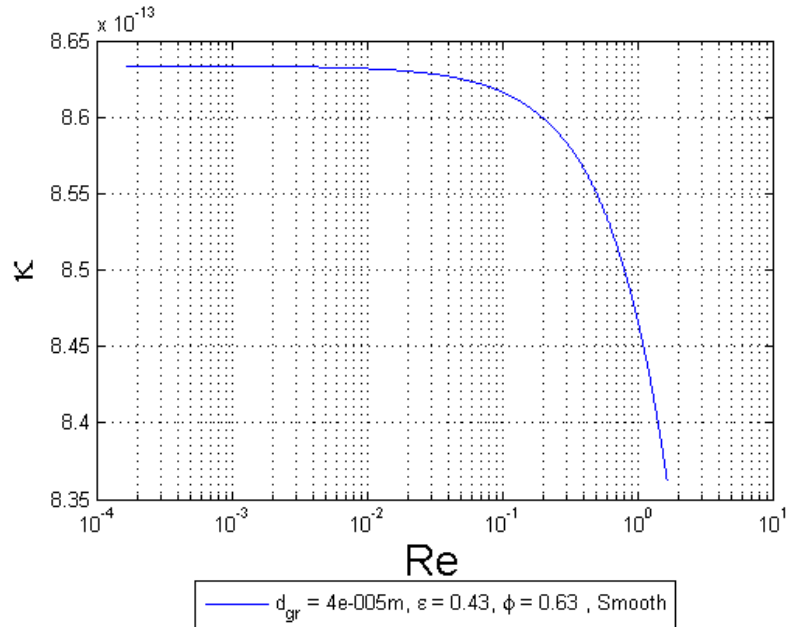


Figure 7.7.: Permeability Estimation Expancel

The parameters for quartz sand were used in the estimation.

$$\Delta P = \frac{Re \cdot \mu^2 L}{\rho d_{el} \kappa} = \frac{0.01 \cdot (1.825 \cdot 10^{-5} Pa \cdot s)^2 \cdot 0.1 m}{1.204 \frac{kg}{m^3} \cdot 0.63 \cdot (40 \cdot 10^{-6} m) \cdot 8.63 \cdot 10^{-13} m^2} = 12720 Pa \quad (7.5)$$

$$Q_{max} = \frac{10^{-2} \cdot (1.52 \cdot 10^{-5} \frac{m^2}{s})}{0.63 \cdot (40 \cdot 10^{-6} m)} \cdot \frac{\pi}{4} \cdot (0.04 m)^2 = 7.58 \cdot 10^{-6} \frac{m^3}{s} = 0.455 \frac{l}{min} \quad (7.6)$$

It should be mentioned that the selected parameters not have any relation to expancel; they were chosen since quartz sand is the material with smallest mean size body diameter in appendix D.

7.4.2. June 1 - Measurement Expancel

Q [l/min]	$\Delta P$ [Pa]	Q [l/min]	$\Delta P$ [Pa]
0.0934	315	0.3311	1977
0.1370	423	0.3738	2326
0.1805	655	0.4370	3104
0.2238	940	0.4790	3617
0.2667	1435		

Table 7.4.: Expancel: Measurement Data

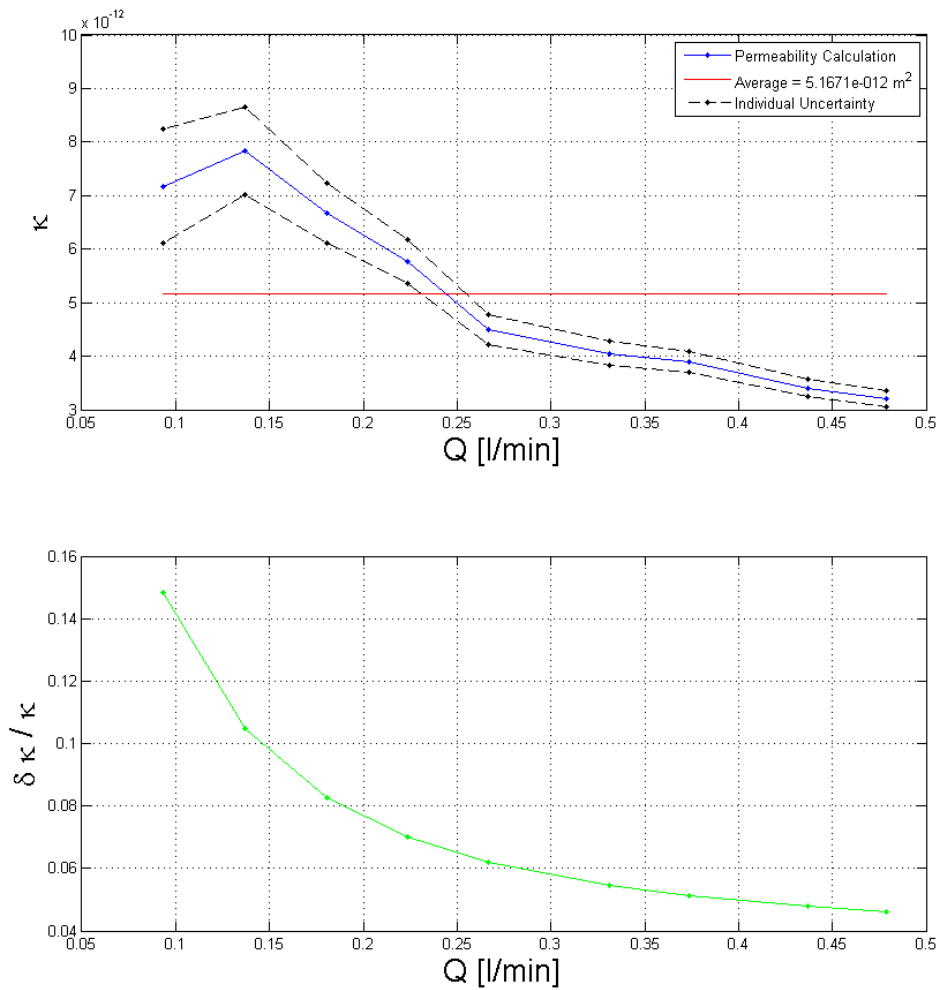
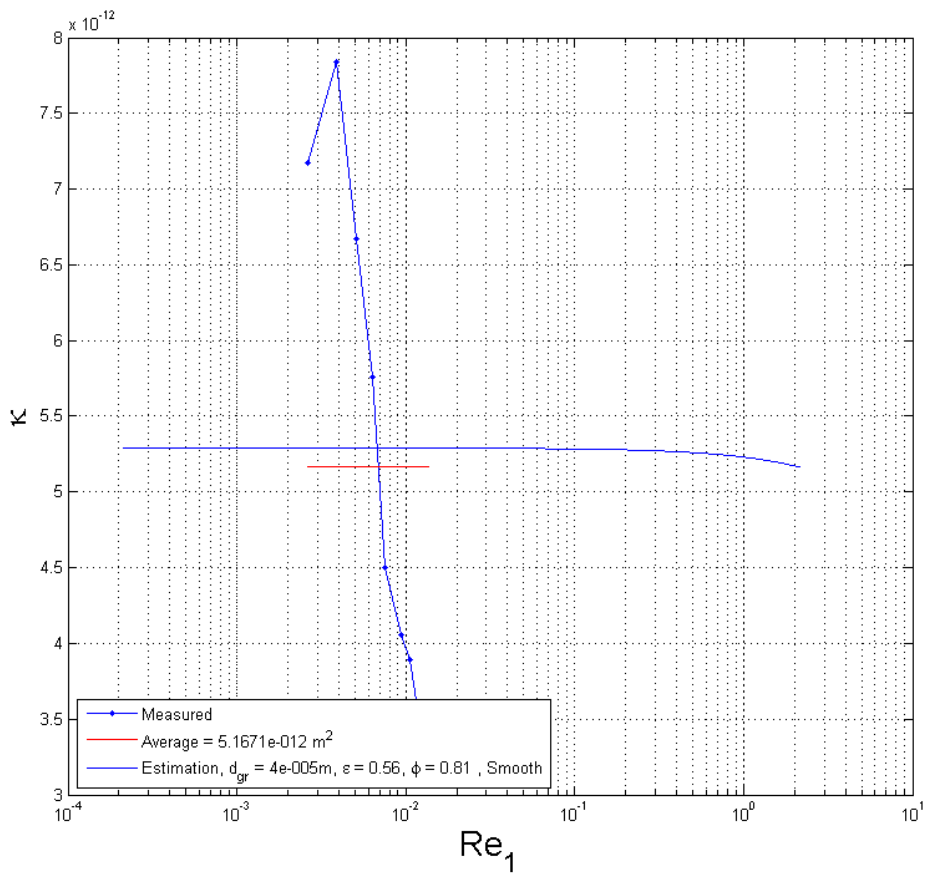


Figure 7.8.: Expancel: Measurement Results and Uncertainties

The compression of the material became visible when the flow rate was increased; therefore, it is reasonable that the slope of the pressure loss rises faster than the volume flow. To obtain a constant value for the permeability, the slope of the volume flow and pressure loss should be the same. This states that the rig not is capable of measurements on a material that change volume under different flow rates.



**Figure 7.9.:** Expancel: Results and Estimation Plotted Together

The parameters of the estimation have been modified to match the average; however, the plot clearly shows that there is no relation between the estimation and result.

**7.5 Discussion**

Taken into account that the rig has been developed and built from scratch this semester with the empirical formulas from Idelchik [6] as the only reference, the development can be said to be satisfactory. However, the pressure loss in the laminar flow regime turned out to be smaller than the accuracy of the pressure indicator. Since the length and pressure drop are proportional, it is suggested to extend the length of the tube. The results show that the uncertainty increase at low pressure losses. It should be fully achievable to get measurement results with less than 10% inaccuracy based on the assumed uncertainties, note that the rig not has been calibrated.

The length and diameter were chosen to match the thermal conductivity rig, it is now clear that the length must be increased. Darcy's Law is applicable for creeping flow only, and the estimations have shown that the Reynolds number based on pore size length scale (equation 3.20) not should exceed  $Re_{max}$ . When the mean body diameter  $d_{gr}$  is known, it can be used to find the maximum superficial velocity  $w_1$ . The superficial velocity can then be used to find the optimal diameter that ensures creeping flow within the measurement limits of the rotameter. With a specified diameter, the length of the tube can be calculated from the desired pressure loss.

The rig was also tested on a material where the flow rates were within the laminar flow range; however, the material turned out to compress itself when the flow rate increased. The permeability was therefore not to be considered as a constant value during the measurements.

**7.6 Further Work**

- The instruments must be calibrated.
- Room temperature has been assumed in the whole rig. To calculate the density of the air more accurate, thermocouples should be placed at the rotameter, and before and after the specimen (position 2, 3, and 4 in figure 5.2).
- To make the rig capable of measurements on materials that shrinks under higher pressures, it is necessary to keep the material equally compressed under the whole measurement. This can be done by compressing the material at atmospheric pressure and maintain it compressed with a filter.
- The length of the tube should be extended to increase the pressure loss at low flow rates.





---

---

PART IV

---

Closure



## THERMAL CONDUCTIVITY

### **8.1** Conclusion

A complete test rig for thermal conductivity measurements has been developed and built. In the prestudy, simulations were performed to assess the temperature and heat flow distribution in the rig. The necessary conductivity of the insulation was found to obtain radial heat flux, and the required power for the heating cartridge was determined. To identify which variables that were most affecting, a single-sample analysis was carried out. The uncertainty of each variable were determined when the instruments and equipment were calibrated. In cooperation with the Department, three different materials were selected for thermal conductivity measurements in lack of the hydrogen storage materials the rig is intended for. Nevertheless, measurements were carried out in a wide temperature range with satisfactory results. Each result has been presented with its uncertainty, roughly around 10%. It turned out to be difficult to compare the results properly with literature models and tabulated data since few of the material properties were known. In addition to the single-sample analysis, it has been suggested to use the t-Distribution to calculate confidence intervals around the mean when multiple measurements are present. In this report, 95% confidence intervals have been calculated based on the three calculations from each measurement with the intention of demonstrating the principle.

Each individual measurement has an uncertainty around 10%. Further investigation of the heat flux may reduce the uncertainty of the height  $\delta h$  and the heat flux  $\delta \dot{Q}_r$ , as mentioned in further work (section 6.6). Based on the statement that the best estimation of a measured variable is the average plus or minus the uncertainty interval (appendix B.4), the measured temperatures at steady state have been averaged. The uncertainty interval was calculated from the calibration measurement in ice water and assumed to be constant for all measurements. What affects the result the most is however positioning of the thermocouples. The result is very sensitive for small deviations in the radial position.

Due to the small dimensions, the rig can reach steady state relatively fast. However, this requires a constant temperature on the side wall. Small temperature deviations interfere with the process and makes the measurement time consuming. The tap water was in particular hard to maintain at a constant temperature, and stated that the rig needs its own cooling system which not relies on a stable tap water temperature. For

## 8.1. CONCLUSION

---

low temperatures, liquid nitrogen turned out to work sufficiently combined with a heater that delivers constant power.

Measurement results indicates that the conductivity for a material increase with the temperature. To ensure that the rig transports the heat radial, the lower conductivity limit was set to  $0.1 \frac{W}{mK}$  for the specimen. For measurements on specimens with lower conductivity, the insulation must be improved. The three conductivity calculations at each measurement have increased the reliability of the results, but several measurements must be performed at the same temperature to validate the measurements.

To sum it up, the measurements have proven that the rig is capable of measurements in a wide temperature range for small specimens. Small dimensions results in a fast responding rig, but does also increase the uncertainties.

## PERMEABILITY

### **9.1** Conclusion

Based on the principles of Darcy's law, a permeability measurement rig has been developed and built. The pressure loss have been assumed to only be caused by the material; hence, the wall friction has been neglected. To estimate the magnitude of the permeability and the corresponding flow rate and pressure loss, an empirical model has been used which is based on material packing and diameter. The estimates of the permeability states the given validity of Darcy's law which only is for slow viscous flow, called creeping flow or Stokes flow. The pressure drop was shown to vary greatly for different pore sizes under the maximum valid flow rate. A single-sample analysis has been carried out where the uncertainties of each variable have been estimated or taken from tabulated data. Without being calibrated, the results indicate that an uncertainty less than 10% should be fully attainable. In cooperation with the Department, three different materials were selected for permeability measurements in lack of the hydrogen storage materials the rig is intended for. The measurements were performed within the flow range of the rotameter. The permeability property is assumed independent of the fluid as long as the size of the molecules not are greater than the void space in the material. This means that the results achieved with air as fluid are valid for hydrogen as well.

The measurements proved that the rig is capable of permeability measurements for non-compressible materials; however, it is clear that the geometry of the rig should be modified. Since Darcy's law only is applicable for creeping flow, the measured permeability is only valid for flow under these conditions. It was not successful to obtain permeability measurements for the selected materials in the valid flow range. The pressure loss turned out to be too small, and it is therefore suggested to extend the length since it is proportional with the pressure loss. Higher pressure losses decrease the uncertainty of the result. In order to obtain proper permeability measurements, it is necessary to know the mean size body diameter of the materials. The geometry of the rig can then be optimized for the flow rate limits to achieve the necessary pressure loss.



## BIBLIOGRAPHY

- [1] Kristoffer Abrahamsen. Development of Thermal Solution for Hydrogen Storage in Porous Structures. Technical report, Norwegian University of Science and Technology, Department of Energy and Process Engineering, 2009.
- [2] A. Bhattacharya, V.V. Calmidi, and R.L. Mahajan. Thermophysical properties of high porosity metal foams. *International Journal of Heat and Mass Transfer*, 45:1017–1031, 2002.
- [3] Yunus A. Çengel. *Heat and Mass Transfer: A Practical Approach (Third Edition)*. McGraw Hill, 2006.
- [4] Targets for Onboard Hydrogen Storage Systems for Light-Duty Vehicles. Technical Report Revision 4.0, U.S. Department of Energy, September 2009.
- [5] James Joosten et. al. The Impact of Increased Use of Hydrogen on Petroleum Consumption and Carbon Dioxide Emissions. Technical Report SR-OIAF-CNEAF/2008-04, U.S. Energy Information Administration, August 2008.
- [6] I.E. Idelchik. *Handbook of Hydraulic Resistance, 3rd Edition*. Begell House, Inc., 1996.
- [7] Robert J. Moffat. Describing the Uncertainties in Experimental Results. *Experimental Thermal and Fluid Science*, 1:3–17, 1988.
- [8] Ronald E. Walpole, Raymond H. Myers, Sharon L. Myers, and Keying Ye. *Probability & Statistics for Engineers & Scientists (Eight Edition)*. Pearson Education International, 2007.
- [9] Stephen Whitaker. Flow in Porous Media 1: A Theroretical Deviation of Darcy’s Law. *Transport in Porous Media*, 1986.
- [10] Frank M. White. *Fluid Mechanics, Fifth Edition*. McGraw Hill, 2005.





## EQUIPMENT AND MATERIAL REFERENCES

- [11] Precision Valve and Gauge, Bosch Rexroth R412004417. [http://www.boschrexroth.com/pneumatics-catalog/content/allplatforms/vornavigation/xmedia/internet/en/pdf/PDF\\_g5386\\_en.pdf](http://www.boschrexroth.com/pneumatics-catalog/content/allplatforms/vornavigation/xmedia/internet/en/pdf/PDF_g5386_en.pdf), May 2010.
- [12] Properties of Expancel 551 DE 40 d42. [http://www.akzonobel.com/expancel/system/Images/AkzoNobel\\_Expancel\\_DE\\_product\\_specification\\_tcm65-31855.pdf](http://www.akzonobel.com/expancel/system/Images/AkzoNobel_Expancel_DE_product_specification_tcm65-31855.pdf), May 2010.
- [13] Pressure Indicator, GE Druck DPI 705. [http://www.gesensing.com/downloads/datasheets/920\\_109a.pdf](http://www.gesensing.com/downloads/datasheets/920_109a.pdf), May 2010.
- [14] USB Single Module Carrier, National Instruments. <http://sine.ni.com/nips/cds/view/p/lang/en/nid/204178>, April 2010.
- [15] Thermocouple Input Module, National Instruments. <http://sine.ni.com/nips/cds/view/p/lang/en/nid/14165>, April 2010.
- [16] Power Supply, Angilent 3612A. [https://www1.elfa.se/data1/wwwroot/assets/datasheets/loE36xxA\\_data\\_en.pdf](https://www1.elfa.se/data1/wwwroot/assets/datasheets/loE36xxA_data_en.pdf), May 2010.
- [17] Properties of Styrofoam HD300. [http://building.dow.com/ap/in/prod/styro\\_hd300.htm](http://building.dow.com/ap/in/prod/styro_hd300.htm), February 2010.
- [18] Thermocouples Type K, Max Sievert AS. [http://www.maxsievert.no/filemanager/download\\_file/file/108126](http://www.maxsievert.no/filemanager/download_file/file/108126), May 2010.



---

---

PART V

---

Appendices



**A.1 Thermal Conductivity Rig**

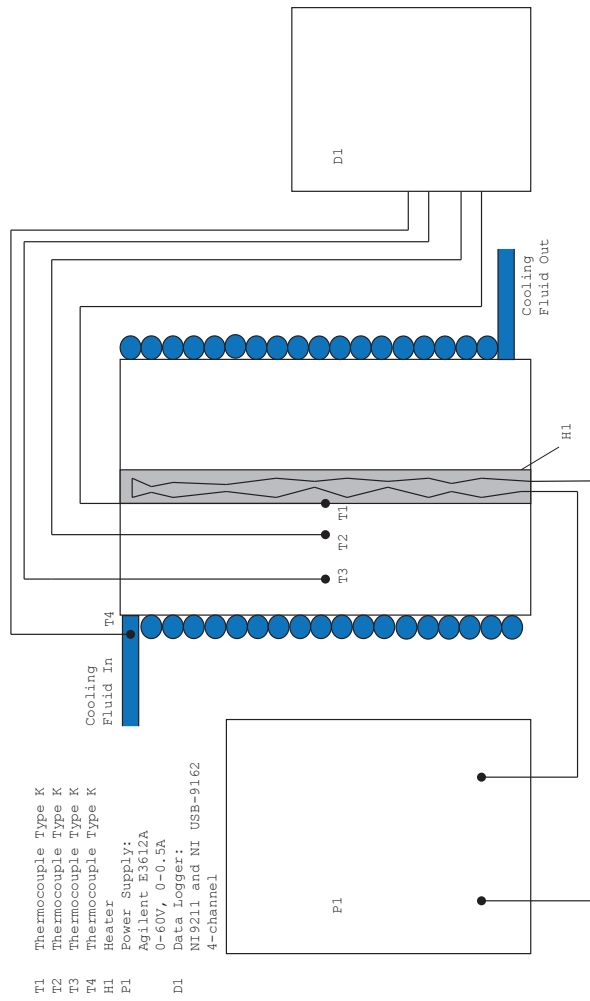


**Figure A.1.: P&ID Conductivity Rig**

**A.2 Permeability Rig**

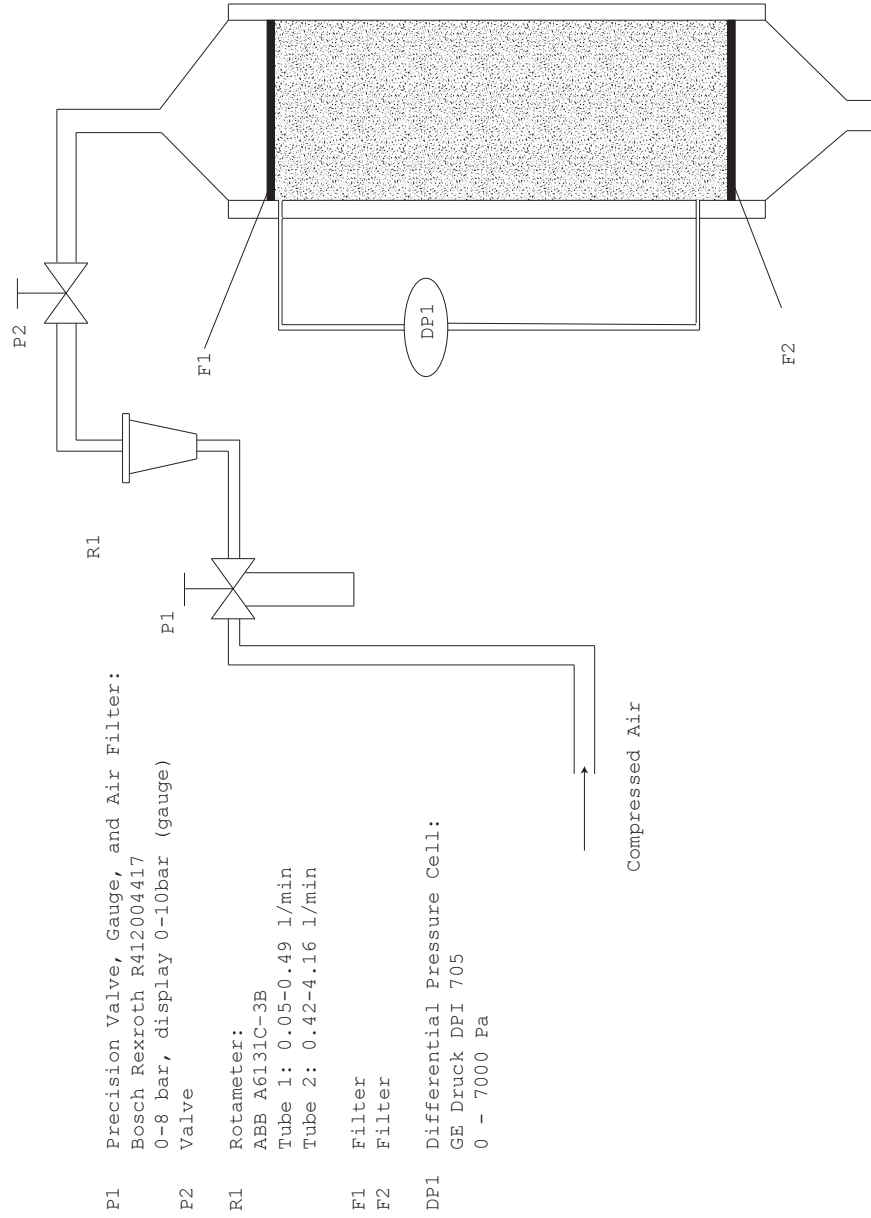


**Figure A.2.: P&ID Permeability Rig**

---

## EXPERIMENTAL UNCERTAINTIES

### **B.1** Basis

This appendix will evaluate a way to quantify uncertainties that will occur under measurements. Uncertainty analysis can tell how much the uncertainty of a variable influences the result; moreover, it can be helpful to identify the ‘weakest link’ in an experimental test setup. Measurement results nowadays should always be presented with uncertainties to consolidate their accuracy.

In addition, the t-distribution will be used to find the expected value within a certain confidence interval when multiple results are present.

### **B.2** Single-Sample Analysis

This section is based on a paper dealing with experimental uncertainties written by Moffat [7]. When considering a result  $R$  that is based on measurements from  $N$  variables  $X_i$ , the total uncertainty can be expressed as:

$$\delta R = \left\{ \sum_{i=1}^N \left( \frac{\partial R}{\partial X_i} \delta X_i \right)^2 \right\}^{\frac{1}{2}} \quad (\text{B.1})$$

The expression  $\frac{\partial R}{\partial X_i}$  describes how sensitive the function  $R$  is for the variable  $X_i$ . Several independent variables are combined in a root-sum-square (RSS) method. Equation B.1 applies when [7]:

- I. Each of the measurements are independent
- II. Repeated observations of each measurement will display Gaussian distributions
- III. The uncertainty in each measurement is initially expressed at the same odds

In order to calculate the uncertainty, it is necessary to have an analytical expression of the result  $R$ :

$$R = R(X_1, X_2, \dots, X_N) \quad (\text{B.2})$$

It is also possible to calculate the uncertainty without an analytical expression by using a computerized uncertainty analysis. Since this report only deals with analytical expressions for the results, it will not be discussed here.

**B.3 t-Distribution and Normal Distribution**

The t-distribution, also known as the Student t-distribution, is similar to the normal distribution as it also is symmetric around the mean of zero and bell shaped. The two distributions are in fact identical when the sample size  $n \rightarrow \infty$ ; however, the deviation of the t-Distribution will grow as the sample size decreases. For  $n < 30$ , it is useful to use t-Distribution.

$$T = \frac{\bar{X} - \mu}{S/\sqrt{n}} \tag{B.3}$$

$\mu$  is the population mean or the expected value,  $n$  number of samples,  $\bar{X}$  is the average, and  $S$  is analog to the standard deviation  $\sigma$  in a normal distribution.

$$\bar{X} = \frac{1}{n} \sum_{i=1}^n X_i, \quad S^2 = \frac{1}{n-1} \sum_{i=1}^n (X_i - \bar{X})^2 \tag{B.4}$$

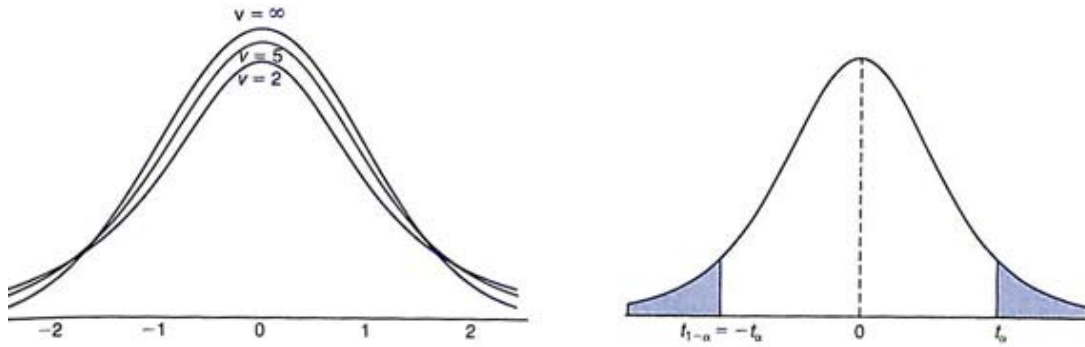


**Figure B.1.:** t-Distribution for Several Degrees of Freedom [8, Figure 8.13 and 8.14]

$v = n - 1$  is the degrees of freedom, the left curve in figure B.1 shows the distribution of  $T$  for  $v = 2, 5, \infty$  degrees of freedom. When sampling from normal distributions,  $\bar{X}$  and  $S^2$  are independent.

In experimental measurements it can be useful to use the distribution to determine the uncertainty between several independent measurements. The deviation from the expected value can be calculated from  $n$  samples when the confidence interval are specified. For a confidence interval of 95%, it means that the probability of the mean being within the specified limits is 95% which is equal to 20 : 1.

$$P(-t_\alpha < T < t_\alpha) = 1 - 2\alpha \tag{B.5}$$

Where  $t_\alpha$  is a tabulated value based on degrees of freedom  $v$ ,  $n$  samples and the confidence interval  $1 - 2\alpha$ .

$$P\left(\bar{X} - t_\alpha \frac{S}{\sqrt{n}} < \mu < \bar{X} + t_\alpha \frac{S}{\sqrt{n}}\right) = 1 - 2\alpha \tag{B.6}$$

[8, Chapter 8.7]

In comparison, the confidence interval for normal distribution is calculated similarly when  $n > 30$ :

$$P\left(\bar{X} - z_\alpha \frac{\sigma}{\sqrt{n}} < \mu < \bar{X} + z_\alpha \frac{\sigma}{\sqrt{n}}\right) = 1 - 2\alpha \tag{B.7}$$



When  $\sigma$  is unknown, it can be replaced with  $S$ .  
 [8, Chapter 9.4]

**B.4 Overall Uncertainty in a Single Measurement**

The sources of uncertainties can be divided into fixed errors and random errors which are called *bias* and *precision errors*, respectively. The uncertainty of the precision errors is calculated as shown in section B.3. The bias errors are however harder to define as they would be corrected if they were known. Moffat introduces a root-sum-square combination of all the fixed errors:

$$B_{X_i} = \{(B_{cal})^2 + (B_{acq})^2 + (B_{red})^2\}^{\frac{1}{2}} \quad (\text{B.8})$$

Where  $B_{cal}$  is the fixed calibration error,  $B_{acq}$  and  $B_{red}$  are the fixed data acquisition and reduction error. Other known fixed errors can be added in the root-sum-square expression.

The best estimate of  $X_i$  is according to Moffat the mean value  $\bar{X}_i$  plus or minus the uncertainty interval:

$$(U_R)_{0.95} = \{(B_{X_i})^2 + (t_{\alpha=0.025} \cdot S_{\bar{X}_i})^2\}^{\frac{1}{2}} \quad (\text{B.9})$$

Where  $S_{\bar{X}_i} = \frac{S}{\sqrt{n}}$ .  
 [7]



## MEASUREMENT MATERIALS

**C.1** Basis

The actual thermal conductivity and permeability have not been found tabulated for any of the chosen materials; therefore, it was necessary to use literature models to estimate the properties. The permeability has been estimated based on a model introduced in section 3.5. The thermal conductivity have been estimated with help from the model in section 2.7 and some tabulated values.

**C.2** Sugar

The measured density and mean body size is tabulated below.

$$\begin{array}{l|l} \rho & 1020 \frac{kg}{m^3} \\ d_{gr} & 0.9mm \end{array}$$

**Table C.1.:** Sugar: Measured Material Properties

The thermal conductivity of sugar and density has been found tabulated to be  $k = 0.58 \frac{W}{mK}$  and  $\rho = 1600 \frac{kg}{m^3}$  [3, Table A-8] at room temperature. Assuming that these values are for solid sugar, the porosity has been calculated:

$$\Phi = 1 - \frac{1020}{1600} = 0.3625 \quad (C.1)$$

The effective conductivity at room temperature has been calculated with the empirical relation presented in section 2.7 using  $k_{\sigma} = 0.58 \frac{W}{mK}$  and  $k_{\beta} = 0.025 \frac{W}{mK}$  [3, Table A-15]. The permeability estimation is found in section 7.2.1.

$$k_e = 0.35 \cdot (0.3625 \cdot 0.025 + 0.6375 \cdot 0.58) + \frac{0.65}{\frac{0.3625}{0.025} + \frac{0.6375}{0.58}} = 0.174 \frac{W}{mK} \quad (C.2)$$

#### **C.3 Sand**

The measured density and mean body size is tabulated below.

$$\begin{array}{l|l} \rho & 2209 \frac{kg}{m^3} \\ d_{gr} & 0.71mm \end{array}$$

**Table C.2.:** Sand: Measured Material Properties

The thermal conductivity and density of sand are given in Çengel to be  $\rho = 1515 \frac{kg}{m^3}$  and  $k = 0.2 - 1.0 \frac{W}{mK}$  [3, Table A-8]. Note that the density of the used material is higher than the tabulated material. The conductivity and density of the solid was not found; therefore, it was not possible to estimate the conductivity.

#### **C.4 Expancel 551 DE 40 d42**

The following data is taken from a data sheet from the supplier [12]:

$$\begin{array}{l|l} \rho & 42 \frac{kg}{m^3} \\ d_{gr} & 40\mu m \end{array}$$

**Table C.3.:** Expancel: Material Properties

As the conductivity for the solid not is available, it is not possible to estimate the effective conductivity. The supplier, Akzo Nobel - Eka Chemicals AB, has been contacted to retrieve material information. Unfortunately, no information regarding thermal conductivity or permeability were available for the current material.

PARAMETERS FOR PERMEABILITY ESTIMATION

Material	With smooth surface			With rough surface		
	$d_p$ , mm	$\epsilon'$	$\phi$	$d_p$ , mm	$\epsilon'$	$\phi$
Polydisperse beach sand	2-3	0.35	0.66	1-2	0.500	0.64
	1.5	0.35	0.76	1.5	0.445	0.92
Bank sand	2.5-5	0.445	0.80	1.5-4.5	0.400	0.79
	1.2-2.5	0.390	0.76			
Activated alumina	1-3	0.500	0.68	1.6	0.640	0.77
	3-5	0.500	0.49	5.25	0.480	0.77
Alumina silica gel	9-10	0.520	0.50	0.2-0.3	0.430-0.460	0.63-0.70
	2.5	0.520	0.56	1.2-5	0.390-0.445	0.76-0.80
Anthracite	3.5	0.480	0.68			
	4.5	0.500	0.49			
Silica gel KSM	1.0	0.540	0.66	3-5	0.490	0.50
	2.1	0.520	0.67	5-25	0.43-0.52	0.68-0.7
Shale	3.5	0.510	0.66	2.6	0.480	0.77
	7-8	0.520	0.07	30-25	0.500	0.62
Crushed stone	12-18	0.465	-	5-10	0.460-0.500	0.54
	18-25	0.475	-			
Gravel	3.7	0.470-0.540	0.73			
	12-20	0.370	0.68			

Figure D.1.: Parameters for Permeability Estimation, [6, Diagram 8-12]



---

## MATLAB SCRIPTS

### **E.1** Introduction

MATLAB has been used to treat the measurement data, this appendix describes briefly some of the scripts. The scripts are attached on the CD.

### **E.2** Thermal Conductivity

#### *E.2.1. conductivity.m*

Calculates the thermal conductivity and plots the temperatures from the logged temperatures, see figure 6.1. `conductivity.m` imports most of the data from an excel file; it is therefore necessary to specify which excel file it shall import and that the file has the same format in sheet1 as the attached `.xlsx`-files. In the MATLAB script it is possible to specify from which measurement step the temperature plot and thermal conductivity calculation shall begin with the variables `startT` and `start`, respectively. In addition, it is possible to use the variable `calibration = [T1 T2 T3]` to calibrate the measurements.

#### *E.2.2. uncertainty\_cond\_plot.m*

Calculates and plots the uncertainty of a thermal conductivity measurement, see figure 6.2. Inputs are  $T = [T1 T2]$ ,  $r = [r1 r2]$ ,  $h$ , and  $Q$  for the temperatures, radial positions, height of the heater, and heat, respectively. In addition, the uncertainties for the mentioned variables must be specified. `uncertainty_cond_plot.m` plots the uncertainty for each variable that is set  $> 0$ , it use the function `uncertainty_cond.m` for the calculation.

### **E.3** Permeability

#### *E.3.1. permplotter.m*

Plots the permeability against pore size length scale Reynolds number. Inputs are the parameters from Idelchik, and the geometry of the rig.

### *E.3. PERMEABILITY*

---

#### *E.3.2. permcalc.m*

Calculates the permeability and plots the result against the volume flow and Reynolds number. Inputs per measurement point are the read value of the rotameter  $X$ ,  $\Delta P$ ,  $P_{gauge}$ , and which float that was used. In addition, the uncertainties of each variable must be specified to calculate the uncertainty. The uncertainties for the rotameter are specified in the function `rotameterpercenttoflow.m`. The permeability will be plotted against the Reynolds number and the estimated value; therefore, it is necessary to specify the mean body diameter  $d_{gr}$ ,  $\phi$ , and  $\epsilon$  as well.



## MAPLE: SOLUTION OF PARTIAL DERIVATIVES FROM UNCERTAINTY CALCULATIONS

### **F.1** Conductivity

$$k := -\frac{Q}{2\pi h} \cdot \frac{\ln\left(\frac{r_2}{r_1}\right)}{dT}$$

$$-\frac{1}{2} \frac{Q \ln\left(\frac{r_2}{r_1}\right)}{\pi h dT} \tag{1}$$

$$dk := \left( (diff(k, r_2) \cdot dr)^2 + (diff(k, r_1) \cdot dr)^2 + (diff(k, Q) \cdot dQ)^2 + (diff(k, dT) \cdot ddT)^2 + (diff(k, h) \cdot dh)^2 \right)^{1/2}$$

$$\frac{1}{2} \tag{2}$$

$$\left( \frac{Q^2 dr^2}{r_2^2 \pi^2 h^2 dT^2} + \frac{Q^2 dr^2}{r_1^2 \pi^2 h^2 dT^2} + \frac{\ln\left(\frac{r_2}{r_1}\right)^2 dQ^2}{\pi^2 h^2 dT^2} + \frac{Q^2 \ln\left(\frac{r_2}{r_1}\right)^2 ddT^2}{\pi^2 h^2 dT^4} + \frac{Q^2 \ln\left(\frac{r_2}{r_1}\right)^2 dh^2}{\pi^2 h^4 dT^2} \right)^{1/2}$$

**F.2 Permeability**

$$K := \frac{4 \cdot Q}{\pi \cdot d^2} \cdot \frac{\mu}{L}$$

$$\frac{4 Q \mu L}{\pi d^2 dP} \tag{1}$$

$$dK = \sqrt{(diff(K, Q) \cdot dQ)^2 + (diff(K, \mu) \cdot d\mu)^2 + (diff(K, dP) \cdot ddP)^2 + (diff(K, L) \cdot dL)^2}$$

$$dK = 4 \sqrt{\frac{\mu^2 L^2 dQ^2}{\pi^2 d^4 dP^2} + \frac{Q^2 L^2 d\mu^2}{\pi^2 d^4 dP^2} + \frac{Q^2 \mu^2 L^2 ddP^2}{\pi^2 d^4 dP^4} + \frac{Q^2 \mu^2 dL^2}{\pi^2 d^4 dP^2}} \tag{2}$$

**F.3** Volume Flow Rotameter

$$Q := \frac{\sqrt{(R \cdot T \cdot (P4 + dP + P_{gauge}))}}{P4 + \frac{dP}{2}} \cdot \left( C_{min} + \frac{(C_{max} - C_{min}) \cdot X}{100} \right) \frac{\sqrt{RT(P4 + dP + P_{gauge})} \left( C_{min} + \frac{1}{100} (C_{max} - C_{min}) X \right)}{P4 + \frac{1}{2} dP} \quad (1)$$

$$\begin{aligned} dQ &:= \left( (\text{diff}(Q, P4) \cdot dP4)^2 + (\text{diff}(Q, dP) \cdot ddP)^2 + (\text{diff}(Q, P_{gauge}) \cdot dP_{gauge})^2 + (\text{diff}(Q, R) \cdot dR)^2 \right. \\ &\quad \left. + (\text{diff}(Q, T) \cdot dT)^2 + (\text{diff}(Q, X) \cdot dX)^2 \right)^{1/2} \\ &\frac{1}{2} \left( 4 \left( \frac{1}{2} \frac{\left( C_{min} + \frac{1}{100} (C_{max} - C_{min}) X \right) RT}{\sqrt{RT(P4 + dP + P_{gauge})} \left( P4 + \frac{1}{2} dP \right)} \right. \right. \\ &\quad \left. \left. - \frac{\sqrt{RT(P4 + dP + P_{gauge})} \left( C_{min} + \frac{1}{100} (C_{max} - C_{min}) X \right)}{\left( P4 + \frac{1}{2} dP \right)^2} \right)^2 dP4^2 \right. \\ &\quad + 4 \left( \frac{1}{2} \frac{\left( C_{min} + \frac{1}{100} (C_{max} - C_{min}) X \right) RT}{\sqrt{RT(P4 + dP + P_{gauge})} \left( P4 + \frac{1}{2} dP \right)} \right. \\ &\quad \left. \left. - \frac{1}{2} \frac{\sqrt{RT(P4 + dP + P_{gauge})} \left( C_{min} + \frac{1}{100} (C_{max} - C_{min}) X \right)}{\left( P4 + \frac{1}{2} dP \right)^2} \right)^2 ddP^2 \right. \\ &\quad + \frac{RT \left( C_{min} + \frac{1}{100} (C_{max} - C_{min}) X \right)^2 dP_{gauge}^2}{(P4 + dP + P_{gauge}) \left( P4 + \frac{1}{2} dP \right)^2} \\ &\quad + \frac{T (P4 + dP + P_{gauge}) \left( C_{min} + \frac{1}{100} (C_{max} - C_{min}) X \right)^2 dR^2}{R \left( P4 + \frac{1}{2} dP \right)^2} \\ &\quad + \frac{R (P4 + dP + P_{gauge}) \left( C_{min} + \frac{1}{100} (C_{max} - C_{min}) X \right)^2 dT^2}{T \left( P4 + \frac{1}{2} dP \right)^2} \\ &\quad \left. + \frac{4 RT (P4 + dP + P_{gauge}) \left( \frac{1}{100} C_{max} - \frac{1}{100} C_{min} \right)^2 dX^2}{\left( P4 + \frac{1}{2} dP \right)^2} \right)^{1/2} \quad (2) \end{aligned}$$